ISAS - INTERNATIONAL SCHOOL FOR ADVANCED STUDIES

Models of Quantum Paraelectric Behaviour of Perovskites

Thesis submitted for the degree of

"Doctor Philosophiæ"

CANDIDATE

Roman Martoňák

SUPERVISOR

Prof. Erio Tosatti

September 1993

TRIESTE

SISSA - SCUOLA INTERNAZIONALE SUPERIORE DI STUDI AVANZATI

TRIESTE

Strada Costiera 11

Models of Quantum Paraelectric Behaviour of Perovskites

Thesis submitted for the degree of

"Doctor Philosophiæ"

CANDIDATE

Roman Martoňák

SUPERVISOR

Prof. Erio Tosatti

September 1993

Acknowledgement

I would like to take this occasion to express my deep gratitude to everybody who has helped me in any manner in course of this work.

Table of Contents

1 Introduction

1.1 Motivation of the work

Consider a regular classical ferroelectric, with all its dipoles ordered and parallel at $T = 0$, so as to minimize some ferroelectric coupling, e.g. a term

$$- J \sum_{\langle ij \rangle} \vec{p}_i \cdot \vec{p}_j \,, \tag{1.1}$$

where $\vec{p}_i$ represents a dipole localized on the site i. Imagine, next, to turn on quantum mechanical effects, for example in the form of a finite amplitude t, for each dipole to hop from the present configuration to another. For small t, or sufficiently large J/t, this process simply adds zero-point fluctuations to the ferroelectric ground state, renormalizing somewhat its mean polarization $\langle \vec{P} \rangle$, as well as the Curie temperature T_c. However, there will be a critical value J_q/t, above which zero-point fluctuations destroy completely, or "melt", long-range ferroelectric order even at $T = 0$. The resulting state has been called a *"quantum paraelectric"* (QPE) [1], as opposed to a *"classical paraelectric"*, where disorder is caused by thermal fluctuations. Quantum paraelectrics characterized by J/t smaller than, but close to, J_q/t, have a very large dielectric response, can be driven into ferroelectricity very easily, and have therefore been named also *incipient ferroelectrics.*

The subject of quantum paraelectricity has a long history. Quantum effects in hydrogen-bonded ferroelectrics were apparently first pointed out by Blinc as early as 1958 [2], and

modeled by de Gennes [3] as an Ising model in a transverse field

$$H = -t \sum_i s_i^x - J \sum_{\langle ij \rangle} s_i^z s_j^z \,, \tag{1.2}$$

where s_i^x and s_i^z are Pauli matrices. This model shows precisely a ferroelectric phase for $J/t > J_q/t$, and a paraelectric phase for $J/t < J_q/t$, at $T = 0$, J_q/t having a finite value, which depends on the dimensionality. Interest renewed in the middle 70's, when two groups in Switzerland [4], [5], separately considered the critical behaviour of a general double-well-plus-spring model displacive ferroelectric, and found anomalous "quantum" critical exponents for the purely quantum ferro-para transition at $T = 0$. The quantum exponents apply strictly at $T = 0$, while at finite T there is a crossover from quantum to classical critical behaviour, sufficiently close to T_c, as later discussed in detail by e.g. Pfeuty [6]. These exponents were measured by Rytz [7] in the perovskite alloys $KTa_{1-x}Nb_xO_3$. Realistic self-consistent phonon calculations for displacive models of $KTaO_3$ have also been performed, which take into account quantum effects in the displacive limit [8], [9].

The present reason for reviving quantum paraelectrics at this time is different, and more speculative. It is based on trying to pursue a certain analogy that quantum paraelectrics have with liquid He^4. He^4 remains fluid down to zero temperature, but crystalizes under pressure, above a critical $P_Q \simeq 25$ atm. As sketched in Fig.1.1, the phase diagram of He^4 has strong analogies to that of a quantum paraelectric, with ordered, classical disordered and quantum disordered (fluid) regions.

However, the quantum fluid region of He^4 has in addition very special properties. He^4 is superfluid, possesses off-diagonal long-range order (ODLRO), and is separated from the classical fluid by a phase transition line (the λ-line). Clearly, helium exhibits phenomena of macroscopic quantum coherence. A natural question to ask is therefore: should we expect something special in the quantum paraelectric systems too, or not ?

A first answer can be given for systems described strictly by the de Gennes hamiltonian

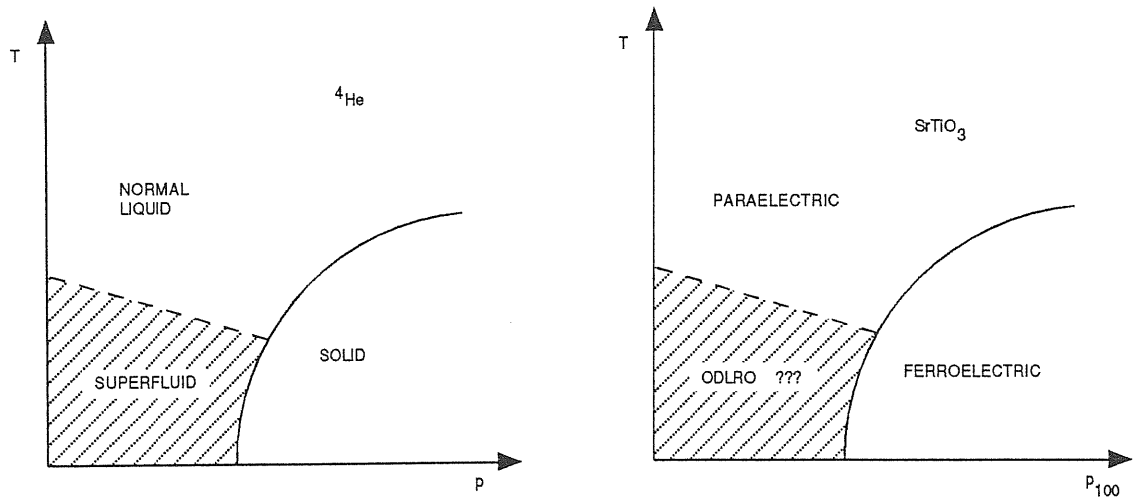

Figure 1.1: The real phase diagram of ^4He and a speculative one of $SrTiO_3$. The region of expected existence of ODLRO in $SrTiO_3$ is hatched.

(1.2), and is negative. The ground state of (1.2) is for all $J/t < J_q/t$ a nondegenerate rotationally symmetric state ("singlet"), with an excitation gap. There is no broken symmetry, and in fact there are, unlike in liquid He^4, no conserved bosons in an extended state. Quantum melting in this case is a strictly local affair.

A similar conclusion applies to the *displacive limit model*, both in its idealized version considered by Oppermann and Thomas [5], and by Schneider at al. [4], or in the more detailed version discussed by Bilz et al. [9] for the perovskites. In the displacive limit, dipoles do not exist until long-range ferroelectric order is established. In other words, the *effective* on-site well is parabolic, without any central barrier and side valleys. Quantum effects simply arise when the quantized level spacing inside this parabolic well gets too large (due to the well being narrow, or the ion mass being small) in comparison with the ferroelectric interaction J. Here too, quantum melting is local (rotational, in fact), and a description by, e.g. self-consistent phonons [9] is probably quite adequate.

However, real systems are endowed with many interesting additional complications, which make them richer than the simple de Gennes double-well hamiltonian (1.2), or than the displacive limit models discussed above. The displacive models, in particular, fail to include the slow, nearly critical fluctuations, which are known to be crucially present [10] in $KTaO_3$ at low temperatures. In simple words, there is in these systems below 40 K or so a well-defined dipole to each cage, even without long-range ferroelectric order. The dipoles are coherent enough to form rather large domains, which fluctuate slowly. The displacive limit models, discussed above, ignore all that. They apply to systems where the standard mean-field assumption of identifying the locale dipole with the mean dipole (which in turn is zero), is justified. We will see that a possible remedy in trying to bring these displacive models to describe better the behaviour of perovskite quantum paraelectrics is to contemplate the existence of an intermediate incommensurate ferroelectric phase, whose quantum melting might be substantially more interesting.

The double-well model (1.2) instead probably describes adequately the hydrogen-bonded ferroelectrics, where each hydrogen is strictly confined to its own double-well, or even the QPE perovskites, where a dipole is delocalized *inside* an individual oxygen cage.

In a perovskite, however, and in $SrTiO_3$ in particular, there are additional ingredients beyond (1.2). First of all, ferroelectricity coexists with antiferrodistortive and elastic degrees of freedom. Even ignoring coupling to these (which represent a very nontrivial complication), there are two effects, both due to the corner-sharing property of the oxygen ions: *an effective ice rule*, and *a quantum mechanical oxygen hopping*, which may cause dipoles to hop from a cage to the next. We will discuss both the ice-rule effects and the dipole hopping, in this order, the latter being more difficult to treat.

Parallel to these theoretical speculations, and in fact initially stimulated by them,

there has been a burst of recent experimental activity on $SrTiO_3$. Müller et al. [11] have found Fe^{3+} EPR evidence of a weak but well defined non-structural phase transition taking place at $T_q \simeq 37$ K. Early $SrTiO_3 - BaTiO_3$ [12] and $SrTiO_3 - PbTiO_3$ [13] alloy studies, and more definitively Ca-doping induced ferroelectricity [14], had clearly indicated the onset of quantum paraelectricity in pure $SrTiO_3$ between 35 and 40 K. The new possibility raised in [11] is that quantum paraelectricity would set in with an abrupt phase transition. Weak anomalies near 30 K have also been observed in sound velocity and internal friction [15], as well as in the phonon dispersion curves [16]. In these quantities, like in the dielectric constant [1], which extrapolates as $\epsilon^{-1} \sim (T - T_0)$ for all $T > 60$ K with $T_0 \sim 37$ K, no sharp critical behaviour was seen. The precise onset temperature of quantum paraelectric phenomena seems thus somewhat property-dependent, as well as slightly sample-dependent [15]. Additional EXAFS evidence is now being proposed [17], reporting a sudden broadening of $Ti-O$ bond length distribution, indicating a very abrupt onset of, or more likely a sharp phase transition into, the quantum paraelectric phase of $SrTiO_3$, taking place near 30 K.

Summarizing this evidence, the quantum paraelectric state of $SrTiO_3$ may be qualitatively described as consisting of large-size ferroelectric domains ($\xi \sim 10 \div 20$ lattice spacings or so). The domains have extensive, slowly quantum fluctuating boundaries, which are responsible for the absence of a net static polarization. If we accept the existence of a phase transition, as first suggested in [11], between the classical paraelectric and the quantum paraelectric state, then we are left with the task of understanding the true nature of the new state, symmetry, and possible order, below T_q.

In this thesis we will review the present state of understanding of these QPE phenomena, reached so far in Trieste, in the attempt to follow up the effects of at least some of the additional couplings present in $SrTiO_3$, as discussed earlier. Although these attempts

are not quite conclusive as yet, also because of the objective difficulty of obtaining quantitative insight for new, complicated quantum models, the physical questions they raise are quite interesting. Here we will present a detailed discussion of the progress made so far.

The thesis is organized as follows. In the rest of this introductory chapter we review in more detail the main relevant experiments, and point to some implications of these for our model building. Chapter 2 is devoted to a general discussion of models to be treated in subsequent chapters. First we recall the well-known displacive versus order-disorder regime aspects of the standard classical model for structural phase transitions, and discuss the extent to which these aspects pertain to the case of QPE perovskites. Correspondingly, we divide the possible models into two classes, those based on continuous and those based on discrete degrees of freedom. As an example of the former class, we propose a Landau-Ginzburg-Wilson hamiltonian for $SrTiO_3$, including elastic couplings, which leads to discuss the existence of an incommensurate phase. Considering the latter class of models, we try to identify their most important ingredients, taking as relevant degrees of freedom the discrete $Ti-O$ bond variables. In Chapter 3, the *classical* incommensurate ferroelectricity arising from elastic couplings is investigated in detail, and the effect of quantum fluctuations is discussed on a heuristic level. In Chapter 4 we then investigate three idealized 2D quantum discrete lattice models. The first is a plain quantum four-state clock model, while the second includes an ice-type constraint. Both models are studied by means of a numerical Path Integral Monte Carlo simulation (PIMC), and the corresponding phase diagrams are determined with reasonable accuracy. On the technical side, in order to overcome the pathologically slow $1/m$ convergence in number of Trotter slices in case of the constrained model, a special method has been invented, which is described in detail in Appendix A. In the last section of chapter 4 we describe our third model, which consists of endowing the constrained four-state clock model with an addi-

tional physical effect, namely the possibility of bond hopping and 'bond vacancies'. For this third model we have so far not been able to set up an accurate numerical simulation technique, allowing us to determine the complete phase diagram in the parameter space at finite temperatures. Some general considerations are presented, based on analogies with Andreev and Lifshitz's work [18] on quantum crystals of He^4, whose main idea is briefly summarized in Appendix B, for the sake of completeness. A particular zero temperature and zero coupling case of this more complete third model is studied numerically, by means of a Variational Monte Carlo technique, the details of which are described in Appendix C. Finally the last, fifth, chapter is devoted to discussion and conclusions.

1.2 Experimental evidence

Before discussing any particular experiments, we find it useful to briefly review the classic phenomenology of *soft modes* in $SrTiO_3$, both structural and ferroelectric, since these modes turn out to be of crucial importance in all the following considerations.

The structure of the high temperature phase ($T > T_a = 105$ K) is *cubic* perovskite which consists of 5 interpenetrating simple cubic lattices and contains 1 formula unit per unit cell. Symmetry analysis [19] shows that in the *center of the Brillouin zone* there is (apart from 3 acoustic modes with $\omega \to 0$) one triply degenerate optical mode Γ_{25} and 3 triply degenerate optical modes Γ_{15}. Each of these latter triplets is for any finite wavevector split into a longitudinal mode and a doubly degenerate transverse mode. Upon cooling, it is the F_{2u} (Γ_{25}-like) *zone-boundary* mode that softens most and goes unstable at $T_a = 105$ K [20], [21]. The crystal undergoes a structural antiferrodistortive phase transition, and the point symmetry group changes from O_h to D_{4h} [22] (we shall say more about the nature of the transition in one of the following subsections devoted to EPR experiments). Below T_a, the soft zone-boundary structural mode folds into a zone-center

one, and splits, due to the lowering of symmetry, giving rise to a single A_{1g} mode and a doubly degenerate E_g mode ($\omega_{A_{1g}} > \omega_{E_g}$). Both modes then harden by further decreasing the temperature below T_a. Apart from the structural mode, also the zone-center F_{1u}, or Γ_{15} mode considerably softens with decreasing temperature. Unlike the structural one, this mode is dipole-active, and would therefore yield ferroelectricity upon condensation. At T_a, this mode splits, too, giving rise to a single A_{2u} mode and a doubly degenerate E_u mode ($\omega_{A_{2u}} > \omega_{E_g}$), both of which continue to soften below T_a, but *never condense*. The lower of the modes, the E_u doublet, softens progressively as T decreases down to $T \sim 35$ K or so, and then saturates at a finite frequency of about 10 cm^{-1}, being *underdamped* over the whole temperature range down to $T \to 0$ [23],[24]. The singlet A_{2u} behaves similarly and saturates at about 20 cm^{-1} [16].

1.2.1 Incipient ferroelectric behaviour of $SrTiO_3$

According to the standard soft-mode theory [25], a strong softening of a particular dipole-active zone-center TO phonon mode brings about a possibility of onset of ferroelectricity in the system, which is marked by a divergence of the corresponding dielectric constant.

The static, or more precisely, low frequency dielectric constant of $SrTiO_3$ has been measured several times [26], [27], [1] (Fig.1.2). It was found to develop a tetragonal anisotropy below T_a, in-plane ϵ_a being larger than ϵ_c, revealing that the *dominant polarization fluctuations* take place in the XY-plane. For temperatures $T > 60$ K, ϵ_a behaves according to the Curie-Weiss law with a critical temperature $T_c \sim 37$ K. Below 60 K, however, considerable deviations from this behaviour are observed and, instead of diverging at 37 K, ϵ_a levels off and gradually stabilizes at a *very high value* of $\sim 2 \times 10^4$. The most striking feature is that for $T < 3$ K this high value is *completely temperature independent*, as Müller et al. have shown in [1], measuring down to 30 mK (this kind of behaviour has then been termed as *quantum paraelectric behaviour*). A very similar kind of behaviour

was observed in QPE $KTaO_3$ [28, 29, 30].

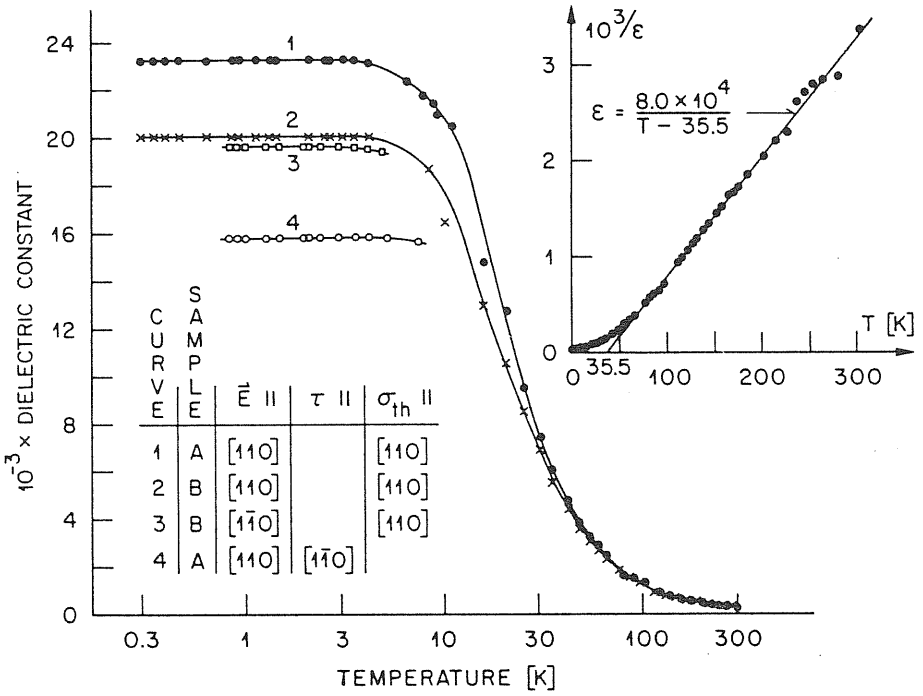

Figure 1.2: Dielectric constants ϵ_{110} and $\epsilon_{1\bar{1}0}$ of the monodomain $SrTiO_3$ samples. (σ_{th} is the stress applied by thermal treatment). Inset: $10^3/\epsilon$ vs. T. After [1].

In $KTaO_3$, apart from the static measurements, frequency resolved dielectric response measurements have also been performed. Maglione et al. [10] measured the *radio-frequency* dielectric response of $KTaO_3$, and found that below $\sim$ 60 K, the dielectric constant ϵ develops in the microwave frequency region a Debye-like additional term,

$$\epsilon = \epsilon_{i.r.} + \frac{\Delta\epsilon}{1 + i\omega\tau_0}. \tag{1.3}$$

The relaxation time τ_0 increases with decreasing temperature, and below 40 K it saturates at a value of about $\tau_0^{-1} \sim 500$ MHz. The saturation of τ_0 appears to be a specific feature of QPE's. The appearance of the slow Debye relaxations is generally a signal of a crossover from displacive to order-disorder regime, and we shall come again to the significance of

this fact in the next chapter. In $SrTiO_3$, no evidence for such slow relaxation has been found in the sub-gigahertz frequency region [31]. However, since there is other evidence for the existence of the crossover to order-disorder regime in $SrTiO_3$ (to be mentioned in the following subsections), the slow relaxation should be also present here. It would be highly desirable to search for it, extending measurements to higher frequencies, because such experiment would provide a direct information about the low temperature cluster dynamics in $SrTiO_3$. At this point, we would like to discuss the link to soft phonon modes, as it is explicitly expressed in the Lyddane-Sachs-Teller (LST) relation.

The low-frequency Debye-like behaviour of the dielectric constant requires that the LST relation be written in its general form [32]

$$\frac{\epsilon(\omega)}{\epsilon_\infty} = \frac{i\gamma_{Ld} + \omega}{i\gamma_{Td} + \omega} \prod_j \frac{\Omega_{Lj}^2 + i\gamma_{Lj}\omega - \omega^2}{\Omega_{Tj}^2 + i\gamma_{Tj}\omega - \omega^2}\,, \tag{1.4}$$

where ϵ_∞ is the high frequency dielectric constant, Ω_{Lj}, γ_{Lj} and Ω_{Tj}, γ_{Tj} are frequencies and linewidths of the longitudinal and transverse IR active phonon modes and γ_{Ld} and γ_{Td} are the longitudinal and transverse relaxation frequencies. As is easily seen, for frequencies below all the phonon resonances this form yields just to a Debye-like behaviour (1.3). To our knowledge, there has not yet been an attempt to verify the validity of LST relation in this general form in the case of $SrTiO_3$ at low temperatures. However, it is clear that the LST relation *cannot* be satisfied in its simpler traditional form, which attributes the *whole* static dielectric constant just to the soft mode, neglecting the contribution of the slow relaxation [23], [24], [16]. This is usually written as

$$\frac{\epsilon_0}{\epsilon_\infty} = \frac{\prod_i \omega_{Li}^2}{\prod_i \omega_{Ti}^2}\,, \tag{1.5}$$

where ϵ_0 is the static dielectric constant. The restricted LST relation (1.5) was discussed in [24] and [23] for the case of the in-plane dielectric constant ϵ_a, and in [16] for the case of ϵ_c. In Ref.[24] and [23], surprisingly, it is claimed that (1.5) is well satisfied for ϵ_a down

to lowest temperatures, while in [16] a discrepancy was reported for ϵ_c, by only a factor of 2 (Fig.1.3). In both places, it was assumed that the frequencies of all modes except for the soft TO branch were temperature independent. In that case, (1.5) implies a relation between the temperature dependence of ϵ_0 and that of the soft mode frequency ω_1

$$\omega_1^2 = \frac{C}{\epsilon_0} , \tag{1.6}$$

where

$$C = \frac{\prod_i \omega_{Li}^2}{\prod_{i>2} \omega_{Ti}^2} \epsilon_\infty , \tag{1.7}$$

and this is the equation actually tested in both cases. We argue that the corresponding conclusions are just incidental, and probably incorrect. We suspect in particular the assignment of the frequency of $\sim$ 173 cm^{-1} to the lowest LO mode in $SrTiO_3$ [23]. It would be desirable to perform new accurate measurements of the LO branches in order to clarify this point.

To end this subsection, we mention that there are several possible ways to remove experimentally the quantum fluctuations, and drive a QPE to proper, classical ferroelectricity. Bednorz and Müller [14] observed that in-plane (XY-type) ferroelectricity can be induced in $SrTiO_3$ by doping the material with Ca. The onset of ferroelectricity was observed at an exceedingly low concentration $x_{Ca} = 0.0018$. By increasing x_{Ca}, the Curie temperature raises fast, and then saturates at $T_S \sim 35$ K. Uwe and Sakudo [33] applied external stress normal to the (100) or (110) face of the crystal, and also observed ferroelectric transitions. In case of (100) stress, the induced polarization developed in the XY plane, in the direction *perpendicular* both to stress, and to the tetragonal axis. With (110) stress, the crystal polarized along the tetragonal axis. We notice that in both cases the spontaneous polarization appeared in the direction *perpendicular to the stress*, along which the stressed crystal actually *expanded*.

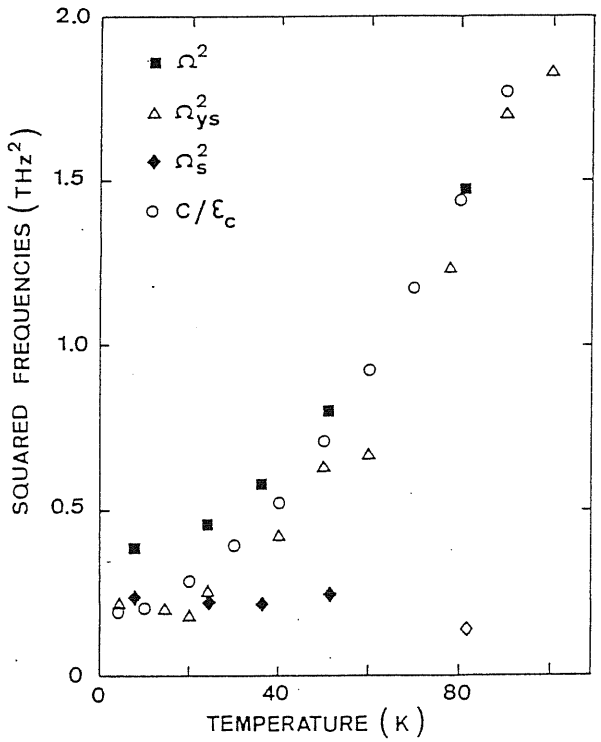

Figure 1.3: Squared frequencies of the low-lying TO modes versus T in $SrTiO_3$. Ω is the frequency of the A_{2u} mode after [16]. Ω_{YS} is the frequency of the E_u mode after [24]. Ω_S is the frequency of the structural E_g mode after [16]. For comparison with the LST relation, C/ϵ_c is also plotted, where ϵ_c is taken from [27]. After [16].

1.2.2 Elastic measurements

Based on general thermodynamic arguments [34], one expects the singularities of a phase transition to reflect in the elastic properties. It has been known for a long time that the 105 K structural phase transition manifests itself as a strong feature on the elastic constants of $SrTiO_3$, [35]. When measurements were extended to lower temperatures, a rather spectacular anomaly was observed in the tetragonal phase at temperature close to 32 K [36], [37]. The elastic compliance s_{11} was observed to increase dramatically, by a factor of almost four, and this behaviour was interpreted as a possible sign of a phase transition into an orthorhombic phase, reported previously by Lytle [38] on the basis of

X-ray diffraction experiment. In both works [36], [37], the sample was made piezoelectric by application of rather strong dc fields of the order of magnitude of 10 kV/cm. No such anomaly in the temperature interval from 105 K down to 4 K was instead reported by Rehwald [39], based on measurements by the pulse-echo method in the frequency range 40 - 200 MHz, with no applied field. Rehwald argued, reasonably, that due to the strong dc fields used in [36], [37], the measured elastic constant actually picked up a contribution from piezoelectric coupling, and claimed that the observed step in s_{11} could be nearly quantitatively explained by this contribution.

Recent study [15] used a vibrating reed resonant method, in which no large dc field was applied across the sample. Experiments were performed at the very low frequency of 3.5 kHz (four orders of magnitude lower than that used in [39]), and both the elastic compliance s_{11} and the corresponding internal friction coefficient Q^{-1} were measured (Fig.1.4). QPE regime related features appear below 50 K. Close to 40 K, there is a pronounced increase of the internal friction, a structured peak. Inside the peak, Q^{-1} rises by a factor of about four with respect to its values in the flat region with low attenuation between 44 and 55 K. Below 20 K, it decreases again, rejoining the ideal straight extrapolation of the flat region between 55 and 44 K. In the temperature region $20 \div 40$ K where the peak of Q^{-1} is present, there is an increase of the compliance s_{11}, which also disappears again below 20 K or so. We believe that these observations can be qualitatively interpreted due to interaction of the acoustic phonon with the (non-critical) ferroelectric domain walls fluctuations. In a critical case like at $T_a = 105$ K in $SrTiO_3$, this coupling gives rise to a sharp singularity. The onset of QPE, between 20 and 40 K, appears instead more as a smooth crossover in the elastic properties.

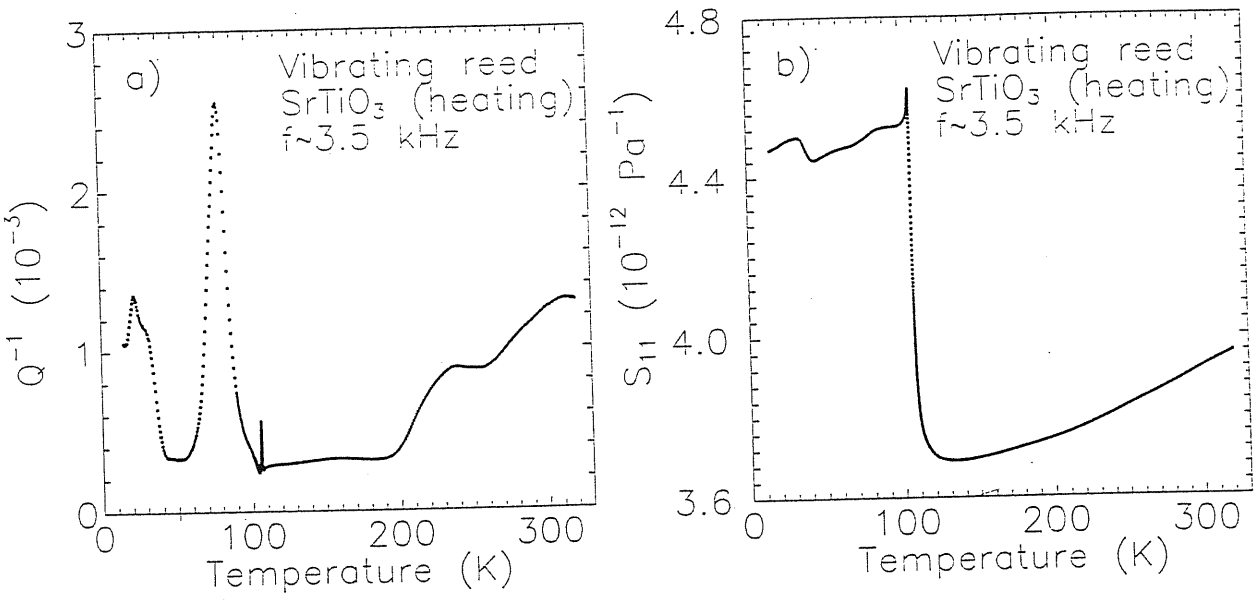

Figure 1.4: Left: Internal friction Q^{-1} (proportional to ultrasonic attenuation) vs. temperature in $SrTiO_3$ single crystal, measured by a vibrating reed resonance technique at frequencies near 3.5 kHz. The excitation is a flexural mode along the [100] direction, corresponding to the S_{11} elastic compliance excitation. Right: Elastic compliance S_{11} measured simultaneously with the internal friction. After [15].

1.2.3 Spectroscopy of the phonon modes

There is a considerable amount of experimental material concerning the spectroscopy of the phonon modes in $SrTiO_3$, and particularly of the soft modes. In this subsection, we will not try to give an exhaustive review of all this work. We rather concentrate on some recent accurate measurements, focusing on the low temperature region ($T < 50$ K) of our interest, which have revealed quite interesting anomalies.

We will start with the acoustic branches. In [40], Axe et al. for the first time pointed out that with decreasing temperature the coupling between the lattice strains and the softening ferroelectric modes becomes more and more important. Such TA–TO coupling can lead to a depression of the effective resulting TA dispersion curve for some $k_0 \neq 0$,

and if sufficiently strong, even to a formation of a minimum in $\omega_{TA}(\vec{k})$. We shall consider this effect in more detail in one of the following chapters. Motivated by the search for such a minimum, in connection with the proposal of Ref.[11], new measurements of the acoustic branches were performed in [41] and [16], by means of neutron and Brillouin spectroscopy, for temperatures below the structural transition at 105 K, with emphasis on the low temperature range below 40 K. In [41], a *polydomain* sample was used. The dispersion curves of TA modes of $SrTiO_3$ were measured for very low values of q in the vicinity of (111) reciprocal lattice point and an anomalous loss of the inelastic structure factor was observed for the [100] branch around a reduced wavevector $\xi = qa/2\pi \sim 0.03$ at $T \sim 40$ K. No anomaly, however, was observed for the [110] branch. This suggests that the TA-TO coupling is anisotropic in the q-space, namely maximal for [100] direction and irrelevant for the [110] direction.

The recent data [16] are particularly reliable since in this work the sample was forced to be a single tetragonal domain by applying an external uniaxial pressure along a $[1\bar{1}0]$ direction. We will briefly comment the main anomalies observed. Since the doublet E_u TO mode softens much more than the singlet A_{2u}, we might expect the TA modes polarized in the XY plane to be more depressed then their counterparts polarized parallel to the tetragonal axis. Contrary to this expectation, just the opposite was found, namely that the TA phonons polarized along the c-axis and propagating in the XY plane have considerably lower frequencies than those polarized and propagating in the XY plane. The former branch is for temperatures below 37 K quite strongly depressed, particularly for propagation along [100] direction, in a *rather narrow* q range near $\xi \sim 0.04$. No proper minimum, however, was found.

Brillouin scattering was used to investigate the acoustic branches propagating in the c direction at very low wavevectors, $\xi \simeq 2.6 \times 10^{-3}$. While the LA phonon hardens with

decreasing temperature (which is the usual temperature dependence), the TA phonon softens progressively, and below 30 K its frequency falls down even more rapidly, until it *saturates* below 10 K or so. This behaviour is reminiscent of the increase observed for the elastic compliance s_{11}, and for the internal friction Q^{-1}, discussed above.

In the Brillouin scattering experiment, apart from phonons, a new finite frequency peak has also been observed in the central peak region, below 37 K, sharper as the temperature decreases further. It might correspond to first order scattering from a new excitation, appearing below 37 K, which however, remains to be identified.

Besides these acoustic branches, an *anomalous* TA branch was also observed by means of the neutron scattering in [16]. Below 105 K, a new mode was observed, polarized along the c-axis and propagating in the XY plane ([100] direction), with frequency *lower* than that of the corresponding TA phonon. The splitting between the TA phonon and the new mode increases very rapidly at temperature near 37 K, particularly for the wavevector $\xi \sim 0.04$. A striking feature of this new mode is that its intensity falls down very rapidly when its wavevector $\vec{q}$ is tilted away from the XY plane.

In [16], the structural mode E_g was also investigated, by means of neutron scattering, and an interesting *structure factor intensity anomaly* was found. In the vicinity of the reciprocal lattice point (002), only the modes polarized along the tetragonal axis should be seen. The doublet E_g is polarized along the c-axis, however, for its normally accepted wavevector, this mode should be inactive at $q = 0$, its intensity proportional to q^2, and therefore for small ξ this mode should not be easily observable. For low enough temperatures, just the contrary was found. The mode is quite strong at $q = 0$, and at very low temperature its intensity *does not depend on* q. In the $(\xi 02)$ measurement, a *maximum* of the intensity was observed around $\xi \sim 0.04$ for $T = 37$ K.

Finally, we mention anomalous hyper-Rayleigh scattering, or second harmonic genera-

tion, observed in [42]. Since both cubic and tetragonal phases of $SrTiO_3$ preserve inversion symmetry, and proper ferroelectricity does not set in, *no* second harmonic generation is expected at any temperature. Contrary to this, hyper-Rayleigh signal appears below 80 K, increasing particularly below 40 K (Fig.1.5), with a behaviour rather similar to that of the static dielectric constant (Fig.1.2). This signal is clearly attributable to scattering from ferroelectric domains, inside each of which the inversion symmetry is broken. In order for this to happen it is necessary that a majority of Ti ions should be displaced off-center below 40 K. This observation therefore represents a *strong support* for the presence of dynamic order-disorder ferroelectric fluctuations in $SrTiO_3$ below 40 K or so. The strong similarity between the increase of hyper-Rayleigh intensity and of low frequency dielectric response at low temperatures further implies that the same slow domain fluctuations, which do not freeze out, but remain dynamical all the way to $T = 0$, are responsible for both.

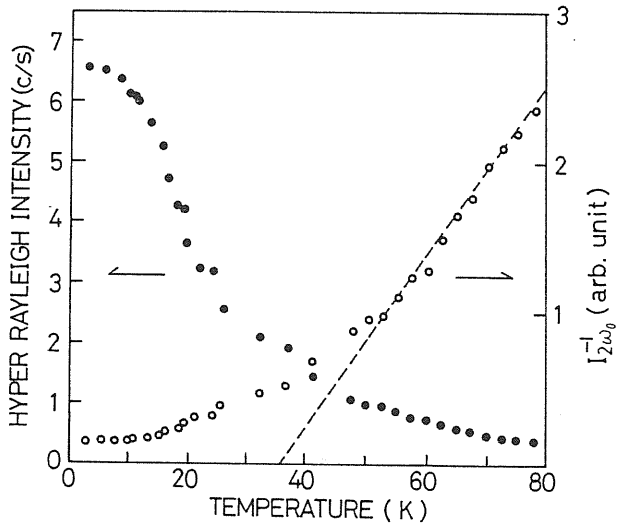

Figure 1.5: Variation of the intensity $I_{2\omega}$ (full points) of hyper-Rayleigh light with temperature. The inverse quantity $I^{-1}_{2\omega}$ (empty points) is also plotted, showing a deviation from a straight line (dotted) at low temperatures. After [42].

1.2.4 The EPR anomaly

Before describing the anomaly itself, we recall some basic considerations related to the EPR measurements and to the way in which these are interpreted. To observe an EPR spectrum, a paramagnetic ion is substituted into a nonmagnetic crystal. Due to the presence of the crystal potential, spin levels, which in the free ion are $(2S + 1)$ times degenerate, become split, and the amount of splitting is related to the strength and the symmetry of the potential. An external magnetic field is then applied which lifts even the remaining degeneracy and the resulting levels are a function of the field orientation relative to the crystal axes. The frequencies corresponding to the transitions between the levels are usually in the microwave region and therefore can be determined by measuring the microwave absorption. A convenient way of representing the experimental situation is to introduce an effective spin hamiltonian, which for our case of tetragonal symmetry reads [11]

$$\mathcal{H} = g\beta\vec{H}\vec{S} + \frac{a}{6}(S_x^4 + S_y^4 + S_z^4 - C) + D[S_\zeta^2 - \frac{1}{3}S(S+1)]\,, \tag{1.8}$$

where a represents the cubic and D the tetragonal splitting, respectively, and ζ is parallel to the tetragonal axis. Because the spin hamiltonian has the point symmetry of the site on which the host atom is placed, EPR spectroscopy is a useful and very sensitive method for investigation of structural phase transitions.

Using Fe^{3+} EPR Unoki and Sakudo [22] for the first time clarified the nature of the 105 K phase transition in $SrTiO_3$ and concluded that the order parameter is the rotation angle ϕ of the antiferrodistortive rotation of the corner-sharing oxygen-octahedra. Its temperature dependence $\phi(T)$ was then determined by Müller et al. (Fig.1.6) also by EPR. In order to explain the observed behaviour Pytte and Feder worked out a microscopic mean-field theory which reproduced $\phi(T)$ very well in the temperature interval 38 K $< T <$ 105 K. For $T <$ 38 K, an additional weak reproducible increase of ϕ was observed (Fig.1.6), as

if at $T = 38$ K there were an onset of some *additional order parameter.* At the time of the observation, no explanation was known or given. Because the antiferrodistortive system has already undergone a phase transition at 105 K, one might think that the additional feature could be caused by coupling of the order parameter ϕ to some other degree of freedom, which has its proper phase transition at T_q. In other words, $\phi(T)$ would in this temperature interval act as a secondary order parameter. If such an assumption were true, then two questions would arise:

1) What might the primary order parameter be ? Is it structural, or of another nature ?

2) Are there possibly other secondary order parameters which exhibit an anomalous behaviour near T_q ?

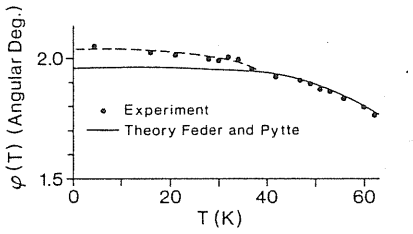

Figure 1.6: Antiferrodistortive rotation-angle measurements in $SrTiO_3$ for $H \parallel [100] - 32°$ in a (001) plane between 4.2 and 50 K at K-band. (After [11].)

Searching for an answer to these questions, a further EPR investigation of $SrTiO_3$ was performed as described in [11]. We shall briefly summarize the results of these measurements, referring for details to the original paper. Attention was concentrated on the temperature dependence of the spin hamiltonian parameters themselves and an anomalous behaviour of these was indeed observed both in the tetragonal and in the $\langle 111 \rangle$ pressure induced trigonal phase. First we describe the effect observed in the tetragonal phase. With the hamiltonian (1.8) and the external magnetic field $\vec{H}$ parallel to the $[11\bar{2}]$ pseudocubic direction, five microwave transitions with $|\Delta M_S| = 1$ are observed. For a tetragonal $\{001\}$ single domain, the distances between the two outer and the two inner spectral lines should

Phase	Parameter	
	δa	$\delta\|D\|$
Tetragonal	-1.0	-0.5
Trigonal	-0.9	-0.6

Table 1.1: *Approximate sizes of EPR parameter anomalies in* 10^{-4} cm^{-1} $=$ *1.068 Gauss* ($g = 2.0037$). *Accuracy* $\sim 20\%$. *(After [11].)*

be, in first order perturbation theory,

$$\Delta H_o^{tet} = \frac{5}{4}a + D \tag{1.9}$$

$$\text{and} \quad \Delta H_i^{tet} = a - 2D\,, \tag{1.10}$$

respectively. On Fig.1.7 both splittings are plotted as functions of temperature. We see that at $T_q \sim 37$ K, ΔH_o^{tet} shows a weak dip, while ΔH_i^{tet} does not show any anomaly. From the latter fact and from (1.10) we deduce that $\delta a = 2\,\delta D$ holds for the dip, and from (1.9) it is then possible to calculate the values of δa and δD. These are given in Tab.1.1 and we point to the fact that both a and D are *reduced* at $T = T_q$, while promptly recovering for $T < T_q$.

Investigation under applied $\langle 111 \rangle$ uniaxial stress revealed a similar transition, only more pronounced. The EPR spin hamiltonian in this case is also characterized by two splitting parameters, a and D_{trig}, which are both reduced in absolute value (Tab.1.1) at T_q, like in the tetragonal phase (Fig.1.7). Moreover, the pressure dependence of T_q was determined. It is plotted on Fig.1.8, on which the phase boundary between pseudotetragonal and trigonal phase is also shown. We see that as long as the sample remains in the pseudotetragonal phase, the temperature T_q is hardly pressure dependent at all. On the other hand, it is strongly pressure dependent in the trigonal phase, T_q decreasing with increasing pressure. Also, the anomaly occurs at about the same temperature on both sides of the tetragonal-trigonal phase boundary.

In both above mentioned cases, apart from the shift of the outer spectral lines, neither

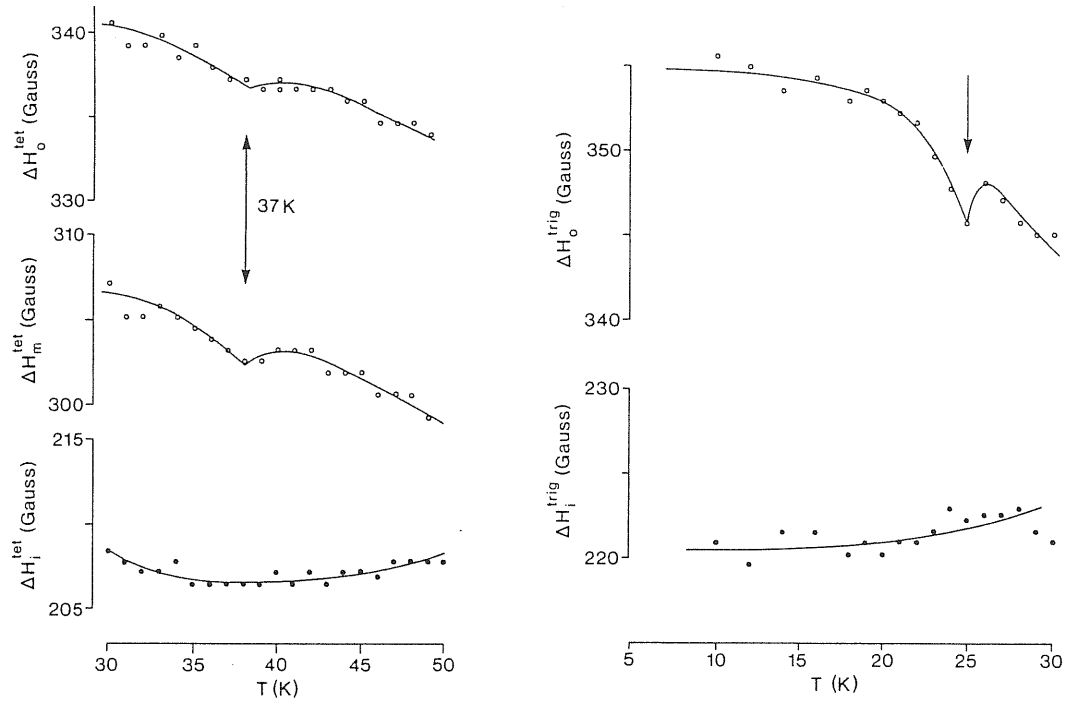

Figure 1.7: Left: Outer and inner Fe^{3+} fine-structure magnetic-field splittings with $\vec{H} \parallel [11\bar{2}]$ measured at a [111] stress of 1.97 kg/mm^2 in the $SrTiO_3$ tetragonal phase between 30 and 50 K due to the {001} domains. The middle splitting H_m^{tet} is due to {100} and {011} domains, which is not further discussed, but clearly shows the anomaly as well. Right: Outer $M = \pm 5/2 \leftrightarrow \pm 3/2$ and inner $M = \pm 3/2 \leftrightarrow \pm 1/2$ fine-structure magnetic resonance field differences with $\vec{H} \parallel [11\bar{2}]$ at a [111] stress of 31.4 kg/mm^2 in the trigonal phase. (After [11].)

their *number* nor *linewidth* change at T_q. This is a striking feature of the data because it assures that *the spatial symmetry of the lattice* (as seen by a Ti site) *does not change at* T_q. A change of the point symmetry of the Ti site (such as in a regular ferroelectric state) would be signaled by an additional splitting of the lines. Similarly, the onset of a static incommensurate or commensurate, spatial modulation would be accompanied by a characteristic line broadening due to the loss of translational symmetry in the direction of the modulation. EPR being perhaps the most sensitive local method to detect structural phase transitions in solids, both possibilities seem to be ruled out. A natural question thus

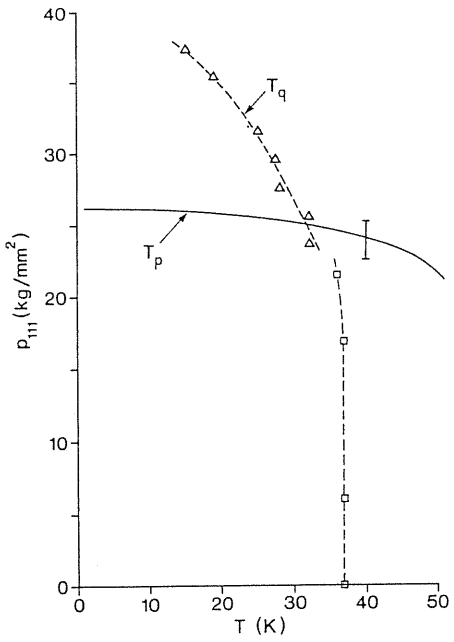

Figure 1.8: Phase diagram of [111] uniaxially p_{111} stressed $SrTiO_3$ as a function of temperature, showing the three-dimensional Potts line between the lower tetragonal and upper trigonal phases, and the dotted line T_q determined in both phases. (After [11].)

is: what does the dip at T_q reflect ? In [11], this point is discussed, considering various possibilities. To ensure that the effect in question is really an intrinsic property of the $SrTiO_3$ lattice, a possible local mode dynamics of the Fe^{3+} impurity has to be excluded first. EPR measurements of the Fe^{3+} ion in MgO, in which the oxygen environment of the probe ion is the same (octahedral) as in $SrTiO_3$, did not reveal any analogous phenomenon. Moreover, the sharpness of the dip clearly points to the collective nature of the effect. Because the concentration of Fe^{3+} ions in the sample was very low, it is highly improbable that these would be substantially involved in the effect, which therefore has to be attributed to the *host lattice itself.* As all the splittings a, D_{tet} and D_{trig} become smaller in absolute value at T_q, the effect mimics a full cubic widening of the lattice. However, there simply is no such static lattice expansion. Detailed X-ray studies [43] reveal instead

that ordinary thermal evolution of lattice parameters (contraction with cooling) abruptly terminates near T_q.

The shape of the EPR dip suggests that this might indeed be a manifestation of enhanced fluctuations at a phase transition. A suitable candidate for the fluctuating quantity which is sensed by the EPR parameters of the impurity ion could be the *local strain.* This idea is further supported by the observation that the additional feature below 38 K on the $\phi(T)$ curve corresponds to the relative increase of ϕ by about 5%, which is close to about 7% observed by Uwe and Sakudo [33] at the onset of *stress induced ferroelectricity.* On the other hand, T_q is very close to the extrapolated Curie-Weiss temperature of 37 K, where $SrTiO_3$ would become ferroelectric, were it not for quantum effects. We are thus led to an idea of a phase transition in which possibly the lattice strains and the ferroelectric mode are involved at the same time, even though we are not yet able to specify the actual primary order parameter.

We extract the following essential message from the experimental evidence reviewed so far:

1. There is a weak phase transition, or very sharp crossover, at $T_q \sim 37$ K in $SrTiO_3$, and although less studied, a presumably similar one at ~ 40 K in $KTaO_3$. It separates the ordinary paraelectric regime for $T > T_q$ from an incipient ferroelectric regime for $T < T_q$.
2. Below T_q, most Ti ions go off-center inside their own oxygen cage, and large oriented domains form. However, these domains fail to grow to critical size, hence no long-range ferroelectric order sets in. The domains can thus be seen as instantaneously forming a sort of incoherent mosaic, with dipoles pointing along the four $(\pm 100), (0 \pm 10)$ directions with equal probabilities.
3. The absence in $SrTiO_3$ of any sign of inhomogeneous broadening in EPR suggests that the domain mosaic is not static in nature, as one would expect e.g., for an incommensu-

rate state, or an impurity-driven disordered domain state. The domain boundaries must remain in motion, even at the lowest temperatures.

4. The persistence of dipole dynamics at $T = 0$ can only be explained as a quantum effect, and is expected qualitatively for a quantum melted ferroelectric state. However, quantum melting in $SrTiO_3$ is 'gentle', leaving large ordered domains and slow fluctuations. This picture is close to that of a classical ferroelectric in its 'central peak' state, close to criticality. Only, the slow central peak fluctuations appear to be of quantum nature in $SrTiO_3$ at low temperatures.

5. Many properties of the physical QPE state for $T < T_q$ are poorly understood, or not at all. Among them, anomalous phonon-like excitations are at present the most striking.

2 Models

2.1 Some aspects of the standard model for structural phase transitions

Microscopic models for classical ferroelectricity have been available for a long time [44]. Among them, very popular are soft-mode lattice-dynamical models [45], and ice models [46]. Ferroelectricity, in fact, represents just a particular case of a more general class of phenomena, that of *structural phase transitions.* An extensive and definitive review of critical phenomena related to classical structural transitions has been provided in Ref. [44]. Here are a few pertinent points.

A useful starting point for our considerations is a classical single mode hamiltonian, as it is usually employed for structural phase transitions [44]

$$H = \sum_l \frac{\vec{p}_l^2}{2M} + \sum_l V(\vec{q}_l) + \frac{C}{2} \sum_{\langle ll' \rangle} (\vec{q}_l - \vec{q}_{l'})^2 , \tag{2.1}$$

$$V(\vec{q}) = \frac{\bar{A}}{2}\vec{q}^2 + \frac{B}{4n}(\vec{q}^2)^2 , \tag{2.2}$$

which consists of a d-dimensional lattice of particles whose displacement is described by n-component vector $\vec{q}_l$. For $\bar{A} < 0, B > 0$, $V(\vec{q})$ has a 'double-well' structure, with minima at $\vec{q}^2 = n|\bar{A}|/B$ and a barrier of height $V = n\bar{A}^2/4B$. The particles are localized in the local double-well potential and are connected by nearest-neighbour harmonic springs. In the quantum case, $\vec{p}_l$ and $\vec{q}_l$ become operators satisfying the canonical commutation rules.

Both classical and quantum version of this model appear to exhibit at most two phases – the ferroelectric and the paraelectric [4]. If the parameters are such that the quantum fluctuations are strong enough to suppress the ferroelectric ordering even at $T = 0$, then this model *does not exhibit any phase transition* as a function of temperature. In other words, quantum paraelectricity *does not* set in with a phase transition. In order to allow for such possibility, a *richer model* is clearly needed. Before considering in detail various possibilities of enriching the above model, we would like to bring attention to those aspects which are related to the crossover from displacive to order/disorder regime, as these will be of particular importance for our model building.

Starting with a generic classical model (2.1), a structural transition problem will approach, depending on parameters, one of two opposite regimes: the *displacive* or the *order-disorder* regime. The criterion which distinguishes between the two regimes is the value of a parameter g, defined as the ratio of the local potential well depth (or barrier height) V to the thermal energy at the transition kT_c, $g = V/kT_c$.

In the displacive limit ($g \ll 1$), fluctuations are unimportant, whence the local distortion and the global order parameter can be identified. The structural order parameter is finite below the critical temperature T_c and zero above T_c. The appropriate description in this case is the standard soft-mode mean-field theory [44], based on continuous degrees of freedom.

In the opposite, order-disorder limit ($g \gg 1$), fluctuations dominate. The local distortion order parameter is generally large, fluctuating, and very different, as temperature grows, from the global order parameter. In particular, the former evolves smoothly with temperature, while the latter of course vanishes critically at T_c. If one further assumes that close to T_c the local distortions remain exactly constant as T varies, then the continuous degrees of freedom can be replaced without harm by a discrete variable.

For a general classical structural transition, it is well-known that close enough to T_c the critical behaviour for dimension $d < 4$ is fluctuation-dominated, at least in simple models with short-range forces. In other words, even a system whose behaviour is displacive well below and well above T_c, will undergo a crossover into an order-disorder regime, close enough to, and on both sides of, T_c. The critical temperature region is characterized by the appearance of fluctuating ordered domains of large size. Inside the domains the order parameter is large, and locally coherent. However, different domains are incoherent [47]. The order parameter dynamics shows in this regime none of the softening typical of the displacive limit. Critical dynamics is instead due to the slow, sluggish relaxation of the domain walls, leading to the famous "central peak" well known from Raman scattering [44].

In a ferroelectric, fluctuating domains give rise to a typical, very slow, Debye-like contribution to the low-frequency dielectric susceptibility, of the form $\Delta\epsilon(T)/(1+i\omega\tau(T))$. If the ferroelectric transition is continuous, both $\Delta\epsilon$ and τ diverge at T_c. The critical exponents of the real system are in the same universality class of a completely discrete model, provided the two have the same symmetry. A discrete model is therefore sufficient to capture the basic physics of the classical ferroelectric-paraelectric transition.

What about a quantum paraelectric ? At high enough temperature, the quantum perovskites $SrTiO_3$, $KTaO_3$, become just ordinary classical paraelectrics, well described by the displacive limit. This classical displacive behaviour is confirmed by IR and Raman spectra showing very well-defined TO modes, hard and narrow. These modes soften down upon cooling, as expected in the displacive picture [48]. However, just above the extrapolated classical Curie temperature T^* (37 K for $SrTiO_3$, 40 K for $KTaO_3$), the picture changes. In $SrTiO_3$, the enhanced anomalous hyper-Rayleigh scattering [42] indicates presence of local disorder, or off-center displacement of the ions, which locally breaks the

inversion symmetry. Various anomalies observed in the spectroscopy of soft and acoustic modes in $SrTiO_3$ point to the existence of large clusters, whose typical size is roughly equal to the reciprocal of the reduced wavevector for which the anomalies are most pronounced, i.e. $\xi^{-1} = 0.04^{-1} \sim 20$ lattice constants at very low T. In $KTaO_3$, NMR data of Rod, Borsa and van der Klink [49] clearly indicate that off-center displacement of Ta ions sets up rather abruptly below $T^* \sim 40$ K. In the microwave region, the slow Debye relaxations typical of the order-disorder regime appear in $KTaO_3$, their typical frequency τ^{-1} again decreasing with temperature [10]. These are the usual signals of crossover into the critical, order-disorder regime of ordinary classical paraelectrics. *This crossover therefore takes place also in the QPE perovskites.* Unlike the classical systems, however, in this case the critical slowing down, i.e. the divergence of τ with decreasing T, appears to be blocked at some *finite* relaxation time τ^*, which in $KTaO_3$ is very long, $(\tau^*)^{-1} <\sim 500$ MHz [10]. Because of this lack of divergence of τ, long-range ferroelectric order is never reached, and the system remains paraelectric even at the lowest temperatures. The failure to order ferroelectrically accompanied by these slow dielectric fluctuations has been attributed to quantum zero-point motion [1]. There is clear evidence showing that fluctuations can be easily removed, the system correspondingly turning into a regular ordered ferroelectric, by applying either pressure [33] or impurity doping [14]. We conclude that when approaching T^* from above, the QPE perovskites are well inside the order-disorder regime. A sort of quantum order-disorder regime appears moreover to persist all the way down to $T = 0$. Between T^* and $T = 0$, we have a sort of "quantum central peak" state – rather than completing its classical slowing down, and undergoing a regular ferroelectric critical point transition, the system hangs indefinitely on the verge of criticality, due to quantum fluctuations.

An important corollary of this discussion is that a discrete lattice model, which lends

itself better to a description of order-disorder critical fluctuations, is more likely to yield, probably even in the details, a better description of the QPE state, rather than a continuous, displacive model. On the other hand, a continuous model allows a good description of coupling to other degrees of freedom. In particular, such coupling allows, already in the classical case, for a well-known *precursor* to the ferroelectric phase transition – namely the onset of a *modulated incommensurate* phase. In the rest of this chapter we shall consider both kinds of models. In section 2.2, we first construct a Landau-Ginzburg-Wilson effective hamiltonian for $SrTiO_3$, including coupling of polarization to elastic strains. This will allow us to investigate the possibility of onset of an incommensurate phase. In section 2.3 we then discuss the main ingredients of an order-disorder description, basic element of which are discrete $Ti - O$ bond variables.

2.2 Landau-Ginzburg-Wilson continuous effective hamiltonian

In this section we shall construct a Landau-Ginzburg-Wilson effective continuous hamiltonian, designed to capture some of the displacive aspects of $SrTiO_3$ at low temperatures, related to the possibility of onset of an incommensurate (INC) phase, to be discussed in Chapter 3. We are guided by existing Landau expansion of the free energy of $SrTiO_3$ (no gradient terms). Several treatments can be found in the literature [50], [23], out of which the most complete one is that of Uwe and Sakudo [33]. They expanded the Helmholtz free energy density f as a function of polarization components P_i, octahedron rotation angles Φ_i and homogeneous lattice strains e_{ij}. Their expression for the free energy density associated with simultaneous onset of all three uniform order parameters in the otherwise cubic phase reads

$$f(P_i, \phi_i, e_{ij}) = f_0 \quad + \quad \frac{1}{2}\gamma_0 \sum_i P_i^2 + D^x (\sum_i P_i^2)^2 + \frac{1}{2} D_n^x \sum_{i \neq j} P_i^2 P_j^2$$

$$+ \quad \frac{1}{2}\kappa_0 \sum_i \Phi_i^2 + A^x(\sum_i \Phi_i^2)^2 + \frac{1}{2}A_n^x \sum_{i\neq j} \Phi_i^2\Phi_j^2$$

$$+\frac{1}{2}\sum_{ijkl} c_{ijkl}e_{ij}e_{kl} \quad - \quad \sum_{ijkl}(g_{ijkl}e_{ij}P_kP_l + b_{ijkl}e_{ij}\Phi_k\Phi_l + t^x_{ijkl}P_iP_j\Phi_k\Phi_l)\,, \qquad (2.3)$$

where the coefficients g_{ijkl} account for the electrostrictive coupling between the components of polarization and lattice strain and the last term corresponds to the 4-th order coupling between the components of the two distinct order parameters.

To proceed in practice, we must somehow simplify the above expression. Assuming the antiferrodistortive mode not to be primarily involved in the relevant physics at low temperatures, we shall not include the angles Φ_i in the expansion. This assumption is probably wrong near and at domain walls, where large local strains may act to rotate Φ_i, but it helps a great deal, and does not seem fatal at this very qualitative stage. We moreover assume that all the relevant physics takes place in the (001) plane, perpendicular to the tetragonal axis. This amounts to setting $P_3 = 0$ and keeping just the polarization components P_1 and P_2, as well as the strain tensor components e_{11}, e_{22} and e_{12}. To be consistent, we shall also allow all the continuum variables (or fields) to be spatially dependent only on the coordinates x_1 and x_2. Again, the large softening of the z-propagating TA mode found by Brillouin scattering speaks against this assumption for actual $SrTiO_3$, however, it is much simpler to deal with strictly 2D gradients.

Now we have to provide the terms containing the spatial gradients of the fields. In spite of the fact that we have two components P_1, P_2 of polarization, the effective hamiltonian *cannot contain* the Lifshitz invariant of the type $P_1\nabla P_2 - P_2\nabla P_1$ [51], because its presence is incompatible with the presence of the center of symmetry. We instead have a coupling between the lattice strains and the components of polarization of the general form

$$\sum_{ijkl} h_{ijkl}e_{ij}\frac{\partial P_k}{\partial x_l}\,, \qquad (2.4)$$

which is a generalization of the form adopted in [52]. The physics of this term is that

once polarization $\vec{P}$ changes as one moves in a given direction, the small but finite lattice deformation that accompanies polarization will also need to change, in a precisely correlated manner. In particular, the lattice will want to remain locally expanded along $\vec{P}$, and locally contracted normal to $\vec{P}$. Apart from this coupling, we must also add terms providing the dispersion of bare optical phonons, at least near $\vec{q} = 0$ (dispersion of acoustical phonons is usually negligible). We therefore introduce a squared gradient term of the form

$$\sum_{ijkl} s_{ijkl} \frac{\partial P_i}{\partial x_j} \frac{\partial P_k}{\partial x_l} . \tag{2.5}$$

In an INC phase the term (2.5) will become, after renormalization due to the coupling, negative for some direction in the (001) plane in the $\vec{k}$-space. To stabilize the dispersion for large $\vec{k}$ vectors we must therefore introduce another term quadratic in $\vec{P}$ and of higher order than 2 in $\vec{k}$. Due to the presence of the center of symmetry this must be of 4-th order in $\vec{k}$ and for simplicity we can take it isotropic like

$$r\,(\nabla^2 \vec{P})^2 . \tag{2.6}$$

The form of the 4-th rank tensors h_{ijkl} and s_{ijkl} is dictated by the point group of the symmetry of the crystal. With all the above approximations we can now recast the effective LGW hamiltonian of the system in the form

$$\begin{aligned}
H^{LGW} &= F_0 + \int f(P_i(\vec{r}), e_{ij}(\vec{r}))\, d^3\vec{r} \\
f &= \frac{1}{2}\alpha(P_1^2 + P_2^2) + \frac{1}{4}\beta_1(P_1^4 + P_2^4) + \frac{1}{2}\beta_2 P_1^2 P_2^2 + \\
&+ \frac{1}{2}c_{11}(e_{11}^2 + e_{22}^2) + c_{12}e_{11}e_{22} + 2c_{66}e_{12}^2 - \\
&- g_{11}(e_{11}P_1^2 + e_{22}P_2^2) - g_{12}(e_{11}P_2^2 + e_{22}P_1^2) - g_{66}e_{12}P_1P_2 + \\
&+ h_1(e_{11} + e_{22})\left(\frac{\partial P_1}{\partial x_1} + \frac{\partial P_2}{\partial x_2}\right) + h_2(e_{11} - e_{22})\left(\frac{\partial P_1}{\partial x_1} - \frac{\partial P_2}{\partial x_2}\right) + \\
&+ h_3 e_{12}\left(\frac{\partial P_1}{\partial x_2} + \frac{\partial P_2}{\partial x_1}\right) + s_1\left[\left(\frac{\partial P_1}{\partial x_1}\right)^2 + \left(\frac{\partial P_2}{\partial x_2}\right)^2\right] +
\end{aligned}$$

$$+ \quad s_2\left[\left(\frac{\partial P_1}{\partial x_2}\right)^2+\left(\frac{\partial P_2}{\partial x_1}\right)^2\right]+s_4\frac{\partial P_1}{\partial x_1}\frac{\partial P_2}{\partial x_2}+s_5\frac{\partial P_1}{\partial x_2}\frac{\partial P_2}{\partial x_1}+$$
$$+ \quad r(\nabla^2\vec{P})^2\,, \tag{2.7}$$

where some of the tensor components have been grouped together. As usual we may assume all the coefficients to be temperature independent except for α. However, since we are in the region in which the temperature dependence of this coefficient is determined by quantum effects, we shall not try to specify it more explicitly and just state that for $SrTiO_3$ under zero stress, $\alpha > 0$ for all $T > 0$.

In Chapter 3, we will show how (2.7) can lead to INC phases, which resolve competition between e and $\vec{P}$ order parameters. According to [53], the INC phase resulting from this kind of effective hamiltonian (without the Lifshitz invariant) is called *type II INC phase*. Having included only polarization components and lattice strains, the softening of a phonon branch leading finally to an onset of INC phase results from the mutual interaction of a polar optical and a non-polar acoustical mode. Actually, this idea was first expressed in 1970 by Axe et al [40]. They spoke about a "phase with sinusoidally modulated spontaneous displacements", which is just the INC phase. The idea was then subsequently formalized by Aslanyan and Levanyuk [52], [54], who considered it as a mechanism of formation of an INC structure in quartz, a type II case, because the order parameter has only one component.

2.3 Discrete lattice models

As discussed in the introduction, the paradigmatic *discrete* model for quantum paraelectricity with a scalar order parameter is the Ising model in transverse field (1.2) [3], [55], which was extensively studied in the 70's, using a variety of techniques [56]. Its relevance is particularly direct for the description of hydrogen-bonded ferroelectrics, like KH_2PO_4. The order parameters in $KTaO_3$ and $SrTiO_3$ are not exactly Ising-like, however. $KTaO_3$

remains cubic down to the lowest temperatures and the order parameter has thus three components. $SrTiO_3$, which acquires a tetragonal structure at low temperatures (below 105 K), can become ferroelectric when doped by Ca and the resulting ferroelectricity is known to be XY-like [14]. In pure $SrTiO_3$, in particular, if the tetragonal axis z is taken along (001), so that below 105 K two neighbouring TiO_3 octahedra rotate by an angle Φ and $-\Phi$ around z ($\langle\Phi\rangle \simeq 5°$ well below 105 K), then ferroelectricity shows a tendency to occur only along either $\pm(100)$ or $\pm(010)$, and more generally in the (001) XY-plane. In the ferroelectric state, the Ti central ion and one of the four coplanar oxygens which surround it in the XY-plane, establish between them a *slightly stronger* bond than the other three. Coupling between different cells is not exclusively dipole-dipole, but should have important electronic contributions (short-range), and elastic contributions (long-range). The elastic coupling mechanism, in particular, is likely to be very strong, as confirmed by the fact that even a small pressure along x is sufficient to yield ferroelectric order along y [33]. Physically, what we believe happens, is that a double-well situation for the central Ti ion (or equivalently for a bridging oxygen between two Ti ions), say along (100), can occur only if the lattice is *locally* expanded along that direction (spontaneously, or due to an external factor). Some of the consequences of coupling of ferroelectricity to elastic modes, leading in particular to incommensurability phenomena, and the possible role of quantum effects will be discussed in the next chapter.

In the present lattice modelling, we shall however ignore these details, and assume simply a short-range ferroelectric coupling J, between first neighbour cells. Each cell has an XY phase variable ϕ, representing the Ti displacement, or the dipole direction, subject to a cubic anisotropy, with minima at $\phi = 0, \pm\pi/2, \pi$. In the large anisotropy limit, a minimal lattice model of ferroelectricity in $SrTiO_3$ is therefore a 3D four-state clock model with first neighbour coupling. This leaves entirely out possible long-range effects

due to dipole-dipole coupling, and to coupling to elastic modes, as mentioned above, as well as additional coupling to the antiferrodistortive order parameter. In order to make quantitative progress, we choose to ignore all these complications for the time being, even though they will probably have to be reconsidered at a later stage.

By introducing at each site the complex variable

$$z_i = e^{i\phi_i} , \tag{2.8}$$

where ϕ_i can take the four values $0, \pm\pi/2, \pi$, the ordinary, classical four-state clock model can be written as

$$\begin{aligned} H^4 &= \sum_i H_i^4 \\ H_i^4 &= -\frac{J}{2}\sum_j \cos(\phi_i - \phi_j) = -\frac{J}{2}\mathrm{Re}(\sum_j z_i z_j^*) , \end{aligned} \tag{2.9}$$

where the sum over j runs over nearest neighbours of i.

It was shown by Suzuki [57] that the classical four-state clock model is mapped in full generality, i.e. independently both of dimensionality, and of range of interaction, onto two decoupled Ising models. Hence, everything is known about the classical behaviour of model (2.9).

However, we must now introduce quantum mechanical effects, in the form of a kinetic energy term, not commuting with the potential energy (2.9). In a perovskite ferroelectric, one can envisage at least two distinct quantum effects, both resulting in dipole tunneling.

The first is quantum hopping of the central positive ion (which will be called Ti, since it is Ti in $SrTiO_3$), from bonding preferentially one oxygen to bonding the next one, within the same cage, or cell (Fig.2.1). The kinetic energy for this is, in the continuous case

$$H^{kin\,1} = \frac{\mu\rho^2}{2}\sum_j \dot{\phi}_j^2 = \frac{1}{2\mu\rho^2}\sum_j \left(-i\hbar\frac{\partial}{\partial\phi_j}\right)^2 , \tag{2.10}$$

where μ and ρ are effective mass and off-center displacement (a very small quantity, of order of 0.03 $\mathring{A}$ [1]) of the Ti ion. In our discrete case, we shall allow the clock variable z_j to hop, for simplicity, into its two nearest orientations, i.e. from z_j into $\pm iz_j$. If we choose to describe the system with a wavefunction $\Psi(z_1, \ldots, z_n)$, the corresponding kinetic piece of hamiltonian reads

$$\begin{aligned} H^{kin\,1} &= \sum_j H_j^{kin\,1}\,, \qquad (2.11) \\ H_j^{kin\,1}\Psi(z_1, \ldots, z_j, \ldots, z_n) &= -t(\Psi(z_1, \ldots, iz_j, \ldots, z_n) + \Psi(z_1, \ldots, -iz_j, \ldots, z_n))\,. \end{aligned}$$

In the last expression, the hopping energy has further been lumped into the constant $t = \frac{\hbar^2}{2\mu\rho^2}$. This term is an obvious generalization of the "transverse field" term in the Ising case. If strong enough, it will cause the dipole in each cell to hop quantum mechanically from one value of ϕ_i to the other, irrespective of the state of dipoles in neighbouring cells, thereby destroying ferroelectric long-range order.

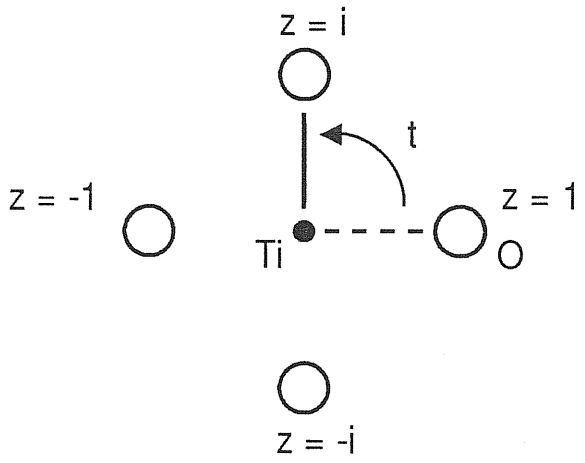

Figure 2.1: Intra-cage bond hopping, corresponding to kinetic energy $H^{kin\,1}$ (2.12).

A second type of quantum effects, which has apparently not been discussed so far, is *oxygen double-well tunneling.* When an oxygen is bonded to a given Ti ion, we can

imagine another energy minimum, more or less equivalent, when that oxygen is bonded to the other Ti ion on the opposite side (Fig.2.2). Quantum hopping processes of the oxygen between these two sites (similar to proton hopping in hydrogen bonds) may play a role in quantum paraelectrics, both because of a relatively small displacement involved, and of the small oxygen mass. However, these processes cause the bond to hop from one cage to the next and therefore, unlike the intra-cage hopping t, they do not obey the (apparently sensible) requirement that the number of bonds per cage should not exceed one. An adequate prescription is thus necessary to include the oxygen tunneling into our scheme.

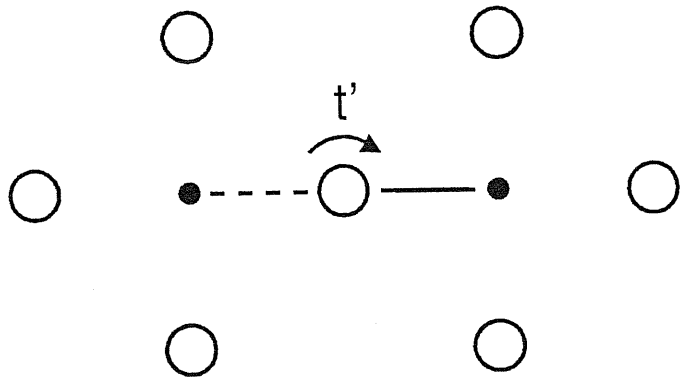

Figure 2.2: Inter-cage bond hopping, due to oxygen tunneling, corresponding to kinetic energy $H^{kin\,2a}$ (2.12), and $H^{kin\,2b}$ (2.13).

We have considered so far two possible implementations of oxygen tunneling. The first is one where we force each cage to retain *one and only one dipole bond* in any given configuration. This is probably close to what happens at very low temperatures. The second is a different scheme, where we introduce the possibility of "bond vacancies", while still forbidding double bond occupancy of any cage. We discuss both schemes in this order.

If each cage is constrained to retain strictly one and only one bond at any given time,

bond hopping becomes extremely problematic. For each bond which hops, a suitable "bond backflow" loop is mandatory, so as to obey the one-bond-per-cage constraint everywhere. In other words, only *concerted rearrangements*, such as ring-shaped currents of bonds, are permitted. The simplest concerted bond hopping loop is shown in Fig.2.3. The associated kinetic energy is a one-body operator, which for a horizontal link $\langle i, j = i + \vec{x} \rangle$ can be symbolically written as

$$H_{ij}^{kin\,2a} = -t' \left(| \leftarrow_j \rangle \langle \rightarrow_i | + | \rightarrow_i \rangle \langle \leftarrow_j | \right) , \tag{2.12}$$

and analogously for a vertical link. In process (2.12), concerted ring bond hopping takes place on the elementary plaquette only. Also, it is ineffective if the initial state is a fully aligned ferroelectric. More general concerted processes should also be interesting, and do not necessarily have this limitation. However, we do not wish to go into this discussion at this stage.

The second possibility we envisage, having particularly in mind the situation at not too low temperatures, is one where we still forbid multiple bond occupancy of a cage, but we allow for the possibility of *bond vacancies*, i.e. cages where the Ti ion is centrally located, or else it moves out of plane, so that it has no in-plane dipole bond at all. The justification for this comes from the necessity to include at temperatures close to T^* and higher, elements which link the present discrete model with the displacive picture, eventually applicable when $T \gg T^*$. At these very high temperatures, the likeliest Ti ion location is indeed the cage center, and there are physically no more bonds to speak of. Introduction of some bond vacancies even at lower temperatures allows for a new bond hopping process, where a vacancy on one cage and a bond on a neighbouring cage can exchange positions. The link oxygen between two cages can "resonate" between two adjacent Ti ions, both of which are free from other bonds. The corresponding piece of

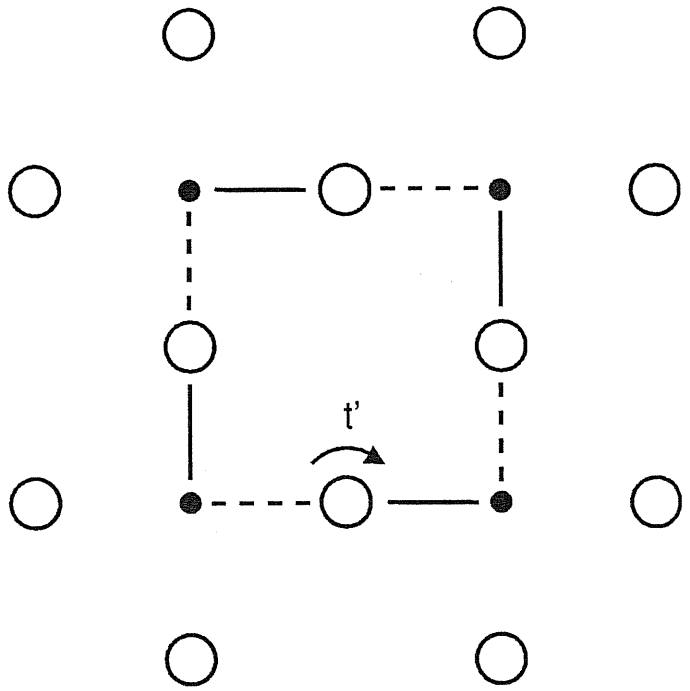

Figure 2.3: The simplest concerted bond hopping mechanism, taking place on the elementary plaquette.

hamiltonian reads symbolically, again for a horizontal link

$$H_{ij}^{kin\,2b} = -t^{'}\,(|\rightarrow_i, \circ_j\rangle\langle\circ_i, \leftarrow_j| + \text{h.c.})\ , \tag{2.13}$$

and analogously for a vertical link, where $\circ_i$ denotes a vacancy on site i. Through processes (2.13), vacancies and bonds become mobile, and the possibility of condensates may arise at sufficiently low temperatures.

Besides potential and kinetic energies, we have also found that the problem of ferroelectricity (both classical and quantum) in a perovskite requires a third, novel ingredient. That ingredient is an anholonomic *constraint*, which in hamiltonian terms can be mimicked by some *infinite* repulsion, or attraction. The physical constraint we consider is that

no oxygen should be bound (i.e. form a dipole) simultaneously to both Ti atoms on the two sides of the link where it belongs. In other words, while a Ti atom has always at most one bond, similarly an O atom can have either zero or one bond, but not two: the configuration of Fig.2.4 is physically meaningless, and should not occur. The constraint can also be included as a hamiltonian term, in the following way. First we introduce for each link an operator

$$P'_{ij} = \delta(z_i - r_{ij})\delta(z_j + r_{ij}) \,, \tag{2.14}$$

which acts as a projector on the forbidden states. In this expression, $r_{ij} = r_j - r_i$, where r_i is the complex number defining the 2D position of site i. The hamiltonian term equivalent to the constraint then reads

$$H^{constr} = \lim_{U \to \infty} U \sum_{\langle ij \rangle} P'_{ij} \,. \tag{2.15}$$

Enforcement of this constraint is analogous to an "ice rule", and has also apparently never been considered before for the perovskites, or any displacive ferroelectric. It is likely to yield nontrivial modifications in the physics. At the classical level, for example, we expect a dramatic reduction of entropy due to the decreased number of available configurations, and a possible change of the critical point universality class. Related effects are expected in the quantum paraelectric problem, which is of direct interest to us.

Finally, we have to choose dimensionality. While the physical system is of course in 3D, we see no major harm in restricting our study to a 2D square lattice of cages. This amounts to treating, so to speak, a single TiO_2 plane, ignoring interplanar coupling. This seems a particularly plausible approximation in the case of $SrTiO_3$, where ferroelectric $Ti - O$ bonds are strictly planar, and do not involve the interplanar bridging oxygens. However, similar reservations to those mentioned in Section 2.2 remain valid in this case, and should not be forgotten, when thinking of real $SrTiO_3$.

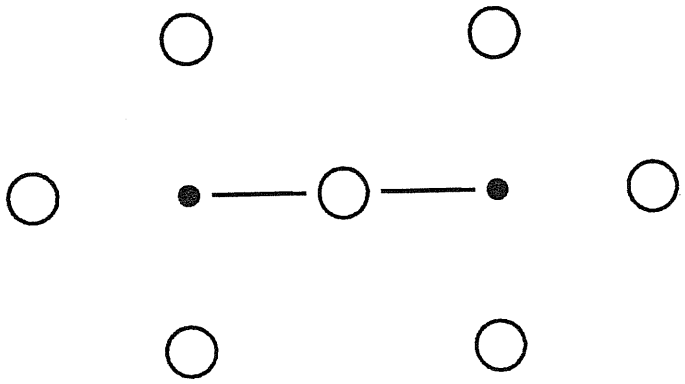

Figure 2.4: Forbidden configuration, with two bonds sharing the same bridging oxygen.

3 The displacive limit model: possibility of a modulated (incommensurate) phase

In this chapter we shall investigate the possibility of the onset of a static incommensurate modulated phase in a hypothetically classical $SrTiO_3$. The reasons for wanting to pursue this kind of phase are many. First of all, the INC state is a regular mosaic of domains of size k_0^{-1} and no net global ferroelectric order parameter. Secondly, any model for displacive ferroelectricity which includes – as it is necessary – the centro-symmetric ferroelastic coupling (2.4) will inevitably run into an INC instability, which pre-empts the actual ferroelectric phase. Third, weak phonon anomalies at $k_0 \simeq (2\pi/a)\xi$ discussed in Chapter 1 are reminiscent of the k_0-phonon softening signaling the onset of an INC phase.

Our starting point will be the LGW hamiltonian (2.7) introduced in section 2.2 of the last chapter. This represents a local free energy expansion, which is not just function of components of the ferro-order parameter and the acoustic displacements, but depends also on their spatial derivatives. The global free energy of the system therefore becomes a functional of spatially dependent components of the order parameter. The equilibrium configuration for given values of temperature and external parameters can then be found as a solution of a variational problem.

3.1 Loss of stability of the high-temperature phase

First we introduce the spatial Fourier transforms of the fields

$$P_i(\vec{r}) = \sum_{\vec{k}} P_{i\vec{k}} \exp(i\vec{k}.\vec{r}) \tag{3.1}$$

$$u_i(\vec{r}) = \sum_{\vec{k}} u_{i\vec{k}} \exp(i\vec{k}.\vec{r}) \tag{3.2}$$

$$e_{ij}(\vec{r}) = \epsilon_{ij} + \frac{i}{2} \sum_{\vec{k}\neq 0} (k_i u_{j\vec{k}} + k_j u_{i\vec{k}}) \exp(i\vec{k}.\vec{r}), \quad i,j = 1,2 \quad , \tag{3.3}$$

where we expressed the lattice strains $e_{ij}(\vec{r})$ through the acoustic displacements $\vec{u}(\vec{r})$ and separated the contribution of homogeneous strains ϵ_{ij}. Substituting these relations into (2.7) we obtain a free energy expansion

$$F = F_0 + V \sum_{\vec{k}} f_{\vec{k}} \tag{3.4}$$

$$\begin{aligned}
f_{\vec{k}} &= \frac{1}{2}\alpha(|P_{1\vec{k}}|^2 + |P_{2\vec{k}}^2|) + \\
&+ \frac{1}{4}\beta_1 \sum_{\vec{k}'\vec{k}''\vec{k}'''} (P_{1\vec{k}} P_{1\vec{k}'} P_{1\vec{k}''} P_{1\vec{k}'''} + P_{2\vec{k}} P_{2\vec{k}'} P_{2\vec{k}''} P_{2\vec{k}'''}) \, \delta(\vec{k} + \vec{k}' + \vec{k}'' + \vec{k}''') + \\
&+ \frac{1}{2}\beta_2 \sum_{\vec{k}'\vec{k}''\vec{k}'''} P_{1\vec{k}} P_{1\vec{k}'} P_{2\vec{k}''} P_{2\vec{k}'''} \, \delta(\vec{k} + \vec{k}' + \vec{k}'' + \vec{k}''') + \\
&+ \frac{1}{2}c_{11}(\epsilon_{11}^2 + \epsilon_{22}^2) + c_{12}\epsilon_{11}\epsilon_{22} + 2c_{66}\epsilon_{12}^2 + \frac{1}{2}c_{11}(k_1^2|u_{1\vec{k}}|^2 + k_2^2|u_{2\vec{k}}|^2) + \\
&+ c_{12}k_1k_2 u_{1\vec{k}} u_{2\vec{k}}^* + \frac{1}{2}c_{66}(k_1^2|u_{2\vec{k}}|^2 + k_2^2|u_{1\vec{k}}|^2 + 2k_1k_2 u_{1\vec{k}} u_{2\vec{k}}^*) - \\
&- g_{11}\left(\epsilon_{11}|P_{1\vec{k}}|^2 + \epsilon_{22}|P_{2\vec{k}}|^2\right) - g_{12}\left(\epsilon_{11}|P_{2\vec{k}}|^2 + \epsilon_{22}|P_{1\vec{k}}|^2\right) - g_{66}\epsilon_{12} P_{1\vec{k}} P_{2\vec{k}}^* - \\
&- g_{11} i \sum_{\vec{k}'\vec{k}''} (k_1 u_{1\vec{k}} P_{1\vec{k}'} P_{1\vec{k}''} + k_2 u_{2\vec{k}} P_{2\vec{k}'} P_{2\vec{k}''}) \, \delta(\vec{k} + \vec{k}' + \vec{k}'') - \\
&- g_{12} i \sum_{\vec{k}'\vec{k}''} (k_1 u_{1\vec{k}} P_{2\vec{k}'} P_{2\vec{k}''} + k_2 u_{2\vec{k}} P_{1\vec{k}'} P_{1\vec{k}''}) \, \delta(\vec{k} + \vec{k}' + \vec{k}'') - \\
&- g_{66}\frac{i}{2} \sum_{\vec{k}'\vec{k}''} (k_1 u_{2\vec{k}} + k_2 u_{1\vec{k}}) P_{1\vec{k}'} P_{2\vec{k}''} \, \delta(\vec{k} + \vec{k}' + \vec{k}'') + \\
&+ h_1(k_1 u_{1\vec{k}} + k_2 u_{2\vec{k}})(k_1 P_{1\vec{k}}^* + k_2 P_{2\vec{k}}^*) + h_2(k_1 u_{1\vec{k}} - k_2 u_{2\vec{k}})(k_1 P_{1\vec{k}}^* - k_2 P_{2\vec{k}}^*) + \\
&+ \frac{h_3}{2}(k_1 u_{2\vec{k}} + k_2 u_{1\vec{k}})(k_2 P_{1\vec{k}}^* + k_1 P_{2\vec{k}}^*) + s_1(k_1^2|P_{1\vec{k}}|^2 + k_2^2|P_{2\vec{k}}|^2) +
\end{aligned}$$

$$+ \quad s_2(k_2^2|P_{1\vec{k}}|^2 + k_1^2|P_{2\vec{k}}|^2) + (s_4+s_5)k_1k_2P_{1\vec{k}}P^*_{2\vec{k}} + rk^4(|P_{1\vec{k}}|^2 + |P^2_{2\vec{k}}|) \; . \qquad (3.5)$$

Now we can investigate the stability of the homogeneous commensurate phase with respect to the formation of an INC modulated phase. For this purpose we need to consider only the quasiharmonic part of the free energy as a function of $P_{1\vec{k}}, P_{2\vec{k}}, u_{1\vec{k}}, u_{2\vec{k}}$, since we are dealing with infinitesimal order parameters. This reads

$$\begin{aligned}
f'_{\vec{k}} &= \frac{1}{2}\alpha(|P_{1\vec{k}}|^2 + |P_{2\vec{k}}|^2) + \frac{1}{2}c_{11}(k_1^2|u_{1\vec{k}}|^2 + k_2^2|u_{2\vec{k}}|^2) + \\
&+ c_{12}k_1k_2u_{1\vec{k}}u^*_{2\vec{k}} + \frac{1}{2}c_{66}(k_1^2|u_{2\vec{k}}|^2 + k_2^2|u_{1\vec{k}}|^2 + 2k_1k_2u_{1\vec{k}}u^*_{2\vec{k}}) + \\
&+ \gamma_1(k_1^2u_{1\vec{k}}P^*_{1\vec{k}} + k_2^2u_{2\vec{k}}P^*_{2\vec{k}}) + \gamma_2k_1k_2(u_{1\vec{k}}P^*_{2\vec{k}} + u_{2\vec{k}}P^*_{1\vec{k}}) + \\
&+ \gamma_3\left[k_1k_2(u_{2\vec{k}}P^*_{1\vec{k}} + u_{1\vec{k}}P^*_{2\vec{k}}) + k_1^2u_{2\vec{k}}P^*_{2\vec{k}} + k_2^2u_{1\vec{k}}P^*_{1\vec{k}}\right] + \\
&+ s_1(k_1^2|P_{1\vec{k}}|^2 + k_2^2|P_{2\vec{k}}|^2) + s_2(k_2^2|P_{1\vec{k}}|^2 + k_1^2|P_{2\vec{k}}|^2) + \\
&+ s_3k_1k_2P_{1\vec{k}}P^*_{2\vec{k}} + rk^4(|P_{1\vec{k}}|^2 + |P_{2\vec{k}}|^2) \quad , \qquad (3.6)
\end{aligned}$$

where we denoted $\gamma_1 = h_1 + h_2$, $\gamma_2 = h_1 - h_2$, $\gamma_3 = h_3/2$, $s_3 = s_4 + s_5$.

It is convenient now to introduce longitudinal and transverse coordinates of P_1, P_2, u_1, u_2 through the relations

$$\begin{aligned}
u_{l\vec{k}} &= u_{1\vec{k}}\cos(\vartheta) + u_{2\vec{k}}\sin(\vartheta) \\
u_{t\vec{k}} &= -u_{1\vec{k}}\sin(\vartheta) + u_{2\vec{k}}\cos(\vartheta) \quad , \qquad (3.7)
\end{aligned}$$

and similarly for $P_{l\vec{k}}$, $P_{t\vec{k}}$. The angle ϑ is the angle between the wavevector $\vec{k}$ and the x-axis. If the system were isotropic in the plane, then these rotated coordinates would be just the eigenvectors of bare longitudinal and transverse phonons. Substituting to (3.6) we get

$$\begin{aligned}
f'_{\vec{k}} &= (\frac{1}{2}\alpha + rk^4)(|P_{l\vec{k}}|^2 + |P_{t\vec{k}}|^2) + \\
&+ \left[\frac{1}{2}(c_1 - c_0\cos 4\vartheta)|u_{l\vec{k}}|^2 + \frac{1}{2}(c_2 + c_0\cos 4\vartheta)|u_{t\vec{k}}|^2 \; + \right.
\end{aligned}$$

$$
\begin{aligned}
&+ \frac{1}{4}(\gamma + \gamma_0 \cos 4\vartheta) u_{l\vec{k}} P^*_{l\vec{k}} + \frac{1}{4}(\gamma' - \gamma_0 \cos 4\vartheta) u_{t\vec{k}} P^*_{t\vec{k}} + \\
&+ \frac{1}{4}(s + s_0 \cos 4\vartheta)|P_{l\vec{k}}|^2 + \frac{1}{4}(s' - s_0 \cos 4\vartheta)|P_{t\vec{k}}|^2 + \\
&+ \sin 4\vartheta \left(c_0 u^*_{l\vec{k}} u_{t\vec{k}} - \frac{1}{4}\gamma_0 (u_{l\vec{k}} P^*_{t\vec{k}} + u_{t\vec{k}} P^*_{l\vec{k}}) - \frac{1}{2} s_0 P_{l\vec{k}} P^*_{t\vec{k}} \right) \Big] k^2 ,
\end{aligned}
\tag{3.8}
$$

where we have introduced the following new coefficients

$$
\begin{array}{lll}
c_0 = -\frac{1}{4}(2c_{66} - c_{11} + c_{12}) , & s_0 = s_1 - s_2 - \frac{1}{2}s_3 , & \gamma_0 = \gamma_1 - \gamma_2 - 2\gamma_3 , \\
c_1 = c_{11} - c_0 , & s = 3s_1 + s_2 + \frac{1}{2}s_3 , & \gamma = 3\gamma_1 + \gamma_2 + 2\gamma_3 , \\
c_2 = \frac{1}{2}(c_{11} - c_{12}) - c_0 , & s' = s_1 + 3s_2 - \frac{1}{2}s_3 & \gamma' = \gamma_1 - \gamma_2 + 2\gamma_3 .
\end{array}
\tag{3.9}
$$

Before proceeding, we have to comment on the longitudinal component $P_{l\vec{k}}$ of the polarization. Our effective hamiltonian (2.7) does not take into account the coupling of the polarization to the macroscopic electric field resulting from the longitudinal part of the optical displacement and therefore does not lead to the splitting between TO and LO phonon frequencies at $k = 0$. Phenomenologically, we could introduce a splitting just replacing by hand the stiffness α in (3.8) by another stiffness α_l corresponding to $P_{l\vec{k}}$. However, at low temperatures we expect the lowest LO phonon frequency to be several times larger than that of the soft TO phonon. Therefore α_l should be considerably larger than α, which means that the longitudinal component $P_{l\vec{k}}$ is hard, and effectively decoupled from the problem. We shall thus use the free energy in the above form and from now on set simply $P_{l\vec{k}} = 0$.

The stability of the homogeneous commensurate phase will be lost if the frequency of one of the branches becomes equal to zero for a wavevector $k \neq 0$. We shall investigate a general situation, not restricting ourselves to wavevectors along any particular direction. Searching for temperature and wavevector at which the frequency of some branch for the first time goes to zero is equivalent to solving the set of equations

$$
\frac{\partial f'_{\vec{k}}}{\partial u^*_{i\vec{k}}} = 0 \tag{3.10}
$$

$$
\frac{\partial f'_{\vec{k}}}{\partial P^*_{j\vec{k}}} = 0 . \tag{3.11}
$$

In other words, it is equivalent to minimizing the free energy with respect to all variables and searching for the $\vec{k}$-point, where this minimum for the first time corresponds to their non-zero values.

Substituting for the elastic constants c_{11}, c_{12}, c_{44} their experimental values for $SrTiO_3$ (taken from [33] and converted to SI units these are $c_{11} = 3.36 \times 10^{11}$, $c_{12} = 1.07 \times 10^{11}$, $c_{44} = 1.27 \times 10^{11}$ Jm^{-3}) we obtain $c_0 = 0.06 \times 10^{11}$, $c_1 = 3.42 \times 10^{11}$, $c_2 = 1.20 \times 10^{11}$ Jm^{-3}. Because $c_0 \ll c_1, c_2$, we can clearly neglect the term which is off diagonal in acoustic displacements in (3.8) (because the elastic properties in the plane are only very slightly anisotropic) and write

$$\begin{aligned} \frac{\partial f'_{\vec{k}}}{\partial u^*_{l\vec{k}}} &= k^2 c_1 u_{l\vec{k}} - \frac{1}{4} k^2 \gamma_0 \sin 4\vartheta P_{t\vec{k}} = 0 \\ \frac{\partial f'_{\vec{k}}}{\partial u^*_{t\vec{k}}} &= k^2 c_2 u_{t\vec{k}} + \frac{1}{4} k^2 (\gamma' - \gamma_0 \cos 4\vartheta) P_{t\vec{k}} = 0 \ . \end{aligned} \tag{3.12}$$

Substituting for $u_{l\vec{k}}, u_{l\vec{k}}$ from these equations to (3.8) we get the free energy $f'_{\vec{k}}$ as a function of $P_{t\vec{k}}$ only

$$\begin{aligned} f'_{\vec{k}} &= \frac{1}{2} \alpha' |P_{t\vec{k}}|^2 \ , \\ \alpha' &= \alpha + \left(\frac{1}{2}(s' - s_0 \cos 4\vartheta) - \frac{1}{16 c_1} \gamma_0^2 \sin^2 4\vartheta - \frac{1}{16 c_2} (\gamma' - \gamma_0 \cos 4\vartheta)^2 \right) k^2 + r k^4 \ . \end{aligned} \tag{3.13}$$

The instability occurs when the expression denoted as α' becomes equal to zero. Therefore we search for its minimum as a function of both ϑ and k. We obtain

$$\sin 4\vartheta \left[s_0 - \frac{1}{4c_1} \gamma_0^2 \cos 4\vartheta - \frac{\gamma_0}{4c_2} (\gamma' - \gamma_0 \cos 4\vartheta) \right] = 0 \ . \tag{3.14}$$

We see that we have a symmetry-determined extremum if $\sin 4\vartheta = 0$ or an accidental extremum if the expression in the square brackets is equal to zero. We shall consider only symmetry determined extrema which occur for $\vartheta = 0$ or $\vartheta = \pi/4$ and equivalent directions. The condition for these extrema to be actual minima is

$$s_0 - \frac{1}{4c_1} \gamma_0^2 - \frac{\gamma_0 (\gamma' - \gamma_0)}{4c_2} > 0 \tag{3.15}$$

when $\vartheta = 0$ and

$$s_0 + \frac{1}{4c_1}\gamma_0^2 - \frac{\gamma_0(\gamma' + \gamma_0)}{4c_2} < 0 \tag{3.16}$$

when $\vartheta = \pi/4$.

Now we investigate the behaviour with respect to k for both cases above. For $\vartheta = 0$ ($\vec{k} \parallel x$, i.e. along (100)) we get

$$f'_{\vec{k}} = \left[\frac{1}{2}\alpha + \left(\frac{1}{4}(s' - s_0) - \frac{1}{32c_2}(\gamma' - \gamma_0)^2\right)k^2 + rk^4\right]|P_{t\vec{k}}|^2 \tag{3.17}$$

for the free energy. In order to have a minimum as a function of k, the coefficient of k^2 in this equation must be negative. This implies

$$(\gamma' - \gamma_0)^2 > 8c_2(s' - s_0) \tag{3.18}$$

as the *necessary* condition for onset of an INC phase. Provided it is satisfied the minimum of (3.17) occurs for a wavevector k_0 which is determined by

$$k_0 = \sqrt{\frac{1}{2r}\left[\frac{1}{32c_2}(\gamma' - \gamma_0)^2 - \frac{1}{4}(s' - s_0)\right]}. \tag{3.19}$$

An INC phase with the modulation wavevector k_0 sets on at a temperature T_I obeying the condition

$$\alpha(T_I) = \frac{1}{2r}\left[\frac{1}{32c_2}(\gamma' - \gamma_0)^2 - \frac{1}{4}(s' - s_0)\right]^2 \quad . \tag{3.20}$$

For $\vartheta = \pi/4$ ($\vec{k}$ along (110)) the equations (3.18), (3.19) and (3.20) are replaced respectively by

$$(\gamma' + \gamma_0)^2 > 8c_2(s' + s_0) \quad , \tag{3.21}$$

$$k_0 = \sqrt{\frac{1}{2r}\left[\frac{1}{32c_2}(\gamma' + \gamma_0)^2 - \frac{1}{4}(s' + s_0)\right]} \tag{3.22}$$

and

$$\alpha(T_I) = \frac{1}{2r}\left[\frac{1}{32c_2}(\gamma' + \gamma_0)^2 - \frac{1}{4}(s' + s_0)\right]^2 \quad . \tag{3.23}$$

3.2 The INC phase and its properties

Now we can turn to the investigation of the properties of the INC phase. Due to the tetragonal symmetry, in both cases analyzed, $\vartheta = 0$ and $\vartheta = \pi/4$, we may have either one modulation direction corresponding to freezing of 2 vectors of the star of $\vec{k_0}$ or 2 mutually perpendicular modulation directions in case when all 4 vectors of the star of $\vec{k_0}$ get frozen. In order to determine which of these possibilities is actually realized it is necessary to go beyond the quasiharmonic part of the free energy, by taking into account the higher order terms of (2.7).

Since the effective hamiltonian (2.7) is a functional of the polarization and displacement fields, the INC pattern corresponding to equilibrium is found as a solution of Euler-Lagrange equations resulting from (2.7). We do not have any particular boundary conditions imposed on the fields and therefore the appropriate solution is the one corresponding to the absolute minimum of the functional. This means that we should find the general solution of Euler-Lagrange equations containing integration constants and then perform an additional minimization with respect to all of these. Such approach would not be an easy one because we would have to solve a system of nonlinear *partial differential* equations. We shall adopt a different approach instead. We assume that the equilibrium solution is a *periodically* modulated phase with the wavevector k which is for the moment unknown. Then it is convenient to make use of the free energy expressed as a function of the Fourier components of the fields (3.5) because the only non-zero components would be those corresponding to the harmonics of the basic wavevector k. Minimizing with respect to those we obtain a system of nonlinear *algebraic* equations which in principle could be easily solved by a numerical iteration procedure.

To write these equations, it is useful to return to the original cartesian components of the vectors in terms of which the free energy (3.5) is expressed. The equilibrium condition

for $P_{1\vec{k}}$ reads

$$\begin{aligned}
\frac{\partial F}{\partial P^*_{1\vec{k}}} &= (\alpha - 2g_{11}\epsilon_{11} - 2g_{12}\epsilon_{22} + 2s_1k_1^2 + 2s_2k_2^2 + 2rk^4)P_{1\vec{k}} + \\
&+ (-g_{66}\epsilon_{12} + (s_4+s_5)k_1k_2)P_{2\vec{k}} + \\
&+ ((h_1+h_2)k_1^2 + \frac{h_3}{2}k_2^2)u_{1\vec{k}} + (h_1 - h_2 + \frac{1}{2}h_3)k_1k_2u_{2\vec{k}} \\
&+ \beta_1 \sum_{\vec{k}'\vec{k}''\vec{k}'''} P_{1\vec{k}'}P_{1\vec{k}''}P_{1\vec{k}'''}\,\delta(\vec{k}-\vec{k}'-\vec{k}''-\vec{k}''') + \\
&+ \beta_2 \sum_{\vec{k}'\vec{k}''\vec{k}'''} P_{1\vec{k}'}P_{2\vec{k}''}P_{2\vec{k}'''}\,\delta(\vec{k}-\vec{k}'-\vec{k}''-\vec{k}''') - \\
&- 2g_{11}i \sum_{\vec{k}'\vec{k}''} k_1' u_{1\vec{k}'}P_{1\vec{k}''}\,\delta(\vec{k}-\vec{k}'-\vec{k}'') - \\
&- 2g_{12}i \sum_{\vec{k}'\vec{k}''} k_2' u_{2\vec{k}'}P_{1\vec{k}''}\,\delta(\vec{k}-\vec{k}'-\vec{k}'') - \\
&- \frac{1}{2}g_{66}i \sum_{\vec{k}'\vec{k}''} (k_1'u_{2\vec{k}'} + k_2'u_{1\vec{k}'})P_{2\vec{k}''}\,\delta(\vec{k}-\vec{k}'-\vec{k}'') = 0\ , \qquad (3.24)
\end{aligned}$$

and differentiating with respect to $P^*_{2\vec{k}}$ we obtain an analogous equation. Equilibrium conditions for the acoustic displacements read

$$\begin{aligned}
\frac{\partial F}{\partial u^*_{1\vec{k}}} &= ((h_1+h_2)k_1^2 + \frac{h_3}{2}k_2^2)P_{1\vec{k}} + (h_1 - h_2 + \frac{1}{2}h_3)k_1k_2P_{2\vec{k}} + \\
&+ (c_{11}k_1^2 + c_{66}k_2^2)u_{1\vec{k}} + (c_{12}+c_{66})k_1k_2u_{1\vec{k}} + \\
&- ig_{11}k_1 \sum_{\vec{k}'\vec{k}''} P_{1\vec{k}'}P_{1\vec{k}''}\,\delta(\vec{k}-\vec{k}'-\vec{k}'') - ig_{12}k_2 \sum_{\vec{k}'\vec{k}''} P_{2\vec{k}'}P_{2\vec{k}''}\,\delta(\vec{k}-\vec{k}'-\vec{k}'') - \\
&- \frac{1}{2}g_{66}ik_2 \sum_{\vec{k}'\vec{k}''} P_{1\vec{k}'}P_{2\vec{k}''}\,\delta(\vec{k}-\vec{k}'-\vec{k}'') = 0 \qquad (3.25)
\end{aligned}$$

and an analogous equation for the derivative with respect to $u^*_{2\vec{k}}$.

The free energy depends also on the homogeneous strains $\epsilon_{11}, \epsilon_{22}$ and ϵ_{12}. Determining the equilibrium conditions with respect to those and solving for the strain components we obtain

$$\epsilon_{11} = a\sum_{\vec{k}} |P_{1\vec{k}}|^2 + b\sum_{\vec{k}} |P_{2\vec{k}}|^2$$

$$\begin{aligned} \epsilon_{22} &= a\sum_{\vec{k}}|P_{2\vec{k}}|^2 + b\sum_{\vec{k}}|P_{1\vec{k}}|^2 \\ \epsilon_{12} &= c\sum_{\vec{k}}P_{1\vec{k}}P^*_{2\vec{k}}\ , \end{aligned} \tag{3.26}$$

where we denoted $$a = \frac{c_{11}g_{11} - c_{12}g_{12}}{c_{11}^2 - c_{12}^2}\ ,\quad b = \frac{c_{11}g_{12} - c_{12}g_{11}}{c_{11}^2 - c_{12}^2}\ ,\quad c = \frac{g_{66}}{4c_{66}}\ . \tag{3.27}$$

We see that it is impossible to fulfill this system with the basic harmonic only, because the bilinear terms originating from the electrostrictive coupling and 3^{rd} order terms originating from the quartic terms in the free energy generate respectively the 2^{nd} and the 3^{rd} harmonic. However, it is actually possible to avoid the numerical iteration procedure, as Michelson has first shown [58]. The general conclusion is that in case when the free energy does not contain the Lifshitz invariant and contains rather a term of 4^{th} order in k, the amplitudes of the higher harmonics in the equilibrium solution are *small* and therefore the INC phase remains practically sinusoidally modulated down to the temperature of the lock-in transition. We shall therefore investigate just the part of the free energy which is projected out from (3.5) by the single plane wave ansatz, consisting in including in the solution just the basic harmonic with the wavevector k_0 found in the last section.

First we analyze the case when the loss of stability occurs for $\vartheta = 0$, i.e. for direction [100]. If only a single modulation direction $\vec{k} = (k_0, 0)$ is present, the only non-zero Fourier components of the polarization will be the *transverse* components $P_{2,\pm\vec{k}}$ which without loss of generality can be considered as real. We notice that the 3^{rd} order electrostrictive terms in (3.5) give zero contribution, because they consist of products of an odd number of basic harmonics. This implies that the equilibrium values of the acoustic displacements are equal to those found in the last section considering just the quasiharmonic part of the free energy. The value of this for the equilibrium acoustic displacements is therefore given by (3.13). To obtain the total free energy we must add to that the contribution of the terms of 4^{th} order in polarization components and also the elastic and electrostrictive

terms containing just the *homogeneous* strains. For those we substitute the equilibrium values (3.26). Writing $P_{2,\pm\vec{k}} = p$ and substituting to (3.26) and (3.5) we recast the total free energy as a function of p (we set the volume $V = 1$)

$$\begin{aligned} F &= F_0 + \alpha' p^2 + \left(\frac{3}{2}\beta_1 + d\right) p^4 \quad , \\ \text{where} \quad d &= 2c_{11}(a^2 + b^2) + 4c_{12}ab - 4g_{11}a - 4g_{12}b \ . \end{aligned} \tag{3.28}$$

The equilibrium value of p is given by

$$p_{eq} = \sqrt{\frac{-\alpha'}{3\beta_1 + 2d}} \tag{3.29}$$

and the *total equilibrium* free energy is

$$F_{eq} = F_0 - \frac{\alpha'^2}{6\beta_1 + 4d} \ . \tag{3.30}$$

If we assume that two mutually perpendicular modulation directions $\vec{k}_1 = (k_0, 0)$, $\vec{k}_2 = (0, k_0)$ are present in the system, we can proceed along the same lines in order to calculate the corresponding equilibrium free energy and compare it with (3.30). The non-zero Fourier components of polarization are now the 4 transverse components $P_{1,\pm\vec{k}_2}$, $P_{2,\pm\vec{k}_1}$ which can again be taken to be real. Writing $P_{1,\pm\vec{k}_2} = P_{2,\pm\vec{k}_1} = p$ we obtain

$$\begin{aligned} F &= F_0 + 2\alpha' p^2 + (3\beta_1 + 2\beta_2 + d')p^4 \quad , \\ \text{where} \quad d' &= 4(c_{11} + c_{12})(a + b)^2 - 8(g_{11} + g_{12})(a + b) \ . \end{aligned} \tag{3.31}$$

The equilibrium polarization and free energy are then, respectively,

$$p_{eq} = \sqrt{\frac{-\alpha'}{3\beta_1 + 2\beta_2 + d'}} \quad , \tag{3.32}$$

$$F_{eq} = F_0 - \frac{\alpha'^2}{3\beta_1 + 2\beta_2 + d'} \ . \tag{3.33}$$

Actually we do not know the coefficients of the gradient terms in the effective hamiltonian (2.7). However, equations (3.30) and (3.33) allow us to decide *within the single plane*

wave ansatz which of the two possible modulation patterns yields the lower free energy knowing only 4^{th} order terms coefficients β_1, β_2, elastic constants and electrostrictive couplings. The latter are known from [33] to be (converted to SI units) $g_{11} = 1.33 \times 10^{10}$, $g_{12} = 3.24 \times 10^9$, $g_{44} = 2.43 \times 10^9$ JmC^{-2}. The clamped values of $\alpha(T)$, β_1, β_2 (which are the appropriate ones for our free energy expansion) can be found in [23] and for $T = 40$ K they read (in SI units) $\alpha = 15.5 \times 10^6$ JmC^{-2}, $\beta_1 = \beta_2 = 0.9 \times 10^{10}$ Jm^{5}C^{-4}. According to (3.30) and (3.33) the condition to be satisfied in order that the two simultaneous modulation directions pattern be the one with lower energy is

$$3\beta_1 - 2\beta_2 > 4\frac{(g_{11} - g_{12})^2}{c_{11} - c_{12}} . \tag{3.34}$$

For the above values of parameters we obtain 9×10^9 for the left hand side and 1.75×10^9 for the right hand side, which means that the condition is well satisfied. *We can therefore conclude that if the loss of stability really occurs along the [100] direction, then the single plane wave ansatz predicts the INC phase to be simultaneously modulated in 2 mutually perpendicular directions.*

Proceeding along the same lines we investigate the case when the stability is lost for $\vartheta = \pi/4$, i.e. along [110] and equivalent directions. We just quote the result for this case. The condition equivalent to (3.34) is

$$10\beta_2 - 6\beta_1 > 2\frac{g_{66}^2}{c_{66}} , \tag{3.35}$$

which for $SrTiO_3$ yields $1.8 \times 10^{10} > 4.65 \times 10^7$ and obviously is well satisfied. The phase with lower free energy is again modulated in two directions.

It is interesting to inspect visually these modulation patterns. We have plotted in particular the [100] ($\vartheta = 0$) case (Fig.3.1). Dipoles are arranged in a kind of *"flux phase"*, with regions of positive and negative "vorticity" alternating along the [100] and equivalent directions. Because the vector field is a superposition of frozen *transverse* optical phonons,

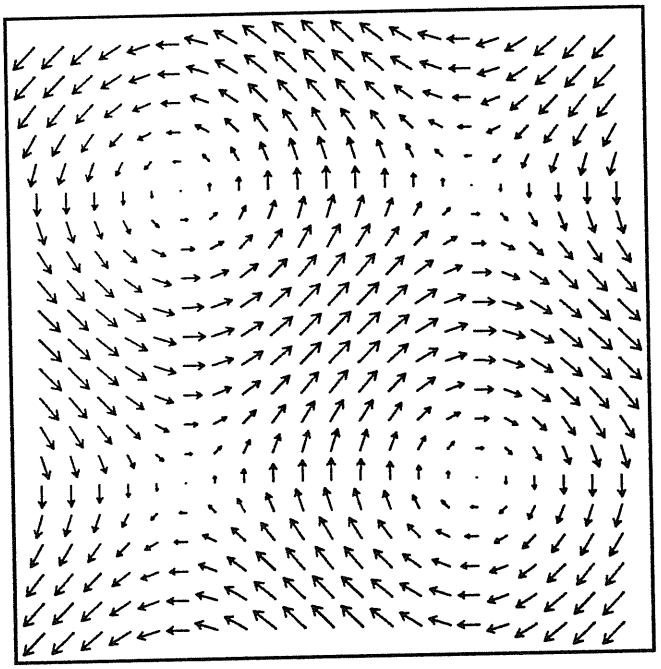

Figure 3.1: The pattern of the polarization in the INC phase with two perpendicular modulation directions.

its divergence is zero which implies zero polarization charge density. The INC modulated phase is also accompanied by non-zero modulated lattice strains. Because the longitudinal component of the acoustic displacement is decoupled and equal to zero, the pattern of this field is the same as that of polarization, as follows from (3.12), possibly differing in sign (determined by the sign of $\gamma' - \gamma_0$). From the equations (3.26) we see that the *homogeneous* strain has no shear component $\epsilon_{12} = 0$, while the normal components $\epsilon_{11}, \epsilon_{22}$ are non-zero and positive, which means that the crystal expands. On the other hand, due to transversality of the frozen phonons involved, the normal components of the *non-homogeneous* strain (3.3) are zero *within the single plane wave ansatz*, while the shear component is non-zero and is plotted on Fig.3.2.

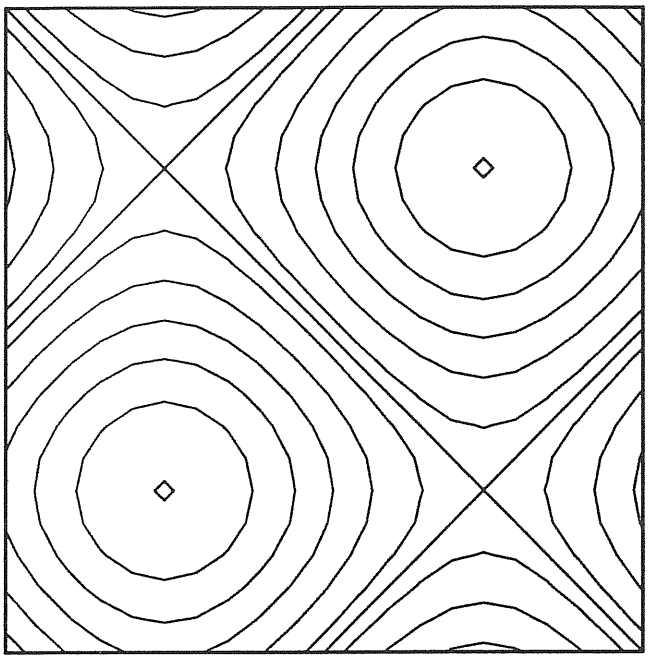

Figure 3.2: The contour plot of the shear strain component e_{12}.

3.3 Quantum mechanics: a new quantum paraelectric state ?

The theory we developed so far in this chapter is classical and refers to an INC distorted phase, which, based on entirely classical reasoning, a displacive model of $SrTiO_3$ might want to take at low temperatures. On the other hand, in the introduction we discussed features of EPR data (lack of inhomogeneous broadening), which are definitely against such possibility. A simple narrow EPR line might be compatible with dynamically fluctuating domains, but certainly not with a static INC state as in Fig.3.1. How is it possible to justify the dynamical picture, and what properties it might be expected to have ?

In this section we shall briefly sketch a possible way to answer these questions. It is known that in case when a Lifshitz invariant present in the effective hamiltonian gives rise to an INC phase [51], the phase degree of freedom of the doubly degenerate order parameter

is governed by the sine-Gordon equation. Adding to the classical effective hamiltonian a corresponding kinetic energy term and introducing non-commuting operators for the phase and its conjugate momentum, one obtains a quantum effective hamiltonian. In the 1D case there are exact results for the quantum sine-Gordon problem due to Haldane [59]. For however small quantum zero fluctuations - i.e. for any finite mass, the ground state is liquid-like, while classically we obtain a static soliton lattice. Such a liquid-like phase can be considered as an incommensurate phase which is quantum melted already at zero temperature by zero-point fluctuations, and suggests, that something similar may be actually going on in our case.

The quantum effective hamiltonian for our model reads

$$H_{qu}^{LGW} = \int \left[\frac{1}{2} m_u \sum_i \dot{u}_i^2(\vec{r}) + \frac{1}{2} m_P \sum_i \dot{P}_i^2(\vec{r}) \right] d^3\vec{r} + H^{LGW} , \tag{3.36}$$

and represents a classical Φ^4 field. The quantum analogue of this is a quantum Φ^4 field theory. *Restricting ourselves to zero temperature*, we may try to assign to the ground state of the system a variational wave function. We may consider for example an approximate ("Jastrow") state of the form

$$\Psi \propto e^{-(\gamma/2) H^{LGW}[\vec{P}(\vec{r}),\vec{u}(\vec{r})]} , \tag{3.37}$$

where $\Psi^2[\vec{P}(\vec{r}), \vec{u}(\vec{r})]$ determines the relative probability of different field configurations, and γ plays a role of a variational parameter. Because this function is formally a functional of the fields $\vec{P}(\vec{r}), \vec{u}(\vec{r})$, it is dependent on an infinite number of some generalized coordinates and therefore still practically intractable. If we were now able to identify which field configurations are the most "important" ones, and introduce for these some suitable coordinates, it would be possible to simplify (3.37) to a more familiar form. In any case, having a wave function for the system, it is *in principle* possible to calculate the average value of any measurable quantity, provided we know the corresponding operator.

This can always be expressed as a function of the coordinates $\vec{r}_{Lj}$ and momenta $\vec{p}_{Lj}$ of the atoms of the crystal, which in turn can be expressed in terms of the amplitudes of the eigenvectors of the lattice dynamical problem. We recall at this point that the meaning of the variables $\vec{P}(\vec{r}), \vec{u}(\vec{r})$ is that of amplitudes of the corresponding TO and TA zone-center mode eigenvectors. Therefore the wave function (3.37) can actually be used to determine the zero-temperature average values of the quantities of experimental interest, and particularly of those measured in EPR experiments, like $\langle \delta\phi \rangle$, $\langle a \rangle$ and $\langle D \rangle$.

The very basic advantage which trial functions like (3.37) have, is that the corresponding probability distributions are identical, by construction, to those of a *classical* system with hamiltonian $H^{LGW}[\vec{P}(\vec{r}), \vec{u}(\vec{r})]$ at temperature $T = 1/k_B\gamma$. Hence, based on our understanding of classical systems, or on classical simulations, etc., we may hope to learn about the physics of the purely quantum system which (3.37) is supposed to approximate.

Classically, an INC phase is necessarily "floating" in 2D – it can only have power law quasi-long-range order due to divergent thermal fluctuations. However, in 3D it will be ordered and stable, apart from a drift of periodicity, up to some critical temperature T_c. Above T_c, the INC lattice disappears, and $\{\vec{P}(\vec{r})\}, \{\vec{u}(\vec{r})\}$ configurations become disordered, or chaotic.

In the previous work [60], it was speculated that the singularity points of the crystalline INC phase – which form a square lattice in Fig.3.1 – might still survive in the disordered state, forming a *fluid* of singularities. In that case, the wavefunction (3.37) would, for $\gamma < 1/k_B T_c$, represent a new kind of quantum fluid – a superfluid of singularities. Although this seems an interesting route to pursue, it has not been possible so far to do so, and this line will not be discussed further at this stage, leaving it for future work.

4 Discrete lattice models

This chapter is devoted to study of discrete lattice models, whose main ingredients were discussed in Chapter 2. Gradually adding these ingredients, one at a time, we obtain in turn a series of three models of increasing complexity, with correspondingly richer behaviour. In the first two sections, we shall heavily rely on a Path Integral Monte Carlo simulation technique. Details of this type of calculation are provided in the Appendix A. In the last section, we shall use a particular sampling algorithm for a Variational Monte Carlo technique, which is described in detail in Appendix C. In the same section, we shall also refer to some ideas related to quantum crystals contained in [18], which are for convenience briefly summarized in Appendix B.

4.1 Plain Quantum Four-State Clock model

In this section we shall consider the simplest of the models, which is defined by the hamiltonian

$$H = H^4 + H^{kin\,1} = \sum_j (H_j^4 + H_j^{kin\,1}) \,, \tag{4.1}$$

where

$$H_j^4 = -\frac{J}{2} \sum_i \cos(\phi_j - \phi_i) = -\frac{J}{2} \mathrm{Re}(\sum_i z_j z_i^*) \tag{4.2}$$

is the classical four-state clock model, and

$$H_j^{kin\,1} \Psi(z_1, \ldots, z_j, \ldots, z_n) = -t(\Psi(z_1, \ldots, iz_j, \ldots, z_n) + \Psi(z_1, \ldots, -iz_j, \ldots, z_n)) \tag{4.3}$$

is the kinetic energy due to hopping of dipole in cell j from one value to another, as discussed in Section 2.3.

4.1.1 Equivalence of the model to two decoupled Ising models in a transverse field

The model (4.1) can be mapped on two decoupled Ising models in a transverse field, regardless of dimensionality. In order to construct the mapping, it is convenient to start from the ϕ_i representation.

We represent the clock variable ϕ_i on each site by two discrete variables, s_i and σ_i, defined respectively by

$$\begin{aligned} s_i &= \sqrt{2}\cos(\phi_i + \frac{\pi}{4}) \\ \sigma_i &= \sqrt{2}\sin(\phi_i + \frac{\pi}{4}) \,. \end{aligned} \tag{4.4}$$

It is easily seen that $s_i, \sigma_i = \pm 1$, and thus the new variables can be regarded as Ising variables. The potential energy term can be immediately written as

$$H_i^4 = -\frac{J}{2}\sum_j \cos(\phi_i - \phi_j) = -\frac{\frac{1}{2}J}{2}\sum_j (s_i s_j + \sigma_i \sigma_j) \,, \tag{4.5}$$

which is just Suzuki's classical decoupling [57].

The kinetic energy term can be written as

$$\begin{aligned} &H_i^{kin\,1}\Psi(s_1,\sigma_1;\ldots;s_i,\sigma_i;\ldots;s_n,\sigma_n) = H_i^{kin\,1}\Psi(\phi_1,\ldots,\phi_i,\ldots,\phi_n) = \\ &-t\left(\Psi(\phi_1,\ldots,\phi_i - \frac{\pi}{2},\ldots,\phi_n) + \Psi(\phi_1,\ldots,\phi_i + \frac{\pi}{2},\ldots,\phi_n)\right) = \\ &-t\left(\Psi(s_1,\sigma_1;\ldots;\sigma_i,-s_i;\ldots;s_n,\sigma_n) + \Psi(s_1,\sigma_1;\ldots;-\sigma_i,s_i;\ldots;s_n,\sigma_n)\right) \,. \end{aligned} \tag{4.6}$$

Because $s_i, \sigma_i = \pm 1$, we have always $s_i = \pm\sigma_i$, and the last expression can thus be rewritten as

$$\begin{aligned} &H_i^{kin\,1}\Psi(s_1,\sigma_1;\ldots;s_i,\sigma_i;\ldots;s_n,\sigma_n) = \\ &-t\left(\Psi(s_1,\sigma_1;\ldots;-s_i,\sigma_i;\ldots;s_n,\sigma_n) + \Psi(s_1,\sigma_1;\ldots;s_i,-\sigma_i;\ldots;s_n,\sigma_n)\right) \,. \end{aligned} \tag{4.7}$$

We see that the Ising variables s_i, σ_i are decoupled both in H_i^4 and in $H_i^{kin\,1}$, and the latter term corresponds to the well-known transverse field. The quantum four-state clock model is thus equivalent to two *decoupled* Ising models in a transverse field equal to the original hopping parameter t, and with a new coupling constant $J/2$.

The Ising model in a transverse field was intensively studied in the 70's. An exact solution for 1D case can be found in [56]. Discussions of higher dimensionalities are given in several places [61, 62, 63]. Quantum Monte Carlo renormalization group study of 1D and 2D case is available in [64]. In 2D at $T = 0$, there is a continuous quantum phase transition at J_q/t between a ferroelectric state and a QPE state. The critical point extends into a line at finite temperature, where a characteristic pattern of quantum-classical crossover is realized [6].

4.1.2 Test of the PIMC scheme on the plain quantum four-state clock model

In order to test the QMC scheme described in the Appendix A, we chose to perform a simulation of a limited extent for the simple unconstrained model, which is equivalent to the quantum Ising model, as discussed in the last subsection. In this subsection we briefly describe the results, since they will also be of interest for comparison with those obtained for the constrained model in the next section.

From the Monte Carlo renormalization group study of Kolb [64] it is known that the limiting value of the ratio t/J for the existence of an ordered state in 2D Ising model in transverse field is $\simeq 3.04$. Using the mapping from the last subsection then results in a limiting value of $J_q^0/t \simeq 0.66$ for our model.

As an initial test, we did a numerical diagonalization of a 2×2 system with $J = 0.5$, and compared the exact canonical results for internal energy and specific heat with those of a PIMC simulation. In order to obtain a good statistical accuracy, we used 1×10^6

MCsteps/site for the simulation, and found excellent agreement (Fig.4.1).

Next, we carried out simulations for three different values of $J = 0.5, 0.75, 1.0$. Each of these three values of J is expected to correspond to a different regime of the system. The results can be described as follows.

We start with $J = 1.0$, where we expect the system to approach the classical behaviour. It should therefore exhibit onset of ferroelectricity with a fully developed critical behaviour of the 2D Ising universality class, which ought to be visible already for the relatively small system sizes studied here. The results of the simulation performed for lattice sizes $L = 6, 10, 20$ are plotted on Fig.4.2. We see that the zero temperature value of the order parameter $|P|$ is about 0.85, only moderately depressed from its classical value by quantum fluctuations. The transition is signaled by a drop of the order parameter as well as by pronounced critical peaks of both the dielectric susceptibility and the specific heat. The susceptibility peak appears at a slightly higher temperature than the specific heat peak, and is also considerably more size dependent. All these results are perfectly compatible with a 2D Ising transition. In order to extrapolate the infinite-size critical temperature we have analyzed our data using the phenomenological renormalization method [65], which treats properly the large finite-size corrections (especially evident for the specific heat peak position). The results of this analysis are given on Fig.4.3 and Fig.4.4. In the case of susceptibility, Fig.4.3, the three curves are near intersection in the vicinity of the point $(1., 1.75)$, which suggests the critical temperature $T_c = 1.0$ and the 2D Ising value of $\frac{7}{4}$ for the ratio of critical exponents $\frac{\gamma}{\nu}$. The same analysis for the specific heat, Fig.4.4, however, suggests instead a higher critical temperature close to $T_c = 1.2$. We consider this discrepancy to be a consequence of small system sizes used as well as of the statistical errors in the results. In any case, a critical temperature $T_c \sim 1.0$ is rather close to its classical value $T_c = 1.1346\ldots$, which further confirms the conclusion that the system for

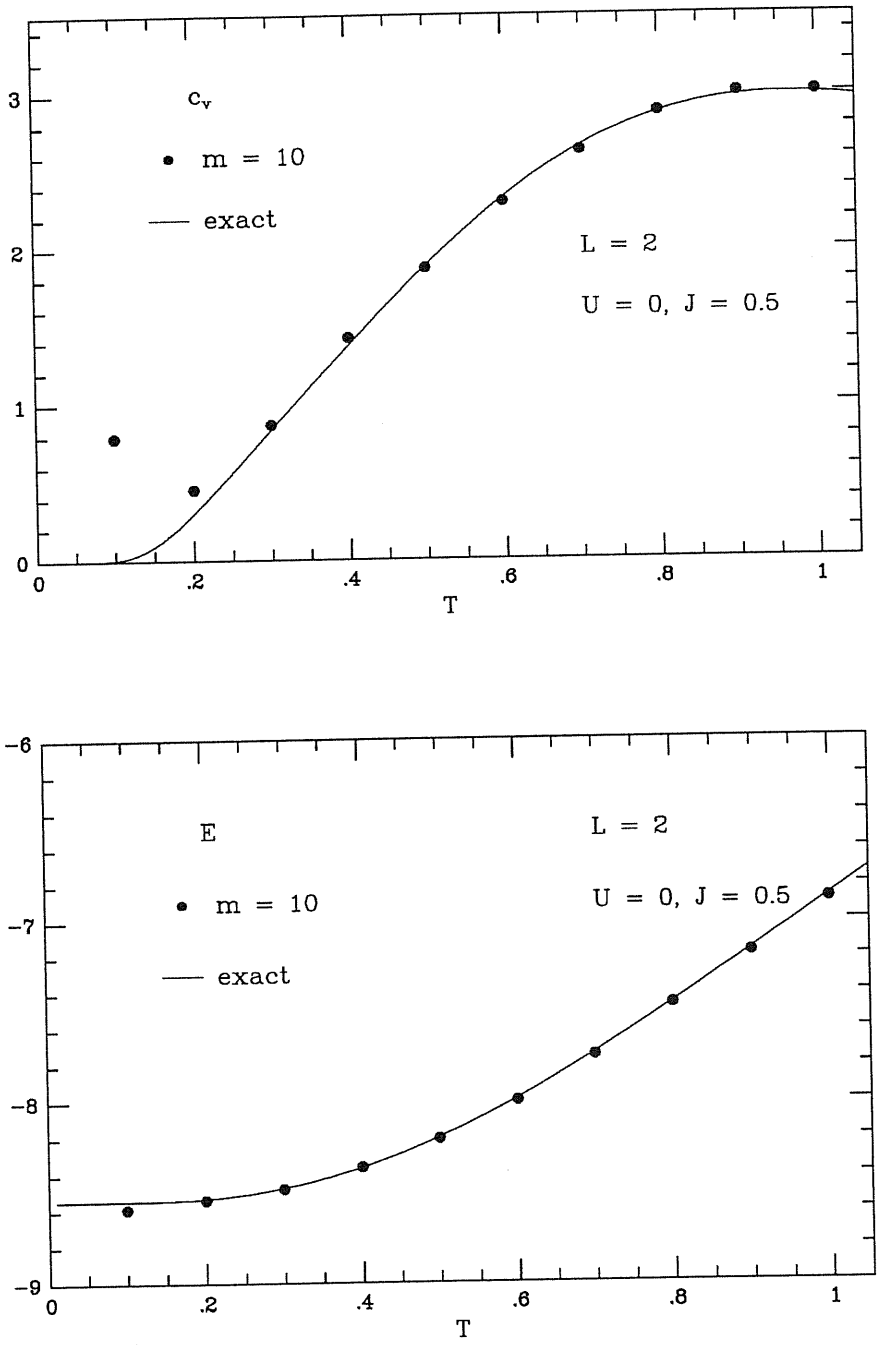

Figure 4.1: Test of the PIMC method: specific heat c_v, and internal energy E for a 2×2 unconstrained system with $J = 0.5$, as obtained from the simulation, to be compared with the exact result obtained from the diagonalization.

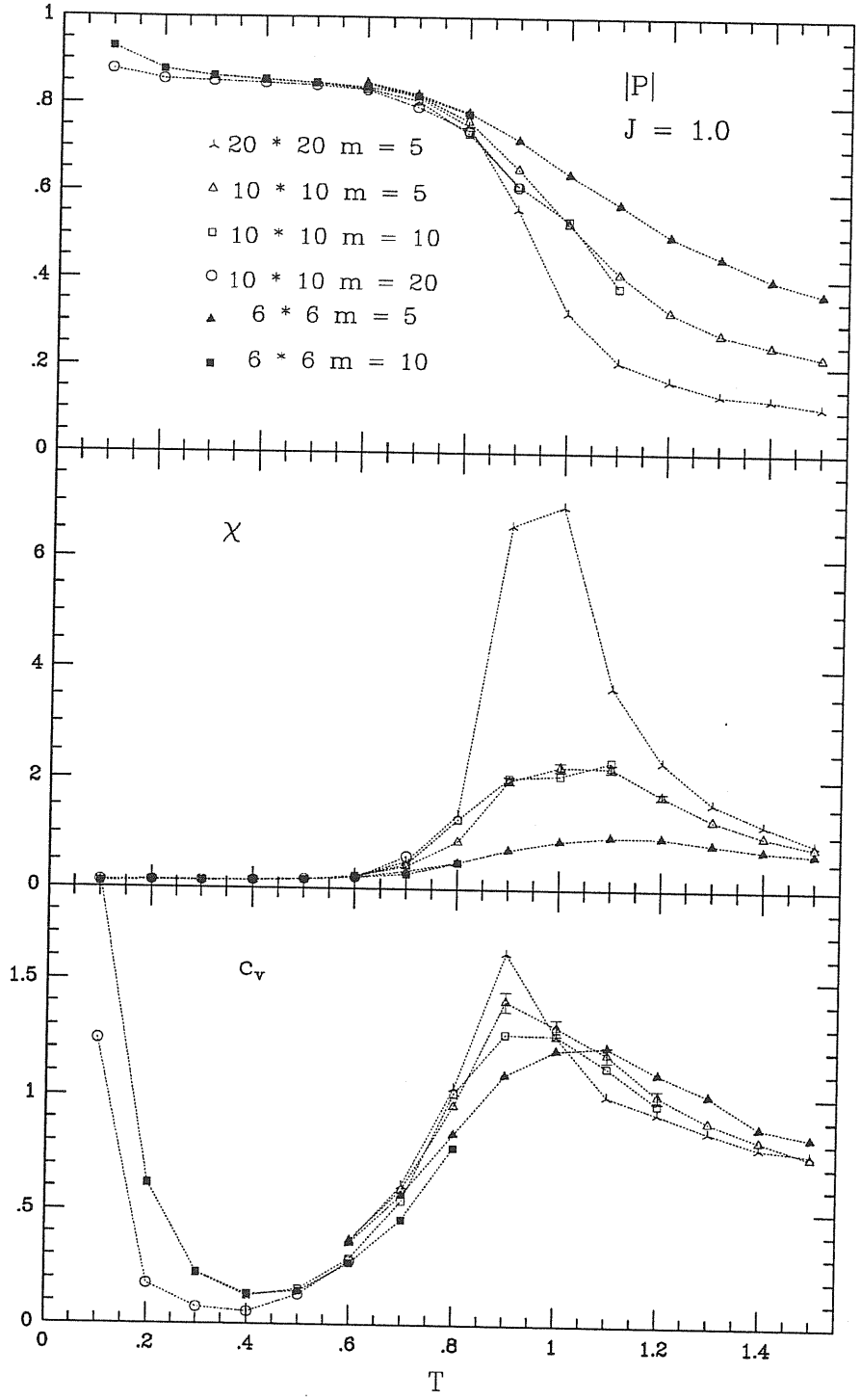

Figure 4.2: Unconstrained polarization $|P|$, dielectric susceptibility χ, and specific heat c_v for $J = 1.$, $U = 0$. Note the classical ferro-para transition near $T_c \sim 1$.

$J = 1.0$ is in a classical regime.

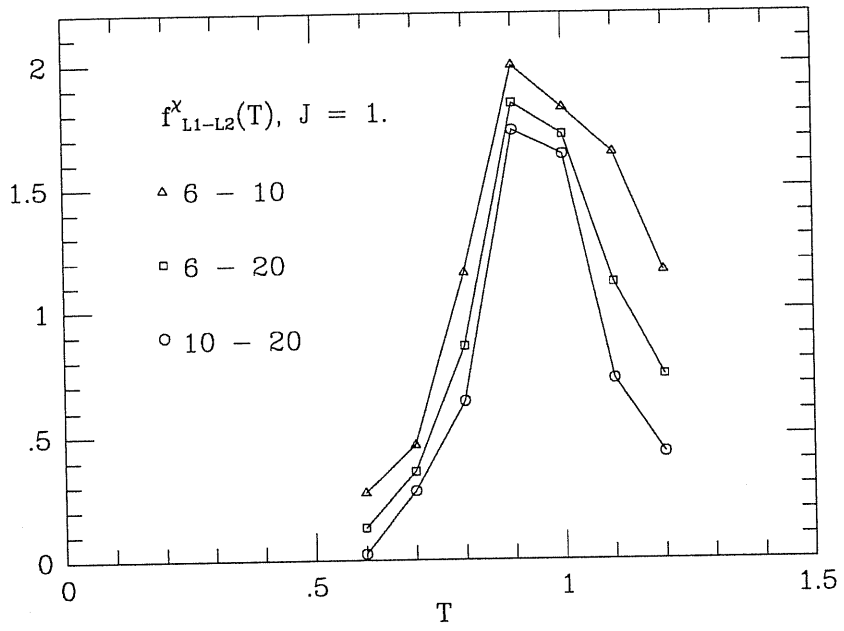

Figure 4.3: Finite size scaling determination of T_c, and $\frac{\gamma}{\nu}$ from the phenomenological renormalization method [65]. On the vertical axis is $f^{\chi}_{L_1L_2}(T) = \ln(\chi(L_1,T)/\chi(L_2,T))/\ln(L_1/L_2)$. All the curves should intersect at the point $(T_c, \frac{\gamma}{\nu})$. Our best estimate for T_c is 1.0, for $J = 1.$, $U = 0$.

For $J = 0.75$ the simulation was also done for three different lattice sizes $L = 6, 10, 20$ and the corresponding results are on Fig.4.5. The zero temperature value of $|P|$ is now about 0.65, which reveals the effect of stronger quantum fluctuations. The ferroelectric-paraelectric transition is seen as a drop of $|P|$ and as a sharp critical peak of the dielectric susceptibility curve near a new $T_c \sim 0.5$. The same finite size scaling analysis of the susceptibility as in the preceding case (Fig.4.6) now agrees with a critical temperature of $T_c \sim 0.5$ and a ratio of critical exponents $\frac{\gamma}{\nu}$ still close to $\frac{7}{4}$. Since the classical transition temperature for $J = 0.75$ is $T_c = 0.851$, the effect of quantum fluctuations has been to reduce T_c quite considerably. An interesting feature in this case is the behaviour of the specific heat. It has a rather flat maximum at temperatures almost twice as high as the transition temperature, with no strong evidence of critical behaviour at T_c itself, for the

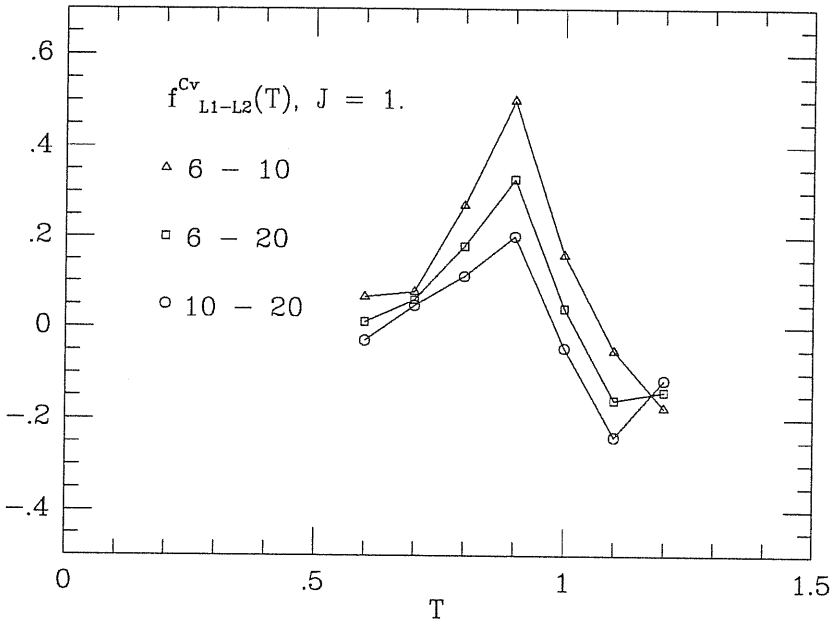

Figure 4.4: Finite size scaling determination of T_c, and $\frac{\alpha}{\nu}$, for $J = 1.$, $U = 0$.

system sizes we studied. This is again a sign that the system is in a quantum regime, and one would have to go to larger sizes to observe the expected crossover [6] from quantum to classical critical behaviour, sufficiently close to T_c.

Finally, for $J = 0.5$, we ran the simulation for only one lattice size, namely $L = 10$. The results are on Fig.4.7. Ferroelectricity seems altogether absent, all the way down to $T = 0$. To clarify further this case, we also performed an extrapolation of the dielectric susceptibility to $m \to \infty$ and found it to saturate at low temperatures (for comparison with the classical case, the susceptibility starts to level off at temperature $T \sim 0.25$, which is slightly less then a half of the classical transition temperature $T_c = 0.567$). This means that the paraelectric state persists down to the lowest temperatures and we therefore conclude that for this value of J the system is in the quantum paraelectric regime.

Apart from the usual long-range order parameter $|P|$, we can also demonstrate the temperature dependence of the nearest-neighbour "short-range order parameter" $\langle \cos(\phi_{ij} -$

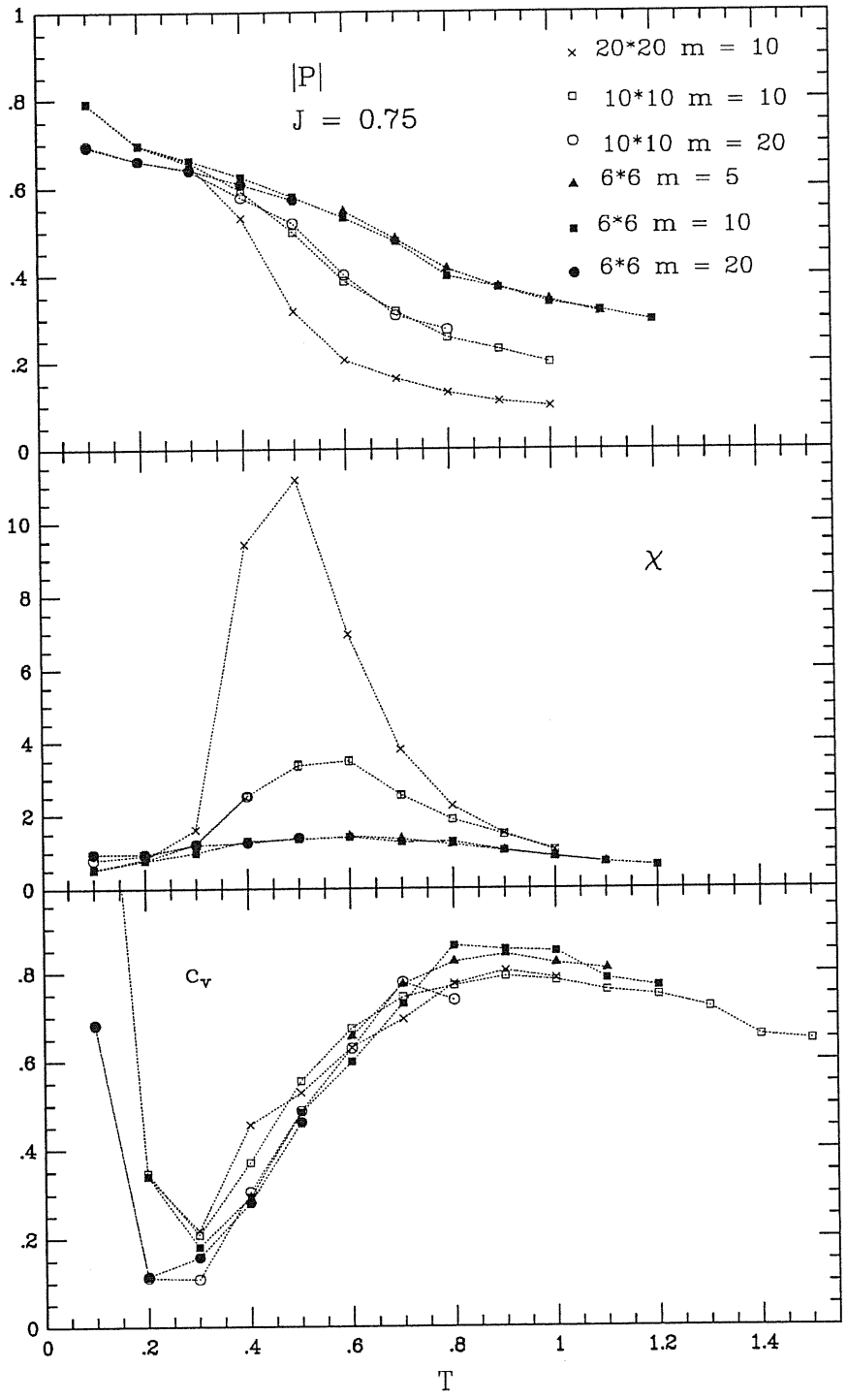

Figure 4.5: Polarization $|P|$, dielectric susceptibility χ, and specific heat c_v for $J = 0.75$, $U = 0$. There still is evidence of a ferro-para transition near $T_c \sim 0.5$. The singularity of c_v is severely depressed by quantum effects.

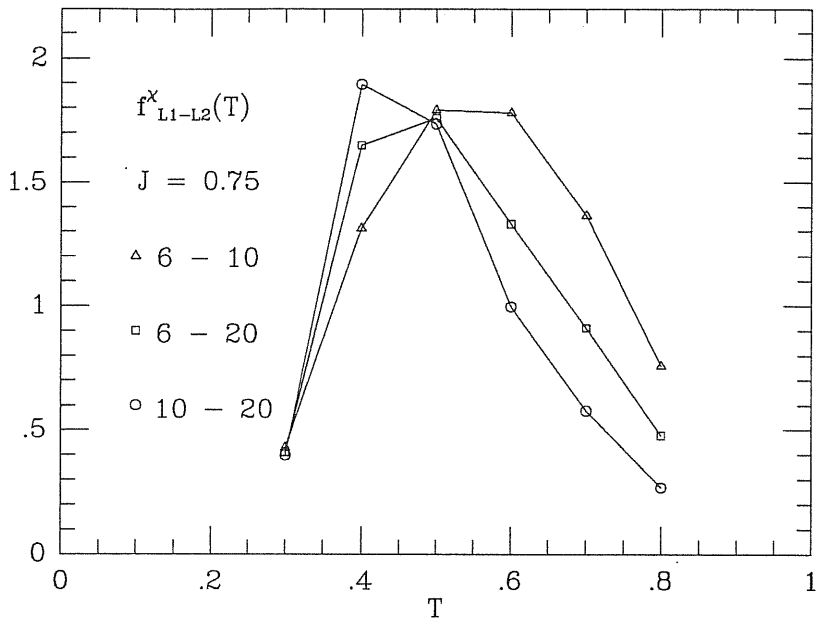

Figure 4.6: Finite size scaling determination of T_c, and $\frac{\gamma}{\nu}$, for $J = 0.75$, $U = 0$. Our best estimate is $T_c \sim 0.5$.

$\phi_{i'j'})\rangle$ (Fig.4.8). Since the system is now paraelectric for all temperatures, $|P|$ must scale to zero with increasing system size L. Its behaviour for a finite L reflects that of the correlation length ξ. The polarization $|P|$ is seen to pass through a moderate *maximum* at temperature $T^* \sim 0.6$, where the same kind of behaviour is clearly visible also on the nearest-neighbour order $\langle\cos(\phi_{ij} - \phi_{i'j'})\rangle$ curve. The correlation length ξ of a system in the quantum paraelectric regime thus has a maximum at a finite T^*. This kind of effect, in the different context of granular superconductors, was found by Fazekas et al. in [66], where a continuous XY-model was investigated. Their conclusion as to the existence of a broad maximum of short range order at $T^* \sim J$ remains therefore valid also in the case of our discrete four-state clock model. Qualitatively, the interpretation of this effect is the following. At zero temperature, the rotors are predominantly in their totally symmetric ground state $|0\rangle + |\pi/2\rangle + |\pi\rangle + |-\pi/2\rangle$, corresponding to the angular momentum $j = 0$, which does not possess a dipole moment. Increasing temperature from $T = 0$, rotor states

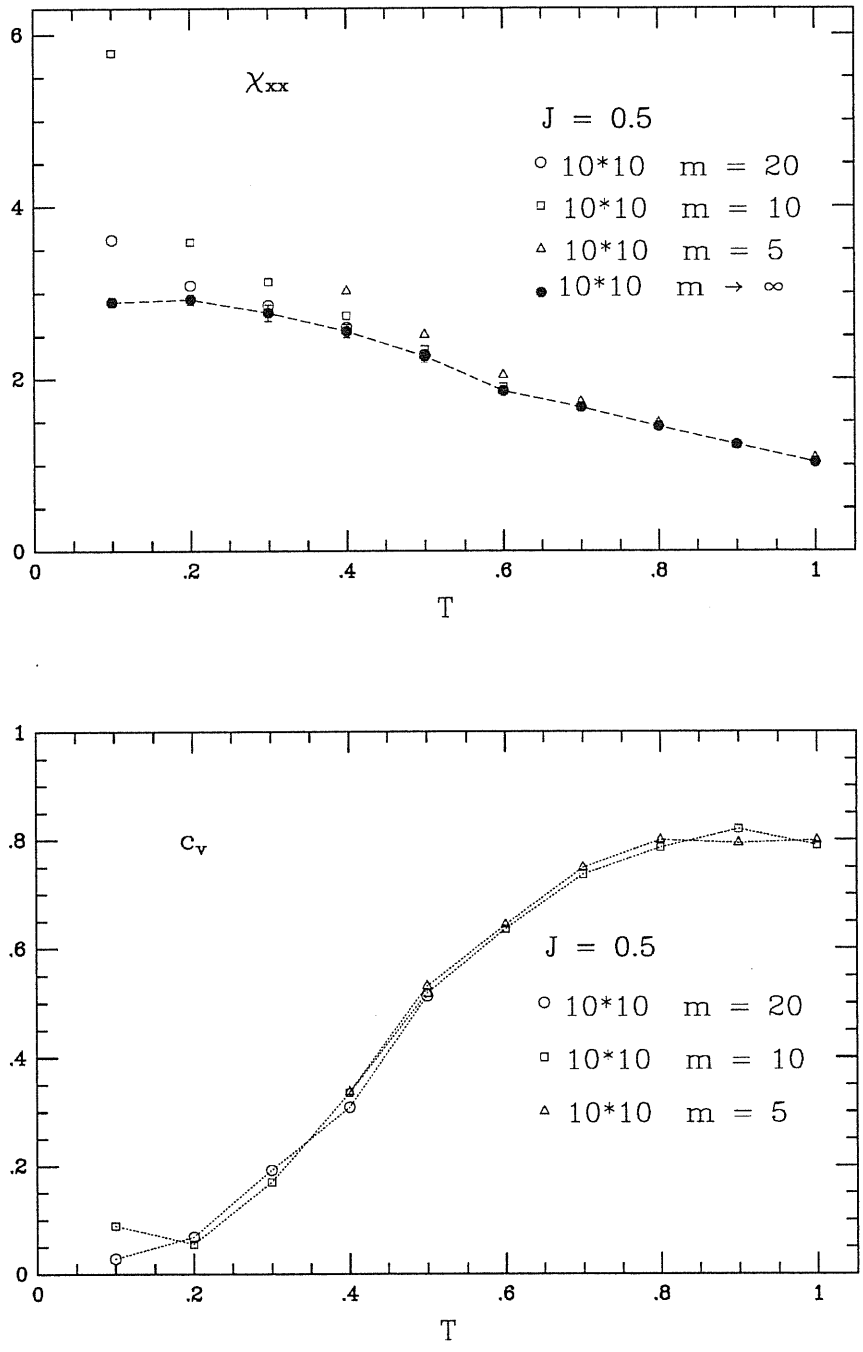

Figure 4.7: Dielectric susceptibility χ_{xx}, and specific heat c_v for $J = 0.5$, $U = 0$. Long-range ferroelectricity is absent. On cooling, the system evolves from classical paraelectric to QPE.

with non-zero dipole moment become thermally excited, and the system starts to develop some kind of short range order due to the coupling J. This order reaches a maximum at finite temperature, and is then eventually disrupted by thermal fluctuations as temperature increases further.

4.2 The constrained quantum four-state clock model

In this section we shall consider the constrained model, defined by the hamiltonian

$$H^{tot} = H^4 + H^{kin\,1} + H^{constr}\ , \tag{4.8}$$

where the constraint

$$H^{constr} = \lim_{U\to\infty} U \sum_{\langle ij\rangle} \delta(z_i - r_{ij})\delta(z_j + r_{ij}) \tag{4.9}$$

eliminates configurations where dipoles on neighbouring cells point towards one another (section 2.3).

4.2.1 General considerations

First of all we notice that the constraint eliminates very large number of configurations. To get an insight, let us consider a 1D case for a moment, and for the sake of simplicity let us force the constraint on each other link only (Fig.4.9). Clearly, the number of allowed configurations in this simplified case represents an upper limit of the number of allowed configurations in the actual 2D case.

Let us denote the total number of configurations in the chain of $2N$ sites as $b(N)$, and that of forbidden configurations as $a(N)$. Adding two new sites to the chain (increasing N by 1) amounts to increasing $b(N)$ by a factor of 4^2. The sequence $b(N)$ is therefore defined by the relation $b(N+1) = 16\,b(N)$, plus the boundary condition $b(1) = 16$, which yields $b(N) = 16^N$.

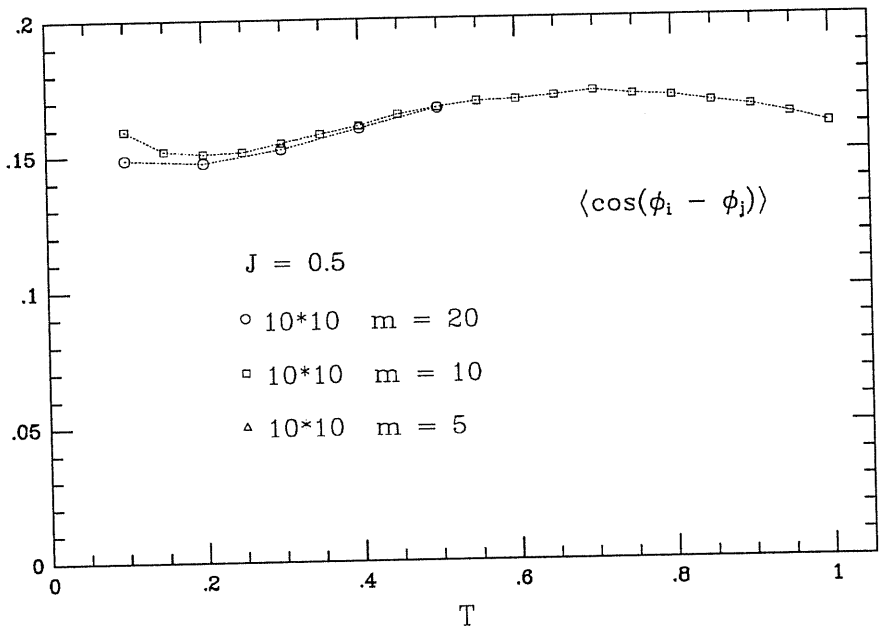

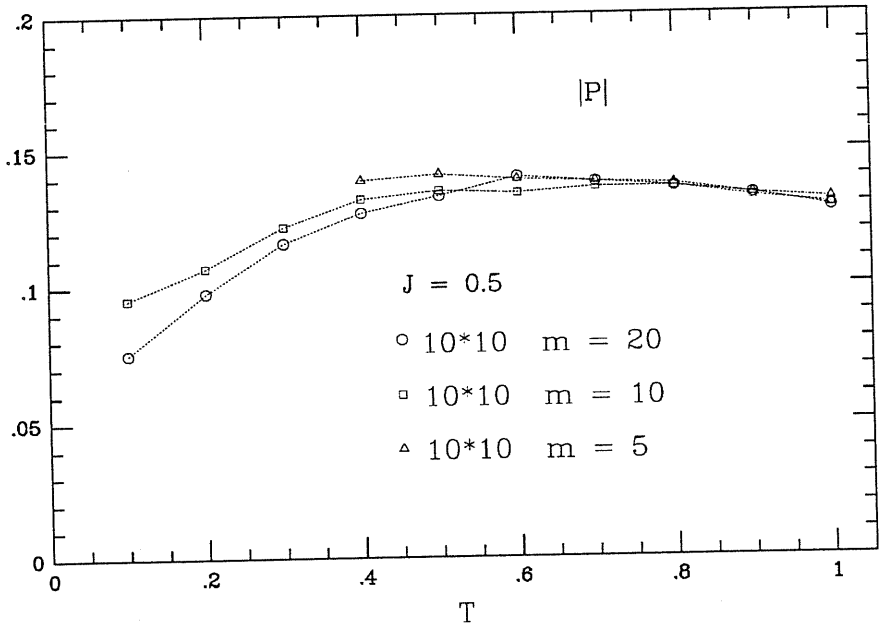

Figure 4.8: Nearest-neighbour "short-range order parameter" $\langle\cos(\phi_{ij} - \phi_{i'j'})\rangle$ and polarization $|P|$ for $J = 0.5$, $U = 0$. Note a mild peak of the short-range order at $T^* \sim 0.6$.

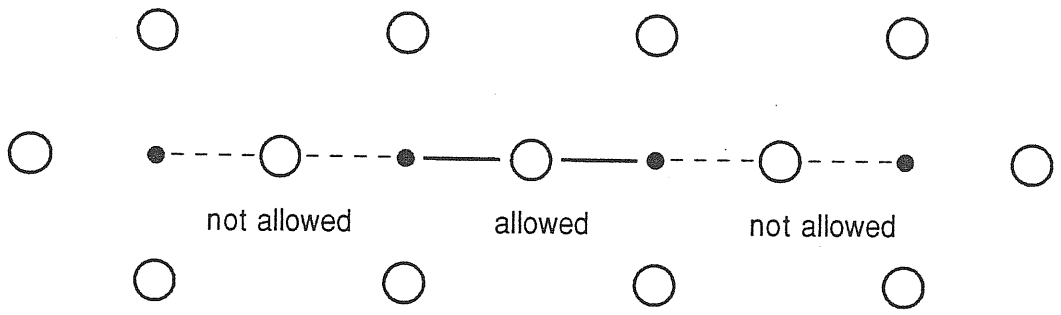

Figure 4.9: 1D model chain of cages with constraint on each other link.

An analogous recursion formula can be found expressing the number of forbidden configurations $a(N+1)$ in the chain of $2(N+1)$ sites through the number $a(N)$ in the chain of $2N$ sites. To do so, we notice that a configuration of the chain of $2(N+1)$ sites is forbidden when *either* the two additional sites are in their single forbidden configuration while the original $2N$ sites are in any of the total of their $b(N)$ configurations, *or* when the additional sites are in any of their 15 allowed configurations, but the original $2N$ sites are in one of their $a(N)$ forbidden configurations. The sequence $a(N)$ therefore satisfies the recursion formula $a(N+1) = 15a(N) + b(N)$ with boundary condition $a(1) = 1$. The explicit expression for $a(N)$ is therefore $a(N) = 16^{N-1} + 15 \times 16^{N-2} + \ldots + 15^{N-2} \times 16 + 15^{N-1}$.

We are interested in the ratio $\frac{a(N)}{b(N)}$ and its limit as $N \to \infty$. Using the above expressions for $a(N)$ and $b(N)$ we find that $\frac{a(N)}{b(N)} = 1 - (\frac{15}{16})^N \to 1$, as $N \to \infty$, which means that in the thermodynamic limit *the constraint eliminates "all" the configurations*, except for a set of zero measure. More precisely, the ratio of dimensionality of the constrained Hilbert space to that of the unconstrained one goes to zero in the thermodynamic limit, which

means that the constrained space is *orthogonal* to the original one. [1]

To start with, we shall investigate the properties of the constrained four-state clock model for the specially simple case $J = 0$. In this limit, it is very easily checked that the ground state of the unconstrained system ($U = 0$) is nondegenerate, and is described by a wavefunction Ψ_g^0, which is just a constant. This state can be seen as the product of N separate identical wavefunctions for each cell, each corresponding to the $j = 0$ angular momentum state of that cell. The corresponding many-body first excited state is infinitely degenerate. If we choose to label the wavefunctions by a wavevector $\vec{k}$, we have for each $\vec{k}$ two independent states, described respectively by wavefunctions (unnormalized)

$$\Psi_{exc1}^0(\vec{k}, z_1, \ldots, z_n) = \sum_i e^{i\vec{k}\vec{R}_i} \mathrm{Re}\, z_i \Psi_g^0 \tag{4.10}$$

$$\Psi_{exc2}^0(\vec{k}, z_1, \ldots, z_n) = \sum_i e^{i\vec{k}\vec{R}_i} \mathrm{Im}\, z_i \Psi_g^0 \,, \tag{4.11}$$

where $\vec{R}_i$ is the ordinary (real) vector defining the position of site i. In the absence of the constraint, i.e. for $U = 0$, the first excited state is separated from the ground state by an energy gap $2t$ (in the rest of this subsection we shall always set $t = 1$).

What about the $U = \infty$ constrained model ? Guided by having solved first the two-site problem, we try as an ansatz for the ground state wavefunction of the constrained system the following (Jastrow-like) product state

$$\Psi_g^\infty(z_1, \ldots, z_n) = \prod_{\langle ij \rangle} (\mid z_i - r_{ij} \mid + \mid z_j + r_{ij} \mid) \,, \tag{4.12}$$

which contains no free parameters. This wavefunction vanishes identically when bond i points towards j *and* bond j points towards i. It is rather close to exact solution for two sites only.

[1] This, incidentally, is quite a common outcome for a constrained many-body problem. For example, the well-known "non Fermi-liquid" behaviour of the 1D Hubbard model results from a very similar orthogonality catastrophe. See, e.g., [67].

	2×2	3×3
E_g^{exact}	-5.831	-12.607
$\langle \Psi_g^\infty \vert H \vert \Psi_g^\infty \rangle$	-5.827	-12.508
$\langle \Phi_g^{exact} \vert \Psi_g^\infty \rangle$	0.9997	0.986
E_{exc}^{exact}	-4.903	-11.906
$\langle \Psi_{excl}^\infty \vert H \vert \Psi_{excl}^\infty \rangle$	-4.866	-11.818
$\vert\langle \Phi_{exc}^{exact} \vert \Psi_{excl}^\infty \rangle\vert^2 + \vert\langle \Phi_{exc}^{exact} \vert \Psi_{exc2}^\infty \rangle\vert^2$	-	0.971
$\langle \Phi_{excl}^{exact} \vert \Psi_{excl}^\infty \rangle$	0.995	-

Table 4.1: *Properties of the ansatz wavefunctions (4.12), (4.13) as compared to exact wavefunctions for small systems,* 2×2 *and* 3×3.

We shall also assume that the first excited state of the constrained system corresponds to $\vec{k} = 0$ and can be obtained as the analytic continuation of the corresponding state (4.10) from $U = 0$ to $U = \infty$. In this way we arrive at the wavefunction

$$\Psi_{excl}^\infty(\vec{k} = 0, z_1, \ldots, z_n) = \sum_i \mathrm{Re}\, z_i \Psi_g^\infty(z_1, \ldots, z_n)\,, \tag{4.13}$$

and analogously for the degenerate state Ψ_{exc2}^∞.

To test these guessed wavefunctions in the real 2D case, defined by the constrained hamiltonian (4.8), we have performed a diagonalization for a 2-site and a 3-site system with periodic boundary conditions (Lanczos diagonalization). In Table 4.1 we show the overlap of trial states (4.12) and (4.13) with the exact wavefunctions, and compare the corresponding ground state and excitation energies. It turns out that (4.12) is an excellent approximation for the ground state of these small systems, and the same is true for the excited state ansatz (4.13). We feel therefore encouraged to adopt (4.12) and (4.13) as reasonable approximations for larger systems, where diagonalization is impossible.

In order to extract properties, such as ground-state energy and correlations, and the excitation gap of the system in the thermodynamic limit, we still need to calculate averages on states (4.12) and (4.13). For a 3×3 system with periodic boundary conditions the constrained Hilbert space contains 57376 states; however for a 4×4 system this number is 284 465 424, and regular sums over the configurations are no longer feasible in a

straightforward way. We have thus adopted a Monte Carlo sampling procedure for this purpose. Energy, for example, is evaluated as the average local energy $E_{loc}(j)$,

$$E = \frac{\langle \Psi \mid H^{kin\,1} \mid \Psi \rangle}{\langle \Psi \mid \Psi \rangle} = (\langle \Psi \mid \Psi \rangle)^{-1} \sum_j \mid \Psi(j) \mid^2 \frac{H^{kin\,1}\Psi(j)}{\Psi(j)}$$

$$= \left(\sum_j \mid \Psi(j) \mid^2 \right)^{-1} \sum_j \mid \Psi(j) \mid^2 E_{loc}(j)\,, \tag{4.14}$$

where j labels the configurations of the whole system (and we recall that we are still discussing the case $J = 0$).

We have calculated the average energies of states (4.12) and (4.13) for system sizes up to 30×30. The relevant information obtained from this calculation is summarized in Fig.4.10 and Fig.4.11. On Fig.4.10 we have plotted the energy gap ΔE versus system size L, which shows that the gap tends to a value close to $\frac{1}{2}$ as $L \to \infty$ and $U \to \infty$. Comparison with the unconstrained gap value $\Delta E = 2$ (for $U = J = 0$) shows that the constraint, even though insufficient to make the paraelectric state unstable and restore ferroelectricity, does all the same act to increase very strongly the tendency to ferroelectricity.

On Fig.4.11 we show a plot of ground state energy per site as a function of L, and we see that the finite size energy corrections scale exponentially with L. This agrees well with the existence of an excitation gap. The correlation length obtained from energy corrections is $\xi \simeq 0.72$, which agrees with absence of long range order. To clarify this point, we calculated the correlation function $\langle z_i^* z_j \rangle$ in the ground state, and find that it falls off very quickly with distance. It was not possible to investigate accurately its large distance behaviour, because the corresponding values were close to zero and suffered from large statistical error. For illustration, we present in Table 4.2 some data for the 10×10 system. This behaviour of the correlation function supports the conjecture drawn from finite-size scaling of the ground state energy, and leaves us with very little doubt that ansatz (4.12) for the $J = 0, U = \infty$ state is disordered.

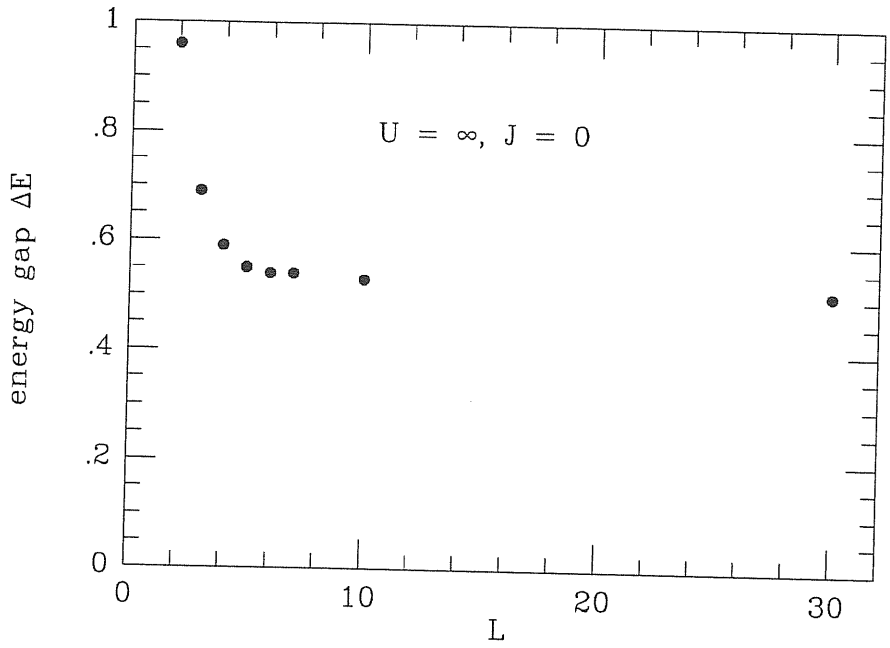

Figure 4.10: Size dependence of the variational energy gap ΔE for $J = 0$, $U = \infty$, between ground state (4.12) and excited state (4.13).

i	j	$\langle z_i^* z_j \rangle$
(1,1)	(1,2)	0.149
(1,1)	(1,3)	$3. \times 10^{-2}$
(1,1)	(1,4)	$(7.2 \pm 2.5) \times 10^{-3}$

Table 4.2: *Correlation function* $\langle z_i^* z_j \rangle$ *of the ground state ansatz wavefunction (4.12) for a* 10×10 *system.*

Unfortunately, we have not been able to construct simple variational states, yielding a similar semi-analytical understanding of the constrained quantum model for a general $J \neq 0$. A simple correlated Jastrow form would necessarily overemphasize the disordered phase, similarly to the case of liquid He^4, where such simple wavefunction strongly overestimates the crystallization pressure. Zero temperature ordering in d dimensions in presence of quantum fluctuations actually corresponds to a classical ordering in $d+1$ dimensions in presence of thermal fluctuations. In a 3D system, long-range order sets on at *much lower value* of short-range order than in a 2D system. A possible way out might be a wave func-

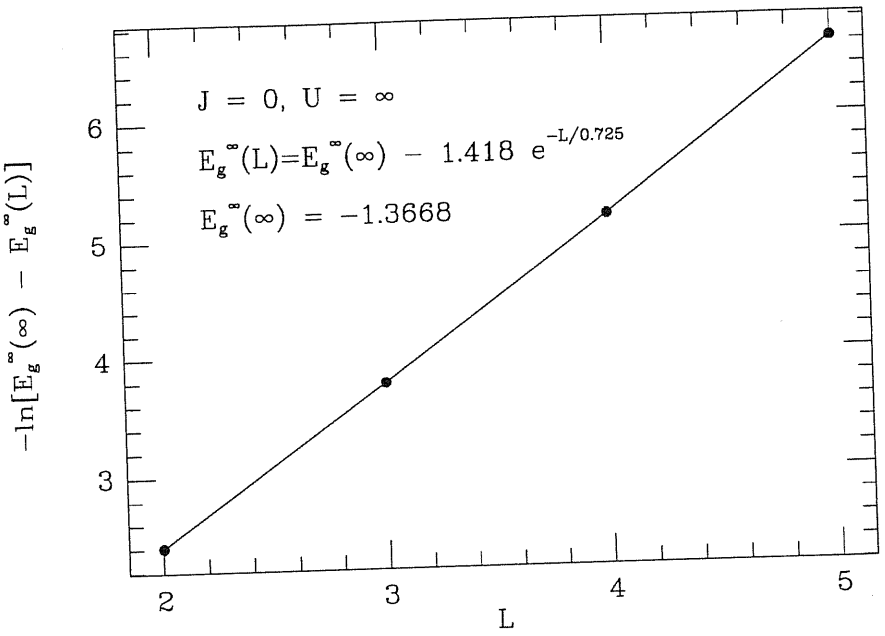

Figure 4.11: Finite-size scaling to the variational ground state energy $E_g^\infty(L)$ for $J = 0$, $U = \infty$. Note the clear exponential behaviour, compatible with a gap, as in the Fig.4.10.

tion analogous to the shadow wave functions, commonly used for He^4, which takes better account of the many-body correlations, however, the corresponding calculation might not be a simple one.

4.2.2 A slave-boson mean field theory

In this subsection we present a mean field theory for the ground state of the constrained model, at $J = 0$. From this, we also get indirectly an estimate for the critical value J_q/t. The main problem is to deal with the rigid constraint which prevents the oxygens from being doubly bonded. This feature of our model is very similar to that which applies to electrons in the infinite U Hubbard model, where the repulsion energy also eliminates double occupancy of a single site. This analogy suggests that we may try to use the method of introducing auxiliary, slave-boson fields, commonly used in the Hubbard model studies [68].

For this purpose it is convenient to work in the occupation number representation. First of all, for each pair of nearest neighbour sites i, j we introduce two Bose operators $b_{ij}^\dagger, b_{ji}^\dagger$. The operator $b_{ij}^\dagger$ creates a bond of the central ion on site i, pointing towards site j, and similarly $b_{ji}^\dagger$ creates a bond of the central ion on site j pointing towards site i. We notice that obviously $b_{ij}^\dagger \neq b_{ji}^\dagger$. Between the central sites i, j, there is a "bridging" oxygen ion, which can be unambiguously labeled by the pair of site labels i, j or j, i. This oxygen ion, depending on the states of central ions on sites i, j, can in fact be in four different states. In order to describe these states, we introduce new Bose operators $e_{ij}^\dagger, p_{ij,i}^\dagger, p_{ij,j}^\dagger, d_{ij}^\dagger$, with the following meaning. The oxygen is in the state $e_{ij}^\dagger |0\rangle$, if none of the central ions is bonded to it. It is in the state $p_{ij,i}^\dagger |0\rangle$, if the ion on site i is bonded to it, and analogously for $p_{ij,j}^\dagger |0\rangle$. Finally, in the state $d_{ij}^\dagger |0\rangle$, both central ions on sites i, j are bonded to it. These oxygen operators represent our auxiliary fields, or slave bosons. In our case they do correspond to real physical states of the oxygen ion. From this point of view, they are in fact real bosons. From the way we introduced all the operators it is clear that these satisfy the following constraints:

$$\sum_j b_{ij}^\dagger b_{ij} = 1 \tag{4.15}$$

$$e_{ij}^\dagger e_{ij} + p_{ij,i}^\dagger p_{ij,i} + p_{ij,j}^\dagger p_{ij,j} + d_{ij}^\dagger d_{ij} = 1 \tag{4.16}$$

$$b_{ij}^\dagger b_{ij} = p_{ij,i}^\dagger p_{ij,i} + d_{ij}^\dagger d_{ij} \tag{4.17}$$

Now we express our hamiltonian (4.8) by means of the new operators. First, the constraint term (2.15) is now easily written as

$$H^{constr} = \lim_{U\to\infty} U \sum_{\langle ij \rangle} d_{ij}^\dagger d_{ij} \,. \tag{4.18}$$

The potential energy term (2.9) is straightforwardly written as

$$H^4 = -J \sum_{\langle ij \rangle} \sum_{kl} \mathrm{Re}(r_{ik} r_{jl}^*) b_{ik}^\dagger b_{ik} b_{jl}^\dagger b_{jl} \,, \tag{4.19}$$

where $r_{ij} = r_j - r_i$, r_i being the complex number defining the 2D position of site i. The hopping term (2.12) is slightly more involved. We work in an enlarged Hilbert space and the hopping of central ion is accompanied by a change of state of the surrounding oxygens. The corresponding expression reads

$$H^{kin\,1} = -t \sum_i \sum_{jj'} b^\dagger_{ij} (d^\dagger_{ij} p_{ij,j} + p^\dagger_{ij,i} e_{ij}) b_{ij'} (p^\dagger_{ij',j'} d_{ij'} + e^\dagger_{ij'} p_{ij',i}) \,, \tag{4.20}$$

where j, j' are both nearest neighbours of i and such that j' is the next-nearest neighbour of j.

Next, we shall treat the *oxygen* operators in the mean-field approximation, replacing them by c-numbers. Before passing to the actual constrained case $U = \infty$, we consider the trivial case of $U = 0$, $J = 0$. The corresponding operator averages are obviously equal for all oxygens and we denote them as

$$\langle e^\dagger_{ij} \rangle = e \tag{4.21}$$

$$\langle p^\dagger_{ij,i} \rangle = \langle p^\dagger_{ij,j} \rangle = p \tag{4.22}$$

$$\langle d^\dagger_{ij} \rangle = d \,, \tag{4.23}$$

where the equation (4.22) expresses the fact that we assume an unbroken symmetry case. The constraints (4.15),(4.16),(4.17) then read

$$\begin{aligned} &\sum_j \langle b^\dagger_{ij} b_{ij} \rangle = 1 \\ &e^2 + 2p^2 + d^2 = 1 \\ &\langle b^\dagger_{ij} b_{ij} \rangle = p^2 + d^2 \end{aligned} \tag{4.24}$$

Since for $U = 0$ the sites are independent, the numerical values of the above averages follow just from the statistical distribution of possible mutual orientations of clock variables on neighbouring sites. It is easily found that in this case $\langle b^\dagger_{ij} b_{ij} \rangle = \frac{1}{4}$, and $d^2 = \frac{1}{16}$, $p^2 = \frac{3}{16}$,

$e^2 = \frac{9}{16}$. Our mean-field hamiltonian then becomes a sum of on-site terms

$$H^{MF} = -\tilde{t} \sum_i \sum_{jj'} b^\dagger_{ij} b_{ij'} \ , \tag{4.25}$$

where $\tilde{t} = tp^2(d+e)^2 = \frac{3}{16}t$. We see that in order to recover the original t we have to renormalize the mean-field $\tilde{t}$ by a factor of $\frac{16}{3}$.

Now we pass to $U = \infty, J = 0$. Obviously, the presence of the constraint H^{constr} amounts to setting $d = 0$. We shall first search for an unbroken symmetry, paraelectric ground state. Following the same line of arguments as above, we have $p^2 = \frac{1}{4}$, $e^2 = \frac{1}{2}$, and we get a renormalized $\tilde{t} = \frac{2}{3}t$. This corresponds to a ground state energy per site equal to $E_g/N = -2\tilde{t} = -\frac{4}{3}t = -1.333t$, which compares very well with the result $-1.3668t$ obtained from our ground state wavefunction ansatz (4.12) (Fig.4.11).

Now we show that for $U = \infty, J = 0$ there is also a broken symmetry, ferroelectric mean-field ground state, whose energy is degenerate with the paraelectric state found above. First of all we notice that the oxygens actually form two interpenetrating square sublattices – one formed by oxygens lying on horizontal links and other formed by those on vertical links. If we want to search for a broken symmetry solution, we have to allow for different oxygen operator averages on these two sublattices, and also the p defining equation (4.22) may not be true anymore. Let us assume that the symmetry is broken along the horizontal axis. Then we shall have nonzero averages e_V,p_V, defined by (4.21),(4.22) for oxygens on links i, j, $j = i + \vec{y}$, and $e_H = \langle e^\dagger_{ij} \rangle$, $p_{H+} = \langle p^\dagger_{ij,i} \rangle$ and $p_{H-} = \langle p^\dagger_{ij,j} \rangle$ for i, j, $j = i + \vec{x}$, where $\vec{x}, \vec{y}$ are unit lattice vectors. As a consequence, the mean-field constraints (4.24) will also be correspondingly generalized. Instead of (4.25) we have now

$$H^{MF} = -\sum_i \left\{ \tilde{t}_1 (b^\dagger_{i,i+\vec{y}} b_{i,i+\vec{x}} + b^\dagger_{i,i+\vec{x}} b_{i,i-\vec{y}}) + \tilde{t}_2 (b^\dagger_{i,i-\vec{x}} b_{i,i+\vec{y}} + b^\dagger_{i,i-\vec{y}} b_{i,i-\vec{x}}) + \text{h.c.} \right\} \ , \tag{4.26}$$

where $\tilde{t}_1 = t p_V e_V e_H p_{H+}$, $\tilde{t}_2 = t p_V e_V e_H p_{H-}$. We can now prove that $e_V = e_H =$

$p_{H+} = \frac{1}{\sqrt{2}}$, $p_V = \frac{1}{2}$, $p_{H-} = 0$, is a selfconsistent ground state solution of (4.26). We get renormalized hopping parameters $\tilde{t}_1 = \frac{16}{3} t/4\sqrt{2}$, $\tilde{t}_2 = 0$, and the corresponding normalized ground state of (4.26) is

$$|\Psi_g\rangle = \prod_i \left(\frac{1}{\sqrt{2}} b^\dagger_{i,i+\vec{x}} + \frac{1}{2} b^\dagger_{i,i+\vec{y}} + \frac{1}{2} b^\dagger_{i,i-\vec{y}} \right) |0\rangle \,. \tag{4.27}$$

The self-consistency condition is easily found to be satisfied, and the solution is clearly ferroelectric. The corresponding energy per site is $E_g/N = -\sqrt{2}\tilde{t}_1 = -\frac{4}{3}t$, and therefore this state is *exactly degenerate* with the paraelectric state already found. Our mean-field theory thus predicts a critical value of $J_q/t = 0$, since the slightest positive J will make the system ferroelectric.

This value of J_q, however, is not compatible with the result obtained in the last subsection from the ansatz (4.12). In the following subsection, we shall resolve this issue by means of a numerical Path Integral Monte Carlo simulation. Before doing so, we present a simple argument which indicates that J_q/t should in fact be finite for the constrained 2D quantum four-state clock model. As can be easily shown, the dielectric susceptibility of a single four-state rotor at zero temperature is $\chi_0 = 1/2t = 1/\Delta E$, where ΔE is the energy gap. Since each rotor has four nearest neighbours, a simple standard mean field scheme would suggest a para-ferro transition at $4\,\chi_0\,J_q = 1$. For a simple, unconstrained model this yields a critical value of $J_q/t = 1/2$, to be compared with the true value 0.66. Since in the constrained case the gap is smaller roughly by a factor of four, the predicted critical value correspondingly becomes equal to $J_q/t = 1/8 = 0.125$. As we shall see later, this value is again reasonably accurate. The basic fact that J_q/t remains finite, in spite of the constraint, will be confirmed. Hence, exact degeneracy of the ferro and para state at $J = 0$ is an artefact of the slave boson approximation.

4.2.3 Accurate simulation of the constrained quantum four-state clock model

Before coming to the actual results of the accurate PIMC simulation of the constrained model, we must again recall the limitations of the method used. It is intuitively clear that already in the classical case, the presence of the constraint acts to reduce very considerably the acceptance ratio of our simple unbiased MC moves (Appendix A). Moreover, in the quantum case, the constraint increases the systematic error due to Trotter decomposition, and a larger number of Trotter slices is needed to approach the true quantum averages. These problems seriously reduce our possibilities of performing a satisfactory finite-size scaling analysis of the results. [2]

As a test of the code, we simulated first a 2×2 constrained four-state clock model, for $J = 0.5$, and compared the results with an exact diagonalization, with very satisfactory agreement (Fig.4.12). The rest of results we present in this section refers to a single system size, $L = 10$. The simulation was performed typically for $m = 10$ Trotter slices in the temperature interval from $0.1 < T < 1$. In the low temperature range ($T \leq 0.4$) we also used $m = 20$ and $m = 40$ Trotter slices. All the quantities were averaged over 4×10^5 MCsteps/site, after discarding the initial 2×10^4 MCsteps/site necessary for equilibration.

In Fig.4.13, we plot the calculated constrained dielectric susceptibility χ versus coupling constant J at low temperatures, $T = 0.1$ and $T = 0.2$. We see a sharp peak, signalling a transition, roughly at $J_c \sim 0.17$ for $T = 0.2$ and at $J_c \sim 0.15$ for $T = 0.1$. The limiting quantum critical value may thus be estimated to be $J_q/t \sim 0.15$, a factor of about *four* smaller than that for the unconstrained model.

On Fig.4.14 we plot the order parameter $|P|$, the dielectric susceptibility χ and the specific heat c_v versus temperature for $J = 0.3$. The system is clearly ferroelectric at low

[2] This will be possible in the future, provided one can construct a suitable algorithm, built to take the constraint automatically into account.

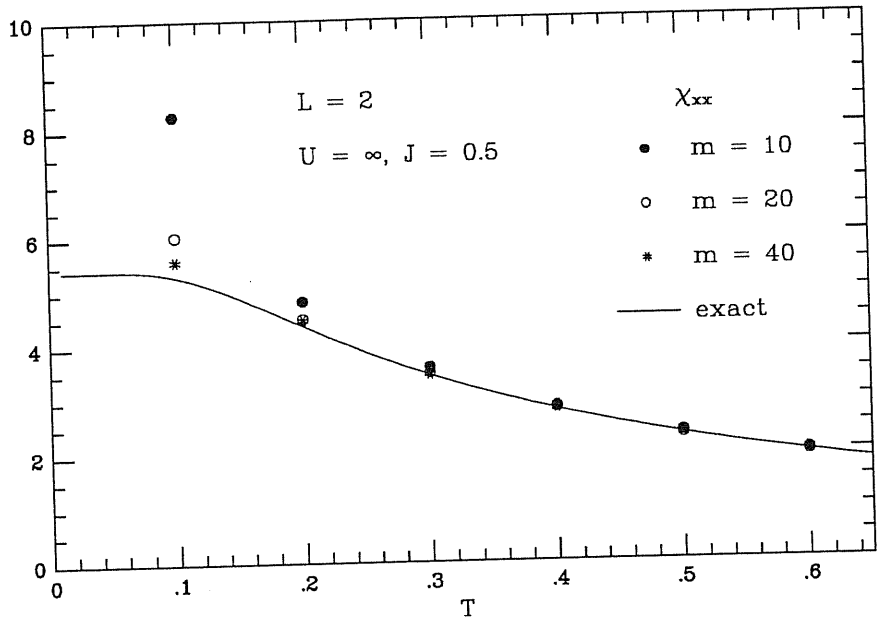

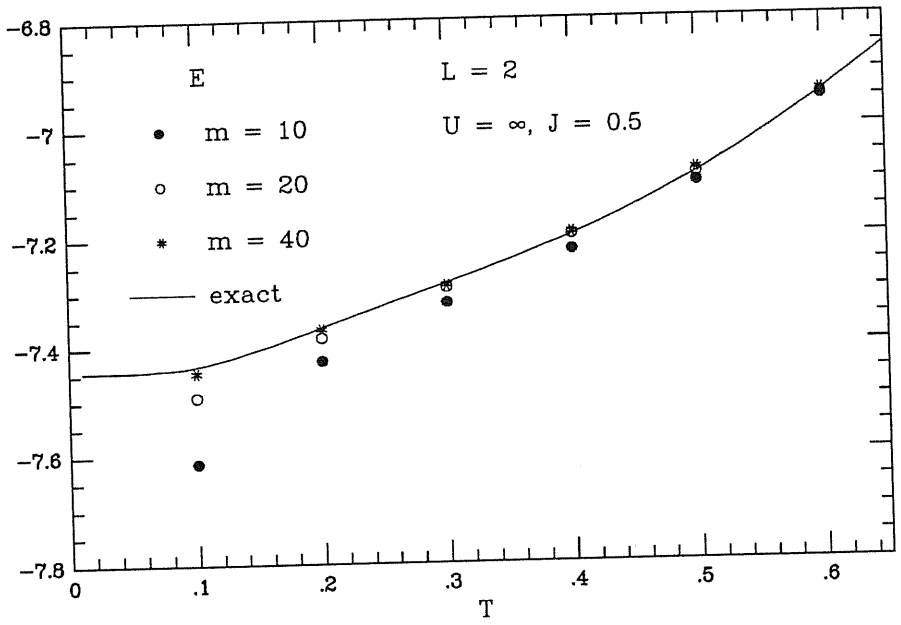

Figure 4.12: Test of the PIMC method: dielectric susceptibility χ_{xx}, and internal energy E for a 2×2 *constrained* system with $J = 0.5$, $U = \infty$, as obtained from the simulation, to be compared with the exact result obtained from the diagonalization.

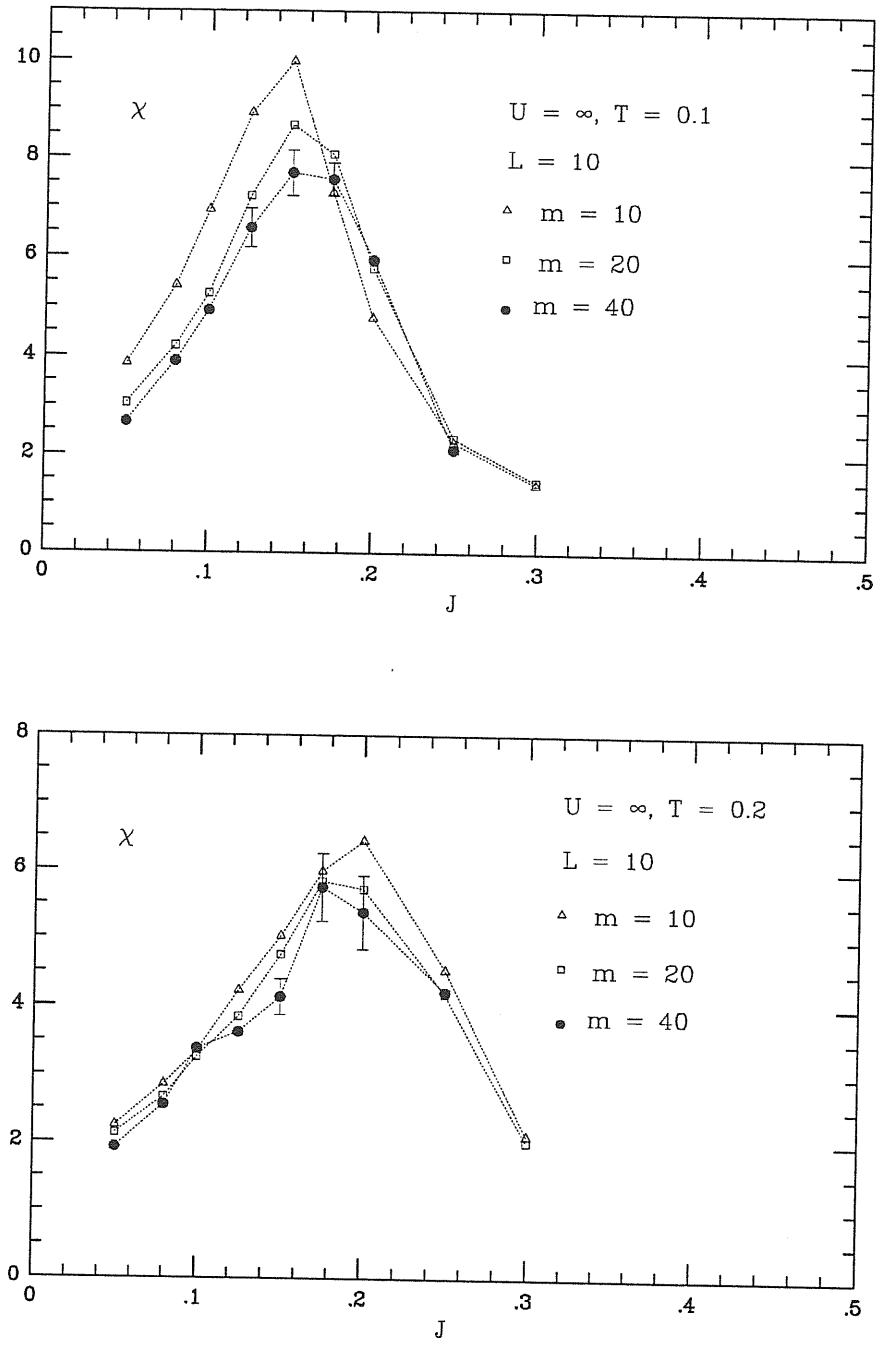

Figure 4.13: Constrained model dielectric susceptibility χ as a function of coupling J, for $T = 0.1$ and $T = 0.2$, $U = \infty$. A ferro-para transition is evident, near $J_q/t \simeq 0.15$.

temperatures. However, the saturation value of the order parameter $|P|$ is ~ 0.5, indicating a strong quantum fluctuation reduction. The susceptibility χ has a peak at $T \sim 0.35$, for this value of J. At the same temperature, however, the specific heat c_v does not show any apparent singularity for this small size. As also found in the previous section, milder specific heat singularities are, however, quite typical for quantum transitions [5],[69].

Fig.4.15 and Fig.4.16 present plots of the same quantities χ_{xx}, c_v and $|P|$, plus in addition the temperature dependence of the nearest-neighbour short range order parameter $\langle\cos(\phi_{ij} - \phi_{i'j'})\rangle$, for $J = 0.05$. For this value of the coupling constant, which is lower than J_q/t, the system should be in the quantum paraelectric regime at low T. Actually, were it not for the J dependence of χ (Fig.4.13), it would be difficult to draw this conclusion just by inspection of the T-dependence of χ_{xx}. In fact, even at the lowest temperatures investigated, χ_{xx} does not seem to saturate, and continues to grow with decreasing T. Further simulation for even lower temperatures in this deeply quantum regime is at the moment not feasible, since the Trotter error would be too large.

Similarly to the unconstrained case, the polarization $|P|$ is seen to pass through a moderate maximum at temperature $T^* \sim 0.3$, and the same behaviour is now just barely visible also on the nearest-neighbour order $\langle\cos(\phi_{ij} - \phi_{i'j'})\rangle$. We note that the specific heat c_v is smooth, with the same broad maximum near $T \sim 0.8$ present also for the ferroelectric case $J = 0.3$. Finally, on Fig.4.17, we show a sketch of phase diagrams for both the unconstrained and the constrained model, as resulting from our simulations.

The two phase diagrams are qualitatively similar. There are only two phases, the ferro and the para. The $T = 0$ QPE phase is nondegenerate, and has a gap. It will transform into a classical paraelectric with temperature, with just a smooth crossover and no phase transition.

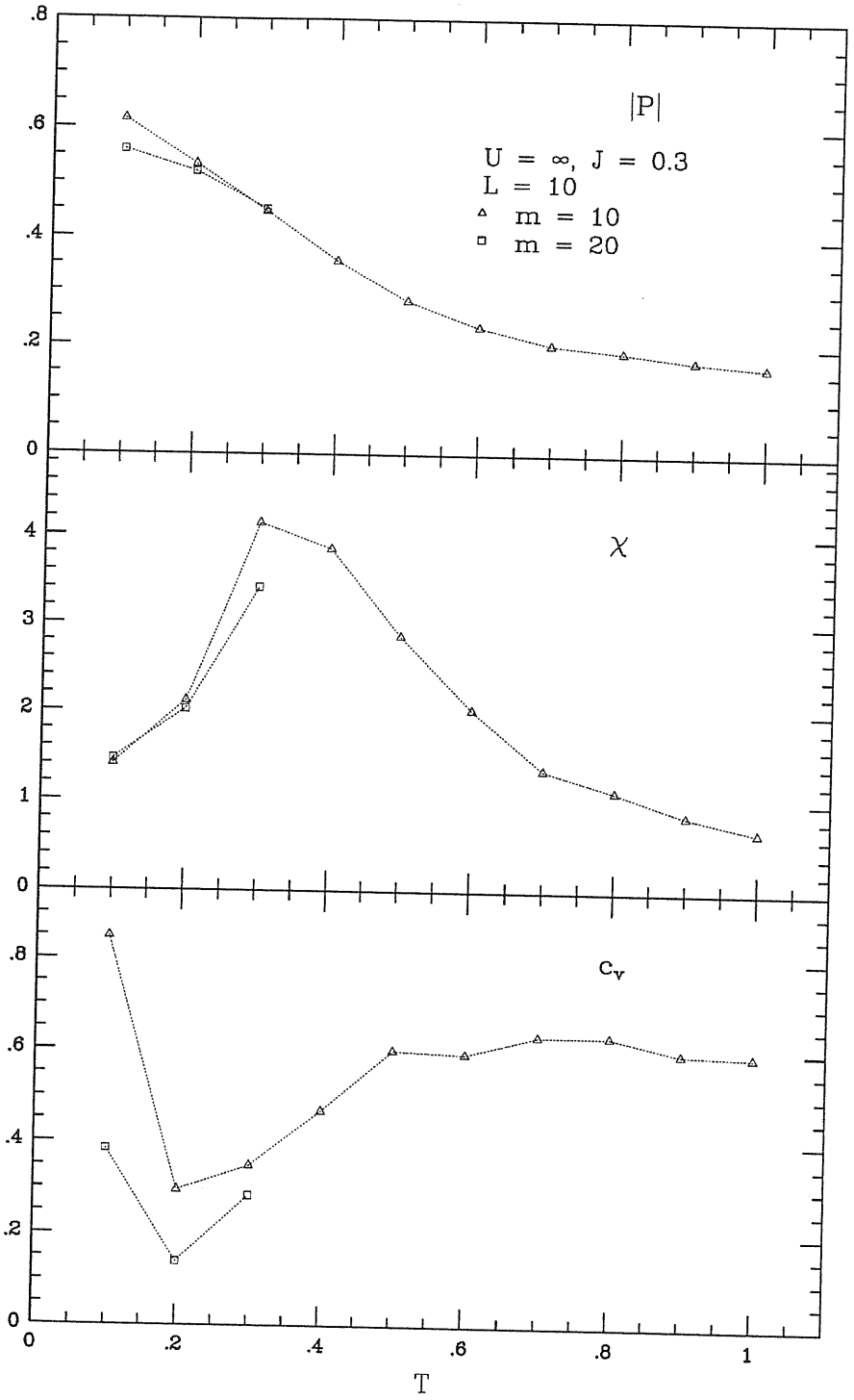

Figure 4.14: Polarization $|P|$, dielectric susceptibility χ, and specific heat c_v for $J = 0.3$, $U = \infty$. There is a clear ferro-para transition near $T_c \sim 0.35$.

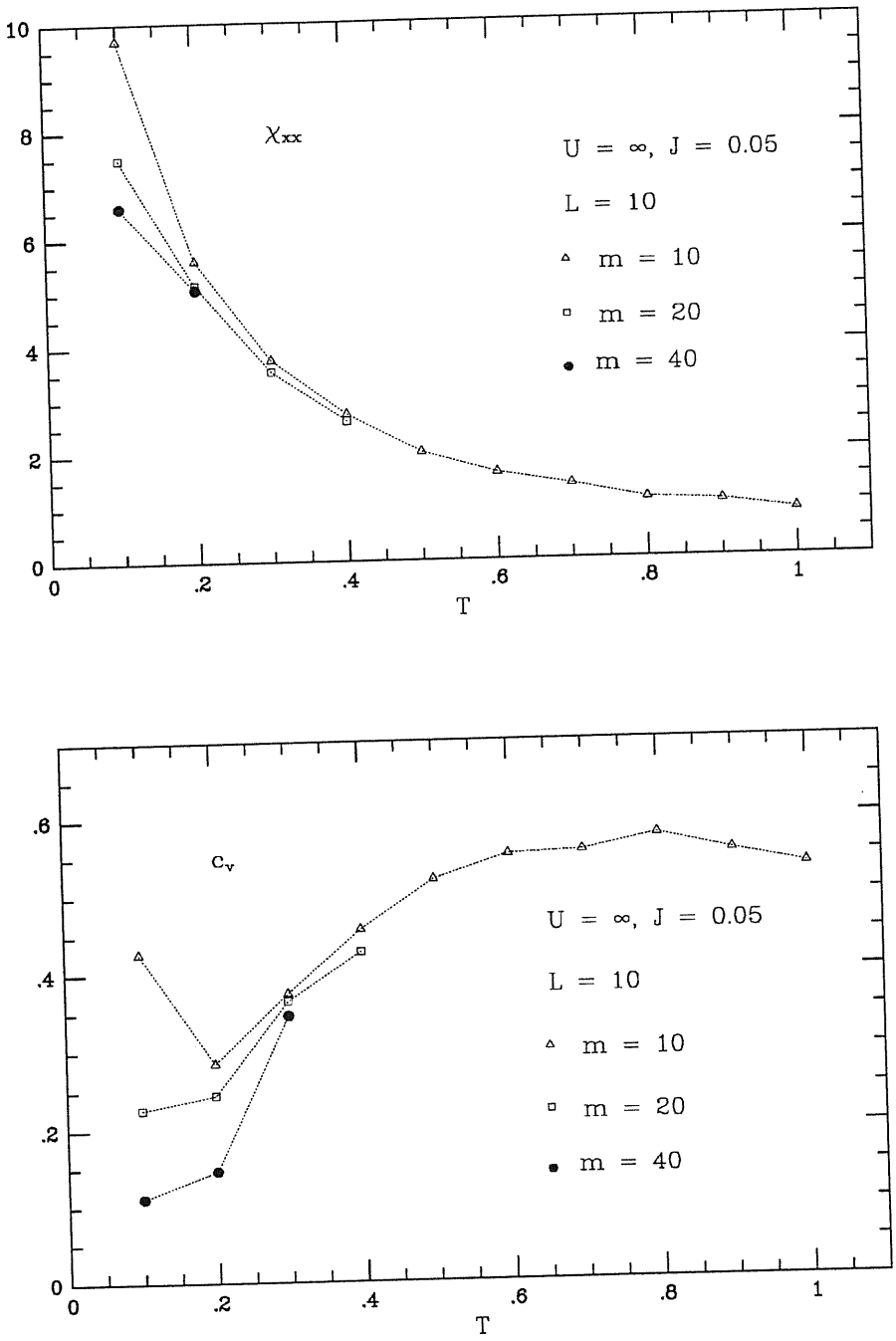

Figure 4.15: Dielectric susceptibility χ_{xx}, and specific heat c_v for $J = 0.05$, $U = \infty$. The low-temperature state is a QPE.

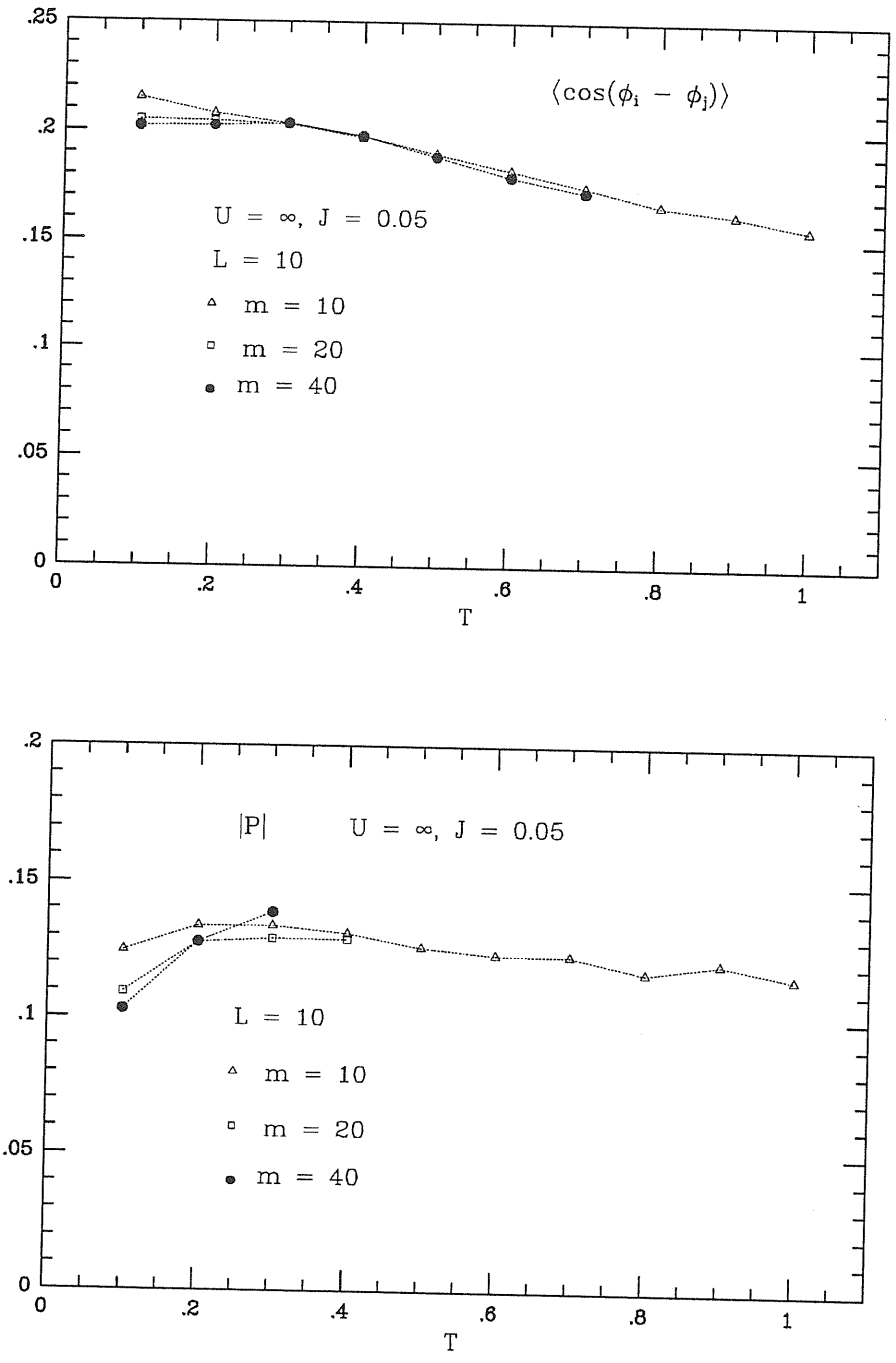

Figure 4.16: Nearest-neighbour "short-range order parameter" $\langle \cos(\phi_{ij} - \phi_{i'j'}) \rangle$ and polarization $|P|$ for $J = 0.05$, $U = \infty$.

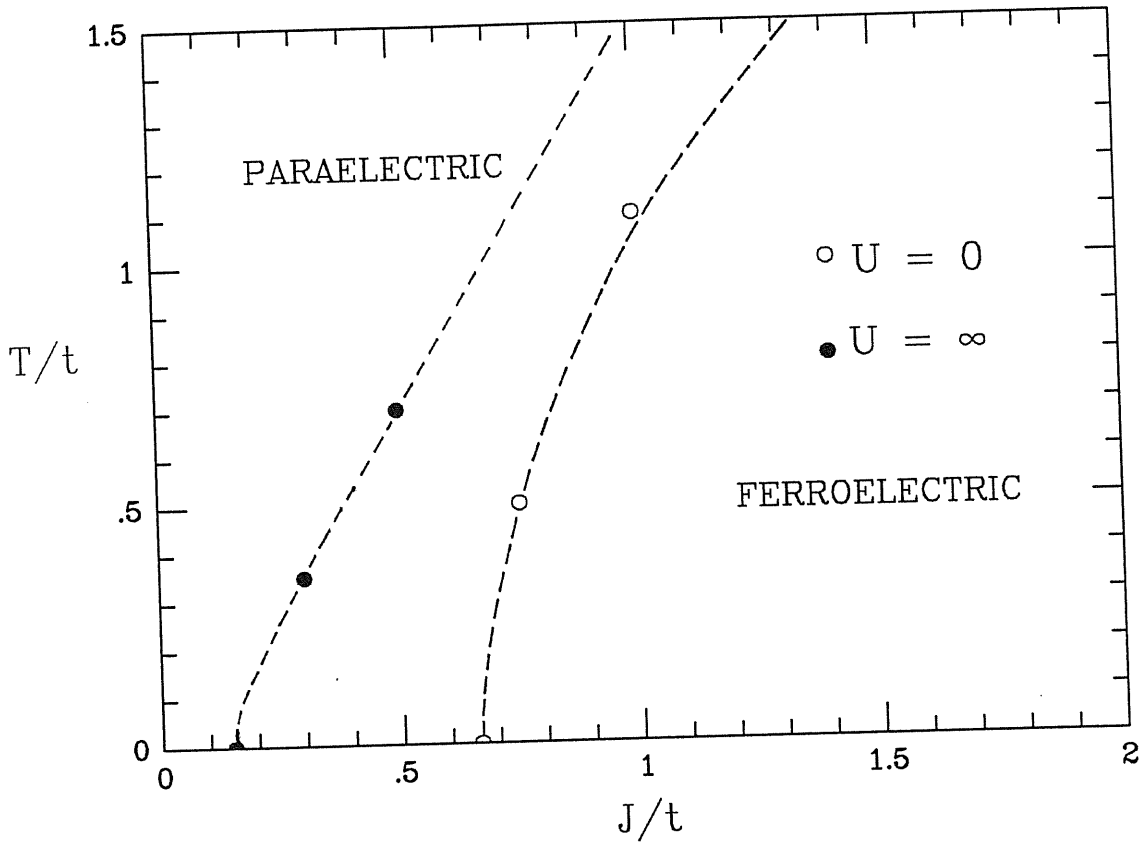

Figure 4.17: Phase diagram of both unconstrained and constrained model in the $(J/t, T/t)$ plane. Note the shift of the phase boundary towards lower J/t due to the constraint.

4.3 Model with bond vacancies

In this section we shall study the last one of our discrete lattice models, which contains and generalizes the previous two. It contains a new ingredient, the possibility of bond vacancies, which at the classical level could just be seen as a way to make connection with the displacive regime, where there are no more bonds. As we shall show, due to quantum effects this new ingredient actually allows for an entirely new piece of hamiltonian, corresponding to the quantum kinetic energy of the oxygen hopping, as discussed in Chapter 2. The resulting model, however, is rather complicated, and so far we have not yet been able to

reach a complete understanding of its phase diagram. We shall describe the picture as we see it at present, and propose a possibility of a new and nontrivial modification to the scenario of the crossover from displacive to order-disorder regime.

4.3.1 The model

The quantum four-state clock model, considered in preceding sections, resulted essentially from a discretization of the local multiple-well potential. It implicitly assumed that at low enough temperatures, *each* Ti ion is close to one of the minima in its local potential, or, in other words, that there is a $Ti - O$ bond in *each* oxygen cage. Imagine now that in some cage there were no bond, and the Ti ion were located near the centre of the multiple well, rather than in a side valley. As suggested in Chapter 2, such configuration could be denoted as a *bond vacancy*, and its energy cost would be close to the well depth V. In the purely classical case and at $T = 0$, each Ti ion would be located exactly in the potential minimum, and obviously there will be no bond vacancies.

Now imagine that due to some quantum process, this bond vacancy, once created in a cage, could become mobile, and hop from a cage to the neighbouring one, exchanging itself with a bond. Analogously to Andreev and Lifshitz's considerations related to the quantum crystal [18] (Appendix B), we may expect that if the amplitude for the bond vacancy hopping were sufficiently large, the system might spontaneously create a *finite bond vacancy concentration* even at $T = 0$. If moreover the vacancies could be considered to be bosons, they would be condensed. For conserved bosons, the resulting ground state would have an off-diagonal long-range order. Even if they were not conserved, the condensed state, if it had to be arrived at by cooling, might imply a phase transition at some finite temperature.

Actually, the *oxygen hopping* discussed in Chapter 2 provides us with a quantum process which, in principle, might be able to delocalize the bond vacancies. The model we

are going to consider in this section is obtained from the constrained quantum four-state clock model of the last section, H^{tot} (4.8), by adding the *kinetic energy term* $H^{kin\,2b}$ (2.13), as well as another term H^{V} which accounts for the energy cost of creating vacancies. The complete hamiltonian H^{vac} reads

$$H^{vac} = H^{4} + H^{kin\,1} + H^{constr} + H^{kin\,2b} + H^{V} \ . \tag{4.28}$$

It is convenient to express all the terms of (4.28) in second quantization, similarly to subsection 4.2.2. Apart from the operators $b_{ij}^{\dagger}$ of the last section, we shall introduce for each site i a new Bose [3] operator $h_i^{\dagger}$, creating a state in which the central ion on site i *has no bond*. The corresponding on-site completeness relation reads

$$\sum_{j} b_{ij}^{\dagger} b_{ij} + h_i^{\dagger} h_i = 1 \ , \tag{4.29}$$

and expresses the condition that in each cage there is either a bond vacancy or just one bond. The term H^{4} remains in the form (4.19), while the terms $H^{kin\,1}$ and H^{constr} have to be written as

$$H^{kin\,1} = -t \sum_{i} \sum_{jj'} b_{ij}^{\dagger} b_{ij'} \ , \tag{4.30}$$

$$H^{constr} = \lim_{U \to \infty} U \sum_{\langle ij \rangle} b_{ij}^{\dagger} b_{ij} b_{ji}^{\dagger} b_{ji} \ . \tag{4.31}$$

The newly added terms are

$$H^{kin\,2b} = -t' \sum_{\langle ij \rangle} b_{ji}^{\dagger} h_i^{\dagger} b_{ij} h_j + h.c. \ , \tag{4.32}$$

and

$$H^{V} = V \sum_{i} h_i^{\dagger} h_i \ , \tag{4.33}$$

where the well depth $V > 0$.

[3] Physically, bonds are composite of (electron pair) + (lattice distortion), and can be thought of as bosons.

Actually, this hamiltonian *conserves* the number of bond vacancies. In reality, their number is determined by the condition of thermodynamic equilibrium, which corresponds to zero chemical potential. In a real system, there will always be a *finite* amplitude for a cage without a vacancy to develop one, and vice versa, and therefore the number of bond vacancies will not be strictly conserved. We will come back to this point later on, and for the moment we limit ourselves to the investigation of the hamiltonian (4.28).

4.3.2 The case $J = 0$

To get a certain insight into the model, which, as formulated in its full generality (4.28), is rather complicated, we first focus on the particular case of $J = 0$. A configuration of the system can be pictorially visualized as on Fig.4.18 – on each site of a square lattice there is either an 'arrow', pointing towards one of the nearest neighbouring sites, or a 'hole'. An arrow can hop to one of the two neighbouring orientations, and the constraint forbids the possibility that two arrows on nearest neighbouring sites might point towards each other. A hole can move, if there is an arrow on a nearest neighbouring site *pointing towards* it - in such case the hole can exchange its position with that of the arrow, while the arrow becomes *overturned.* One may expect that if the ratio of hopping parameters t'/t is not too small, being, say, of the order of one, or larger, then in the typical configurations, around each hole there will very probably be at least one arrow pointing towards it, allowing it thus to move. Actually, in case of $SrTiO_3$, to which our model should eventually apply, we have a good reason to believe that this condition should be well satisfied. The value of t and t' should depend, first of all, on the masses of the respective ions, Ti and O. The mass of O is three times lower than that of Ti, and therefore we expect that t' should be at least comparable to, or perhaps even larger than t.

The picture that emerges is thus that of 'holes' moving more or less freely through the system, overturning the arrows. An instructive, although undoubtedly crude approxima-

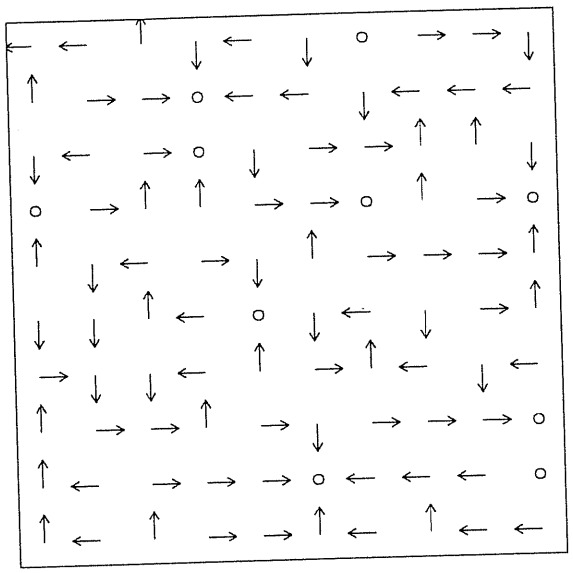

Figure 4.18: A typical configuration of the system containing bond vacancies in the ground state, corresponding to choice of parameters $t = t' = 1, J = 0, U = \infty$. Note arrows pointing towards holes on neighbouring sites.

tion might be to consider the arrows just as a kind of medium, which renormalizes the hole hopping parameter t'. The resulting effective hamiltonian for the holes would then be that of *hard-core lattice bosons*, with some new hopping parameter $\tilde{t'}$ and a chemical potential μ

$$H^{eff} = -\tilde{t'} \sum_{\langle ij \rangle} \left(h_i^\dagger h_j + h_j^\dagger h_i \right) + H_{hc} - \mu \sum_i h_i^\dagger h_i \,, \tag{4.34}$$

where the term H_{hc} forbids the double occupancy of each site. The value of $-\mu$ will be equal to the energy cost of creation of a hole, which, apart from the well depth V, will also contain a contribution from t, because presence of a hole is equivalent to absence of a t hopping ion, with its proper contribution to the energy.

A formal mean-field treatment of hard-core lattice bosons is provided in the paper by Matsubara and Matsuda [70], making use of a mapping on a spin $\frac{1}{2}$ system. Here we just quote some important points of their analysis, the main result of which is a possibility

of a superfluid phase transition. In order to understand the behaviour of the transition temperature as a function of the chemical potential, it is useful to plot the average number of bosons versus temperature for different values of μ, as shown on Fig.4.19. For chemical potential lower than a certain critical value $\mu_c = -z\tilde{t'}$, where z is the number of nearest neighbours, the number of bosons monotonously drops with decreasing temperature, until at $T = 0$ there are no bosons in the ground state. There is no transition at any temperature. For μ slightly larger than μ_c, the number of bosons falls with decreasing temperature, until at some finite T_c the system *becomes superfluid.* On further decreasing temperature, the number of bosons *remains constant* down to $T = 0$. It is easy to show that the *mean-field* condensate fraction in the ground state is just equal to $n_0/n = 1 - n$. Increasing the value of μ, the transition temperature increases too, until for $\mu = 0$ it reaches its maximal value $T_o = z\tilde{t'}/2k$, when the ground state is just half-filled. As is easily seen, the Fig.4.19 is symmetric with respect to half-filling, which is a consequence of the particle-hole symmetry.

From the spin system analogy of [70] it is also intuitively clear, in which way would the above picture be modified by the presence of a term that does not conserve the number of bosons, as discussed in the end of the last subsection. Such term in the spin system is equivalent to an external magnetic field in the XY plane, within which the superfluid ordering takes place. In presence of the field which couples to the order parameter, strictly speaking, there is no real, sharp phase transition. Depending on how strong the field is, the transition will be smeared out to some extent.

The above tentative picture, if true for our bond vacancies, suggests a *new* possible scenario for the crossover from displacive to order-disorder regime. At high enough temperatures, $kT \gg V$, each Ti ion will be uniformly distributed among the minima and the centre of its multiple well. As temperature decreases, some of the ions would go off-center,

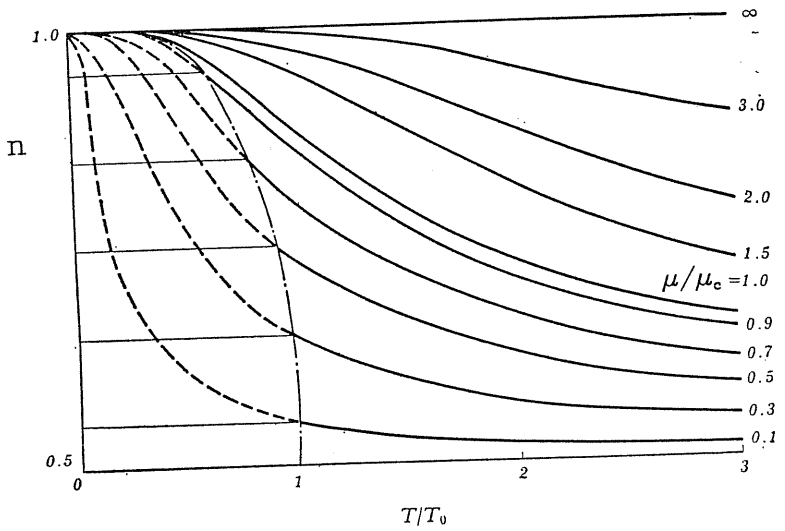

Figure 4.19: Average number of hard-core lattice bosons versus temperature for different values of chemical potential μ, as found by mean-field treatment [70]. The figure is actually symmetric with respect to the $n = 1/2$ line, and only the upper half, corresponding to $\mu > 0$ is shown.

towards one of the minima, creating bonds and reducing the number of bond vacancies. This corresponds to the crossover from the displacive to order-disorder regime, and classically, all the bond vacancies would disappear at $T = 0$. In our model, however, if t' is strong enough and V not too large, this process will be *blocked* at some finite temperature, due to a quantum phase transition. The system will keep some number (in a mean-field treatment, a constant number) of bond vacancies down to $T = 0$, and moreover, these will be superfluid. The transition itself may be accompanied by critical or non-critical fluctuations of the total number of vacancies. All these "strong" properties (ODLRO, superfluidity, sharp phase transition) will be smeared out to some extent by vacancy non-conserving processes.

In order to provide some quantitative, though still preliminary, basis for the above considerations, we have studied the ground state of the hamiltonian (4.28) for $J = 0$, using a variational ansatz for the wavefunction Ψ_g, much in the spirit of the last section.

We shall again use the complex representation, and allow the variable z_i to be equal to 0 in case of a bond vacancy. We assume the ansatz in a product form and write

$$\Psi_g(z_1, \ldots, z_n) = \prod_{\langle ij \rangle} \phi_0(z_i, z_j, r_{ij}) \, . \tag{4.35}$$

If both sites i, j are occupied by vacancies, we set the function $\phi_0(z_i, z_j, r_{ij}) = d_{00}$. If just one of the sites is occupied by a bond vacancy, then $\phi_0(z_i, z_j, r_{ij})$ acquires one of three different values: $\phi_0(z_i, z_j, r_{ij}) = d_{01}$, if the arrow on the other site is perpendicular to the vector r_{ij}; $\phi_0(z_i, z_j, r_{ij}) = d_{02}$, if the arrow points *towards* the vacancy and $\phi_0(z_i, z_j, r_{ij}) = d_{04}$, if the arrow points *from* the vacancy. The quantities $d_{00}, d_{01}, d_{02}, d_{04}$ represent our four variational parameters. Finally, if there is no bond vacancy on the sites i, j, we take the function $\phi_0(z_i, z_j, r_{ij})$ to be equal to the normalized exact solution of the two site problem for sites i, j. This choice is different from that adopted in (4.12), where we took instead $\phi_0(z_i, z_j, r_{ij}) = (\mid z_i - r_{ij} \mid + \mid z_j + r_{ij} \mid)$, since it turned out that with a *non-zero* number of bond vacancies the latter choice yielded slightly *higher* variational energy.

We calculated the average energy of the state described by (4.35), again by means of a Monte Carlo sampling, as we did in the last section. The details of the sampling algorithm we used are reported in the Appendix C. We have investigated just one system size $L = 10$, and one set of parameters $t = t' = 1, V = 0$. We performed the sampling for several values of the bond vacancies number, corresponding to different fillings of the system. For each filling, all four variational parameters $d_{00}, d_{01}, d_{02}, d_{04}$ were optimized, typical optimal values being close to $d_{00} = 3.20, d_{01} = 1.04, d_{02} = 1.28, d_{04} = 0.94$. The results of this calculation are shown on Fig.4.20. The energy first decreases, as the number of bond vacancies grows, until it reaches a minimum for filling equal to 0.2, which would be the equilibrium filling for $V = 0$. This behaviour of the energy agrees with (B.24), and it is clear that for not too large positive V, the energy curve would still develop a minimum for some smaller filling. For a certain value of V, the minimum will be at zero

filling, and for this and higher V, the ground state will contain no bond vacancies. The essential conclusions of our intuitive considerations thus seem to be confirmed, and we believe that at least for $J = 0$, the above scenario may in principle be correct.

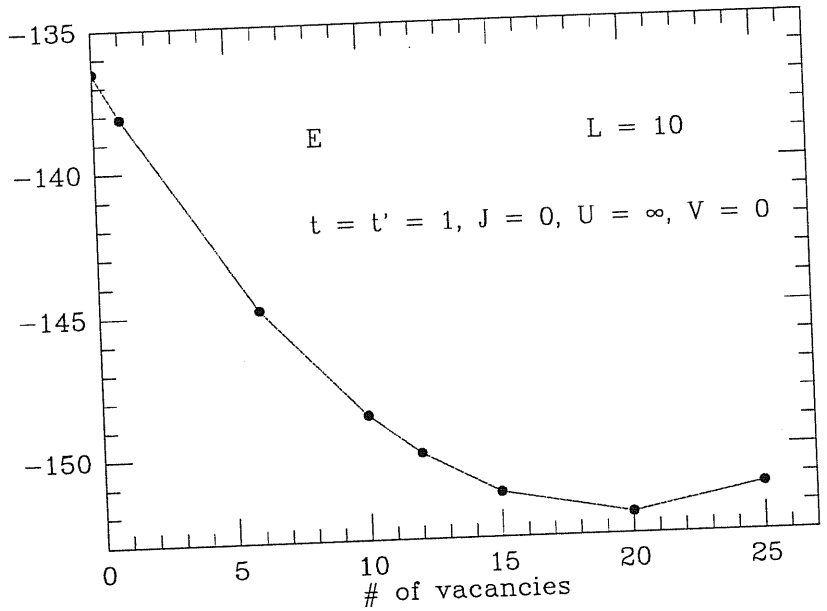

Figure 4.20: Variational ground state energy of the $L = 10$ system with $t = t' = 1, J = 0, U = \infty, V = 0$, as a function of number of vacancies. Note the minimum on the curve, which determines the equilibrium number of vacancies.

4.3.3 The general case of $J \neq 0$

The crucial question in this subsection is how much of the scenario might survive in case of $J \neq 0$, or how it might be modified. As a matter of fact, we know that at temperatures below 37 K, $SrTiO_3$ is already very close to ferroelectricity, and strong, nearly critical polarization fluctuations are present. The system can order in two different ways; apart from the off-diagonal long-range order of the bond vacancies, it can develop also a diagonal long-range order in bond orientation. The question that naturally arises is whether the two kinds of order can coexist. In other words, this amounts to ask what does the $T = 0$ phase diagram of the system look like in the J, V plane (for some fixed $t \sim t'$). Essentially,

there are three possibilities, as shown on Fig.4.21. In cases a) and b), the two kinds of ordering exclude each other. If, however, the real phase diagram is that of the case c), then it is interesting to ask further, what are the properties of the phase with both kinds of order simultaneously present.

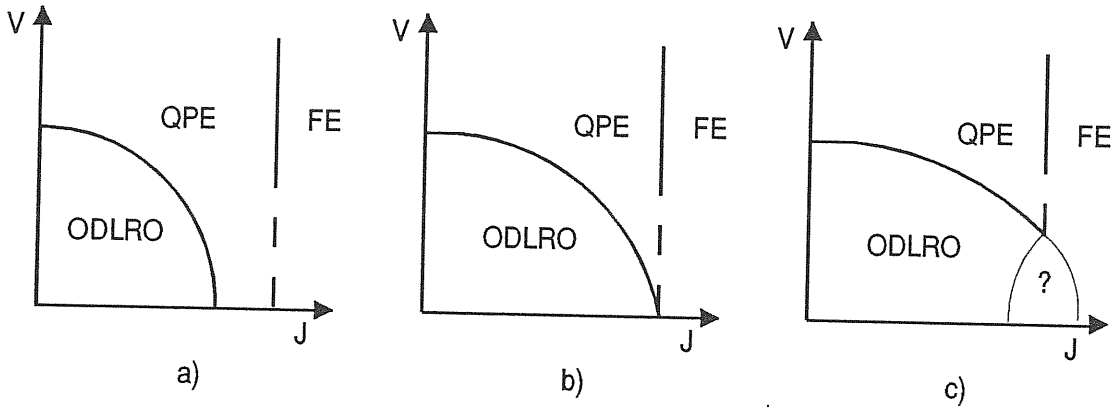

Figure 4.21: Tentative $T = 0$ phase diagrams of the system with bond vacancies in the J, V plane, for $U = \infty$ and some fixed $t \sim t'$.

We can speculate about the role that the aligned clusters play in the motion of bond vacancies. As we see it, the clusters would rather tend to *frustrate* this motion. In the pictorial description of the last subsection, a hole can only move *overturning* the arrows, which, in turn, increases the energy of the ferroelectric coupling. As a result, the holes, if still present, might tend to become localized on the *domain walls*, where the same ferroelectric coupling would favour them. Further work is required to clarify this, probably subtle interplay.

To summarize, so far we have not been able to provide answers to the questions raised above. We have no quantitative prediction for the $J \neq 0$ case, which would allow us to decide whether the model considered can for some reasonable values of its parameters actually exhibit a finite temperature non-ferroelectric phase transition, such as that observed

in $SrTiO_3$.

5 Discussion, and conclusions

In this thesis, we have studied the physics of the simplest models of QPE systems. The selection of a meaningful hamiltonian is particularly delicate, and we have been able to make only some tentative steps towards modeling the real perovskite quantum paraelectrics $SrTiO_3$ and $KTaO_3$. Several main points have emerged in this selection process.

The first is that ferroelectric phenomena are not alone, in these crystals, and experimental facts speak instead clearly of a rich interplay between ferroelectric, strain, and in case of $SrTiO_3$, also antiferrodistortive order parameters. This makes the system rather complicated to treat. Even restricting, as we did initially, to ferroelectricity and strain alone, and accepting the mean-field approximations typical of the displacive limit, the resulting quantum field theory is far from transparent, involving possible quantum melting of an incommensurate modulated phase.

The second is that (unfortunately) only models capable of describing order-disorder fluctuations should be considered really adequate, since experimentally quantum perovskites appear to crossover into an order-disorder regime, *before* entering a sort of quantum central peak state at low temperatures. Therefore the displacive, mean-field picture is inadequate to describe this situation. We have therefore done most of our work on discrete lattice models, and chosen mainly techniques, which can describe adequately fluctuations, quantum as well as classical. The basic element in our discrete lattice models is the $Ti-O$

dipole, also called a "bond".

A third point, which has emerged, is that we might expect in a perovskite ferroelectric at least two different quantum tunneling processes. The first is bond tunneling between the n equivalent positions inside the octahedral cage ($n = 4$ in tetragonal $SrTiO_3$, $n = 6$ in cubic $KTaO_3$). The second is bond tunneling between one cage and the next. This second process will occur whenever an oxygen which is bonded to one Ti hops to bond the other Ti, as in the Fig.2.2.

A fourth point is that there are two strong constraints which restrict both classical and quantum mechanical motion, if the model is to make physical sense for real perovskites. A first constraint, probably valid at low temperatures, is that there should not be more than one bond per cell. In other words, so long as we are in the order-disorder regime, and the Ti atoms are instantaneously off-center, each can engage one and only one of the surrounding oxygens. The second, more interesting constraint, is that two neighbouring cages must not simultaneously possess bonds which point towards one another. This constraint comes from the physical impossibility of an oxygen to be engaged in two bonds simultaneously, and constitutes a kind of ice-rule. The necessity of an effective ice-rule in displacive perovskite ferroelectrics (or, for that matter, in cuprate high T_c superconductors !) does not seem to have been noted and made use of before, and might have far-reaching consequences.

A fifth point is that it should make sense to include the possibility of bond vacancies, corresponding to Ti sites which, by sacrificing some potential energy V, will not fall into a bond with any of the neighbouring oxygens. This potential energy cost might be overcompensated by a kinetic energy gain, in presence of strong inter-cell bond hopping, in turn related to oxygen tunnelling. These zero-point vacancies might condense with a sharp phase transition.

Guided by these considerations, and after an initial discussion of a fully continuous free energy model, we have selected a short-range, 2D lattice quantum four-state clock model, as the simplest toy model of quantum paraelectrics. Of the ingredients mentioned above, two in particular pose some difficulty, namely the inter-cell bond tunneling, and the ice-rule constraint. Our strategy has been therefore to start off first without these two ingredients, with the simple quantum four-state clock model, and then to add the complications only gradually and successively. Since handling of bond hopping is very dependent from the presence of the ice constraint, it was necessary to include the latter first. Thus, the second discrete model considered in this work is an ice-rule constrained quantum four-state clock model.

The main method adopted for the present study of the unconstrained and constrained 2D quantum four-state clock model is Path Integral Monte Carlo (PIMC), plus finite size scaling when possible. For the unconstrained case this calculation is meant to reproduce known results, since, as we show, the model maps onto two uncoupled quantum Ising models (Ising model in a transverse field), well studied and characterized in the 70's. The ice-rule constrained model is instead new and non-trivial. A Monte Carlo strategy has been devised, in order to eliminate a pathologically slow $1/m$ convergence with the number of time slices m, to recover even for the constrained model the usual, more comfortable $1/m^2$ convergence. Although we cannot push finite size scaling to produce critical exponents for this case, we have obtained a reasonably accurate phase diagram.

There are, both in the constrained and in the unconstrained model, only two phases, the ferroelectric and the paraelectric states. However, the ice-rule constraint greatly reduces the number of excited configurations, and this in turn reinforces ferroelectricity. As a result, the extrapolated $T = 0$ critical ratio of potential to kinetic coupling parameters is $J_q/t \simeq 0.15$, a factor of about four smaller than that $J_q^0/t \simeq 0.66$ of the unconstrained

model. The classical critical temperature will also be raised with respect to the unconstrained case, although we did not pursue this aspect in detail. We would not be surprised if a future closer analysis of both classical and quantum critical behaviour should reveal different universality classes, for the unconstrained and the ice-rule constrained 2D clock models.

What have we learned on the nature of the QPE state in the constrained and unconstrained quantum four-state clock model ? We have found that the state is fully symmetric, and has an excitation gap in both cases. However, the gap ΔE is very severely reduced by the ice-rule constraint. This reduction is at least a factor of four at $J = 0$, but seems even stronger for finite J. So long as the ground state is nondegenerate with an excitation gap, transformation from the classical paraelectric state at high temperatures to the QPE state at low temperatures is predicted to be a smooth crossover, not a phase transition. The finding is in line with traditional views on QPE's [71]. It does not explain, however, the phase transition phenomena found by Müller et al. in pure, tetragonal $SrTiO_3$, and also those seen in $KTa_{1-x}Nb_xO_3$, at low x, well below the onset of long-range ferroelectric order [7].

A new, very interesting perspective is finally found by introducing the possibility of "bond vacancies". Because of their ability to favor bond hopping and thus to gain the system kinetic energy, these vacancies might be present even at absolute zero, similar to Andreev and Lifshitz's speculations for solid He^4. In this modeling, the abrupt onset of quantum paraelectricity corresponds to condensation of such vacancies, probably physically tied to the boundary walls between fluctuating ferroelectric domains. This possibility is appealing, and will be further pursued in the future.

It is clear from the above that although we are gradually building some concrete understanding for a series of problems and models which have not been studied at all so

far, we are still a long way from relating to some of the phenomenology of QPE materials discussed in Chapter 1. It is not obvious what a condensate of bond vacancies might look like. The role of strain and antiferrodistortive couplings does not really seem marginal, in the experiments, and we have not yet begun to treat them. Finally, no attempts at studying excitations – which instead have been shown to be very anomalous – has yet been possible. All this work is left for the future.

Appendix A
The Path Integral Quantum Monte Carlo technique

In this appendix we shall describe the Path Integral Quantum Monte Carlo algorithm implemented for the simulation of the constrained model (4.8). The first problem to be resolved is the choice of a convenient decomposition of the hamiltonian in order to apply the Trotter formula.

Since we are interested in the $U \to \infty$ limit of the hamiltonian (4.8), we need to be especially careful. Splitting naively H^{tot} into the sum of a kinetic and potential energy yields in the limit $U \to \infty$ a very poor convergence of the Trotter expansion, because the commutator of the kinetic energy operator and the unbounded potential energy operator is also unbounded. The error decreases slowly, as $1/m$, with the number of Trotter slices m, analogously to that of Ref. [72]. In order to avoid this problem, we have to get rid of the unbounded term in the hamiltonian. For this purpose it is useful to introduce a projector P

$$P = \prod_{\langle ij \rangle} (1 - P'_{ij}) = \prod_{\langle ij \rangle} P_{ij} \,, \tag{A.1}$$

which projects out the forbidden states. The partition function of (4.8) in the limit $U \to \infty$ then can be written as

$$Z = \mathrm{Tr}\, P e^{-\beta PHP} \,, \tag{A.2}$$

where we again denote by H the unconstrained hamiltonian (4.1)

$$H = H^4 + H^{kin\,1} = \sum_i (H_i^4 + H_i^{kin\,1}) = \sum_i H_i \,. \tag{A.3}$$

It is now convenient to use both *row and column* indices i, j to label the sites of the square lattice, and write the hamiltonian as

$$H = \sum_{ij} H_{ij} = \sum_{(i+j)\ odd} H_{ij} + \sum_{(i+j)\ even} H_{ij} = \sum_{(i+j)\ odd} A_{ij} + \sum_{(i+j)\ even} B_{ij} \,, \tag{A.4}$$

where A_{ij} is just a re-naming of H_{ij} for the $(i+j)$ odd sublattice, and B_{ij} that for the even sublattice. Since both H, and P, contain only nearest neighbour interactions, we have

$$\left[PA_{ij}P, PA_{i'j'}P\right] = \left[PB_{ij}P, PB_{i'j'}P\right] = 0 \,, \tag{A.5}$$

which provides us with a useful decomposition of the hamiltonian for application of the Trotter formula. The whole lattice is decomposed into two interpenetrating sublattices, A and B, each sublattice consisting of noninteracting sites in an external field determined by the configuration of the other sublattice. This scheme is actually a version of the well-known checkerboard decomposition [73].

To proceed, we write the partition function of the system as

$$Z = \mathrm{Tr} P\, e^{-\beta PHP} = \sum_{\{z_{ij}\}} \langle z_{ij}|P \left[e^{-\frac{\beta}{m}\left(\sum_{ij} PA_{ij}P + \sum_{ij} PB_{ij}P\right)} \right]^m |z_{ij}\rangle \,, \tag{A.6}$$

where m is an integer, and $|z_{ij}\rangle$ are eigenstates of the complex coordinates z_{ij} (2.8).

We define the m-th approximant to the partition function by

$$\begin{aligned} Z_m &= \sum_{\{z_{ij}\}} \langle z_{ij}|P \left[e^{-\frac{\beta}{m}\sum_{ij} PA_{ij}P} e^{-\frac{\beta}{m}\sum_{ij} PB_{ij}P} \right]^m |z_{ij}\rangle \\ &= \sum_{\{z^1_{ij}\}} \cdots \sum_{\{z^{2m}_{ij}\}} \langle z^1_{ij}|Pe^{-\frac{\beta}{m}\sum_{ij} PA_{ij}P}|z^2_{ij}\rangle \langle z^2_{ij}|Pe^{-\frac{\beta}{m}\sum_{ij} PB_{ij}P}|z^3_{ij}\rangle \\ &\quad \cdots \langle z^{2m-1}_{ij}|Pe^{-\frac{\beta}{m}\sum_{ij} PA_{ij}P}|z^{2m}_{ij}\rangle \langle z^{2m}_{ij}|Pe^{-\frac{\beta}{m}\sum_{ij} PB_{ij}P}|z^1_{ij}\rangle \,, \end{aligned} \tag{A.7}$$

where we have inserted a complete set of intermediate states between each two exponentials. Due to (A.5), the matrix elements between the intermediate states in the last expression factorize, and we get

$$Z_m = \sum_{\{z_{ij}^1\}} \cdots \sum_{\{z_{ij}^{2m}\}} \tag{A.8}$$
$$\prod_{k,(i+j)\,odd} \langle z_{i+1,j}^k, z_{i,j+1}^k, z_{i-1,j}^k, z_{i,j-1}^k, z_{i,j}^k | Pe^{-\frac{\beta}{m} P A_{ij} P} | z_{i+1,j}^{k+1}, z_{i,j+1}^{k+1}, z_{i-1,j}^{k+1}, z_{i,j-1}^{k+1}, z_{i,j}^{k+1} \rangle$$
$$\prod_{k,(i+j)\,even} \langle z_{i+1,j}^k, z_{i,j+1}^k, z_{i-1,j}^k, z_{i,j-1}^k, z_{i,j}^k | Pe^{-\frac{\beta}{m} P B_{ij} P} | z_{i+1,j}^{k+1}, z_{i,j+1}^{k+1}, z_{i-1,j}^{k+1}, z_{i,j-1}^{k+1}, z_{i,j}^{k+1} \rangle ,$$

where $|z_{i+1,j}^k, z_{i,j+1}^k, z_{i-1,j}^k, z_{i,j-1}^k, z_{i,j}^k\rangle = |z_{i+1,j}^k\rangle |z_{i,j+1}^k\rangle |z_{i-1,j}^k\rangle |z_{i,j-1}^k\rangle |z_{i,j}^k\rangle$. It is easily seen that the matrix elements in the last equation are *diagonal* in the quantum numbers $z_{i+1,j}^k, z_{i,j+1}^k, z_{i-1,j}^k, z_{i,j-1}^k$, and can therefore be written as

$$\langle z_{i+1,j}^k, z_{i,j+1}^k, z_{i-1,j}^k, z_{i,j-1}^k, z_{i,j}^k | Pe^{-\frac{\beta}{m} P H_{ij} P} | z_{i+1,j}^k, z_{i,j+1}^k, z_{i-1,j}^k, z_{i,j-1}^k, z_{i,j}^{k+1} \rangle$$
$$= C(z_{i+1,j}^k, z_{i,j+1}^k, z_{i-1,j}^k, z_{i,j-1}^k, z_{i,j}^k, z_{i,j}^{k+1}) . \tag{A.9}$$

This diagonality imposes a conservation rule on the 2+1 D classical system on which our 2D quantum system maps. The mapping now follows from

$$Z_m = \sum_{\{z_{ij}^1\}} \cdots \sum_{\{z_{ij}^{2m}\}} \prod_{k,i+j\,odd} C(z_{i+1,j}^k, z_{i,j+1}^k, z_{i-1,j}^k, z_{i,j-1}^k, z_{i,j}^k, z_{i,j}^{k+1})$$
$$\prod_{k,i+j\,even} C(z_{i+1,j}^k, z_{i,j+1}^k, z_{i-1,j}^k, z_{i,j-1}^k, z_{i,j}^k, z_{i,j}^{k+1}) , \tag{A.10}$$

and each term in the above product can be interpreted as a Boltzmann factor of a parallelepiped with vertical faces rotated by 45° with respect to the axes of the original 2D lattice (Fig.A.1). Each of its corner points is a four-state clock rotor. The corresponding classical system can thus be seen as a (2+1) D lattice of such parallelepipeds. The conservation rule restricts *the rotors on both sides of the vertical edges of each parallelepiped to be in the same state.* The Boltzmann weight (A.9) of each parallelepiped then depends on the state of all four rotors at its vertical edges, as well as on the state of both rotors at

the centers of its horizontal faces. The mutual state of these latter rotors, sitting at the centers of the horizontal faces, *is not restricted* in any way.

The calculation of the matrix elements $C(z^k_{i+1,j}, z^k_{i,j+1}, z^k_{i-1,j}, z^k_{i,j-1}, z^k_{i,j}, z^{k+1}_{i,j})$ is straightforward. It requires just diagonalization of the 4×4 on-site problem of a four-state clock rotor H^{kin}_i [1] in an external field, represented by H^4_i and the projector P. In our simulation we performed this diagonalization numerically. All the matrix elements turned out to be non-negative, and therefore no sign problem was present. [1]

We proceed to identify the estimators for the thermodynamic quantities. For convenience we write the partition function approximant Z_m symbolically as

$$Z_m = \sum_{\{z^1_{ij}\}} \cdots \sum_{\{z^{2m}_{ij}\}} \prod_{k,i,j} C_{kij} \,. \tag{A.11}$$

The internal energy per site of the system then reads

$$E_m = -\frac{1}{N}\frac{1}{Z_m}\frac{\partial Z_m}{\partial \beta} = \langle E_{est} \rangle \,, \tag{A.12}$$

where

$$E_{est} = -\frac{1}{N}\sum_{k,i,j} \frac{1}{C_{kij}}\frac{\partial C_{kij}}{\partial \beta} \tag{A.13}$$

is the corresponding estimator. For the specific heat per site c_v we obtain

$$\begin{aligned} c_{vm} &= -\frac{1}{N}\beta^2 \frac{\partial E_m}{\partial \beta} \\ &= \frac{1}{N}\beta^2 \left\{ \langle E^2_{est} \rangle - \langle E_{est} \rangle^2 + \langle \sum_{k,i,j} \left[\frac{1}{C_{kij}}\frac{\partial^2 C_{kij}}{\partial \beta^2} - \left(\frac{1}{C_{kij}}\frac{\partial C_{kij}}{\partial \beta} \right)^2 \right] \rangle \right\} \,, \end{aligned} \tag{A.14}$$

and we see that it is not just equal to the fluctuation of the internal energy, as in the classical case. The hamiltonian of our effective classical system is itself temperature dependent.

[1] Since bonds cannot interchange in the present model (4.8), there is no question as to their statistics, which is irrelevant.

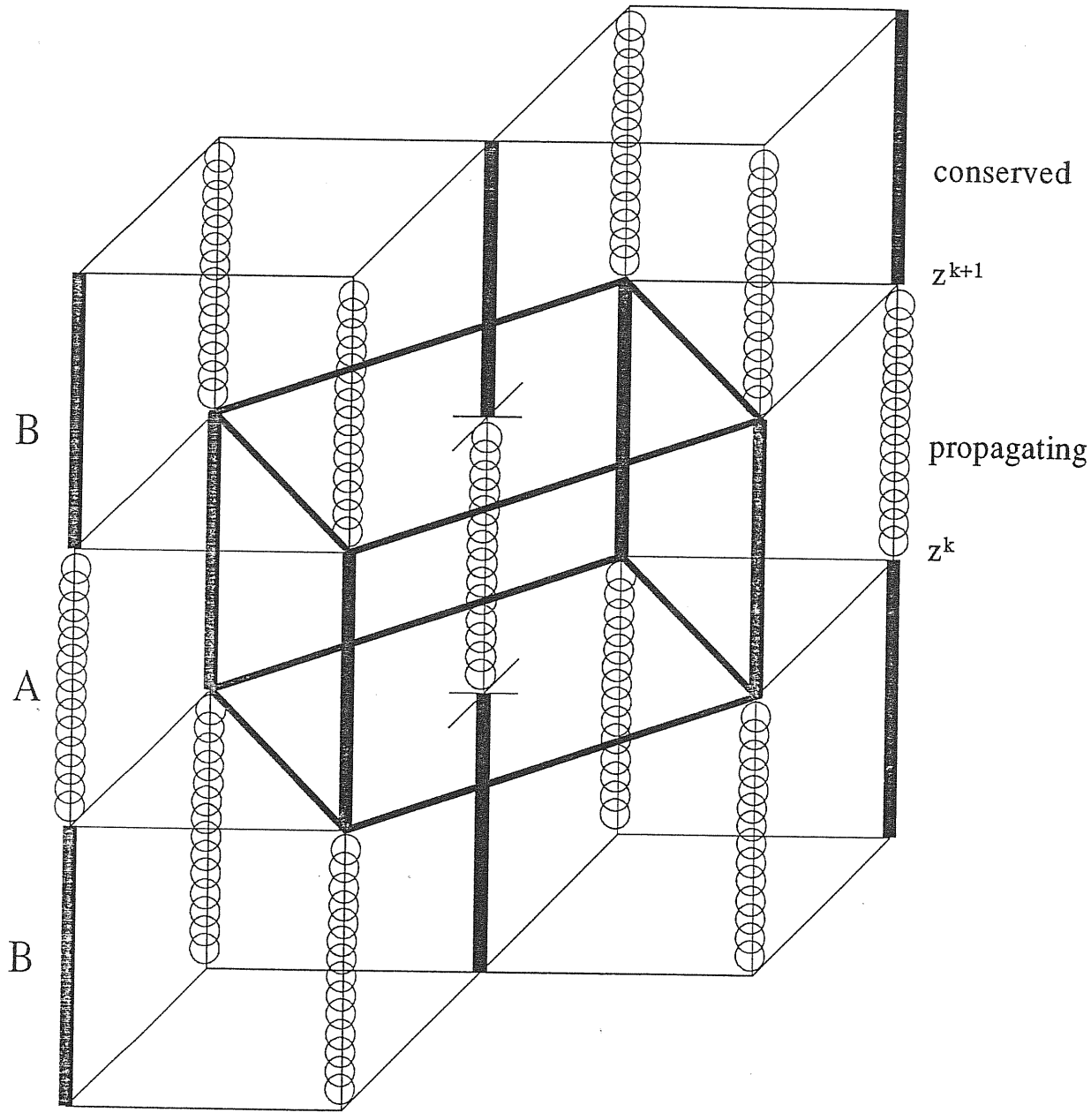

Figure A.1: The (2+1)D classical system. The imaginary time (Trotter) direction is vertical. Vertical dark lines connect sites, which must be flipped together, springs connect independent sites.

In order to calculate the order parameter, which in our case is the polarization of the system, and the corresponding susceptibility, we have to consider an external field F applied on the system. If we choose this to point, e.g. along the x-axis, the matrix elements $C(z^k_{i+1,j}, z^k_{i,j+1}, z^k_{i-1,j}, z^k_{i,j-1}, z^k_{i,j}, z^{k+1}_{i,j})$ in (A.10) are replaced by

$$\begin{aligned} &C(z^k_{i+1,j}, z^k_{i,j+1}, z^k_{i-1,j}, z^k_{i,j-1}, z^k_{i,j}, z^{k+1}_{i,j}) \rightarrow \\ &C(z^k_{i+1,j}, z^k_{i,j+1}, z^k_{i-1,j}, z^k_{i,j-1}, z^k_{i,j}, z^{k+1}_{i,j}) \exp(\frac{\beta}{m} F \mathrm{Re}\, z^k_{i,j}) \end{aligned} \tag{A.15}$$

and we obtain for the equilibrium polarization per site P_{xm}

$$P_{xm} = \frac{1}{\beta N Z_m} \frac{\partial Z_m}{\partial F} = \langle P_{xm\,est} \rangle \,, \tag{A.16}$$

where

$$P_{xm\,est} = \frac{1}{Nm} \sum_{k,i,j} \mathrm{Re}\, z^k_{i,j} \tag{A.17}$$

The static dielectric susceptibility $\chi_{xx\,m}$ then turns out to be

$$\chi_{xx\,m} = \frac{\partial P_{xm}}{\partial F} = \beta N \left[\langle P^2_{xm\,est} \rangle - \langle P_{xm\,est} \rangle^2 \right] . \tag{A.18}$$

The last two quantities are suitable to study the system either in the paraelectric phase, where $\langle P_{xm\,est} \rangle = 0$, or in the ferroelectric phase not very close to the transition, when the order parameter does not undergo the finite-size flipping among the four possible orientations, and $\langle P_{xm\,est} \rangle$ remains a well-defined quantity during the simulation time. For the behaviour of the system right across the phase transition, it is convenient to monitor the modulus rather than the components of the order parameter. We have

$$P_m = \langle P_{m\,est} \rangle = \langle \sqrt{P^2_{xm\,est} + P^2_{xm\,est}} \rangle \,, \tag{A.19}$$

and the corresponding susceptibility is given by

$$\chi_m = \beta N \left[\langle P^2_{m\,est} \rangle - \langle P_{m\,est} \rangle^2 \right] . \tag{A.20}$$

Finally, we have sampled a "short-range order parameter" $\langle\cos(\phi_{ij}-\phi_{i'j'})\rangle$, where ij and $i'j'$ are nearest neighbours. This can be calculated as

$$\langle\cos(\phi_{ij}-\phi_{i'j'})\rangle = \frac{1}{2Nm}\langle\sum_{k,i,j}\left[\mathrm{Re}({z^k_{i,j}}^* z^k_{i+1,j}) + \mathrm{Re}({z^k_{i,j}}^* z^k_{i,j+1})\right]\rangle\,. \tag{A.21}$$

Our (2+1) dimensional classical system is simulated in a standard way using the Metropolis algorithm. The trace operation requires periodic boundary conditions along the imaginary time direction. We have used periodic boundary conditions for both space directions as well. In order to satisfy the conservation rule, we must always move the pairs of rotors on both sides of the vertical edges of the parallelepipeds simultaneously. It is therefore convenient to consider the vertical edges as being a kind of "rigid rods", and take these as new variables, which now can be moved independently (Fig.A.1). One randomly chosen rod was moved at a time, without any kind of collective moves. Unlike in simulation of the classical four-state clock model [74], we did not restrict the flips of the rods and allowed these to flip from present position to each of the remaining three.

We carried out almost all calculations by fixing the value of the ferroelectric coupling J and of the number of Trotter slices m, and then running a series of simulations for different temperatures. The final configuration of a simulation at a given temperature was used as the initial configuration for a run at the next higher temperature, always heating the system. As the initial configuration at the lowest temperature, we always took the ferroelectric state, completely ordered both in space and in the imaginary time directions. The only exception is the data shown on Fig.4.13, where the corresponding runs were carried out at constant temperature, decreasing the value of J. We typically used $1 \div 2 \times 10^4$ MCsteps/site to equilibrate the system and $2 \div 4 \times 10^5$ MCsteps/site for calculating averages. The CPU time needed to perform 1 MCstep/site was about $14\,\mu s$ using an HP720 RISC machine.

In order to estimate the statistical accuracy of our results we measured the MC correla-

tion time of the chain of values generated for various quantities in course of the simulation. We did this by using the standard method of dividing the chain in blocks of variable size described in [75], [76].

Finally, we would like to comment briefly on the convergence of the averaged quantities as a function of the number of Trotter slices m. It is well-known [73] that the error in the average value of an operator due to the Trotter decomposition is an even function of m and therefore the results of a QMC simulation can, in principle, be extrapolated to $m \to \infty$ in the form

$$A_m = A_\infty + \frac{a}{m^2} + \frac{b}{m^4} + \dots . \tag{A.22}$$

This kind of extrapolation, to be meaningful, would require very high accuracy for at least two values of m (to determine a), or three values of m (to determine b), etc. For most data presented in this paper such procedure was not needed. Except at the lowest temperatures, it was generally sufficient to inspect data for $m = 5, m = 10$ or $m = 10, m = 20$ (sometimes for all three values of m) to see that further increasing of m would not change the value of the quantity under consideration within our statistical accuracy. The values of m we have used were always a result of a compromise between the requirement of convergence and that of keeping a reasonable acceptance ratio, since, of course, the acceptance ratio falls with increasing m and problems with loss of ergodicity of the system begin to appear.

Appendix B
The quantum crystal of Andreev and Lifshitz

In this appendix we briefly summarize some of the ideas contained in [18], which are relevant for our considerations in section 4.3.

Imagine a *classical* crystal at $T = 0$, in which there is an atom on each site of a regular periodic lattice. In order to make the number of atoms different from the number of lattice sites, it is necessary to create a *defect*, either a vacancy, or an interstitial. Such process would cost a finite energy ϵ_{cl}, and classically is not possible at $T = 0$. The perfect crystalline state is therefore stable.

Now, still at $T = 0$, turn on the quantum fluctuations. The atoms will not be anymore localized precisely on the lattice sites, which correspond to the points of minimal potential energy. They will be spread around this points over some characteristic distance, which is a measure of the strength of the fluctuations. As long as this distance is small compared to the lattice constant, however, the one-to-one correspondence between an atom and a site is preserved, and nothing particular happens.

Increasing further the strength of the quantum fluctuations, the wavefunctions of the atoms on neighbouring sites start to overlap. Imagine that a defect were created *now*, and to be specific, let it be a vacancy. There would be a finite amplitude t' for a process, in which one of the nearest neighbouring atoms tunnels over a distance of one lattice

constant, and fills the vacant site. Due to such mechanism, the vacancy has become mobile. Although the number of atoms is no more equal to the number of lattice sites, the crystal is *still periodic*. The state of the vacancy is thus characterized by a quasimomentum $\vec{k}$, and its energy eigenvalues $\epsilon(\vec{k})$ will form a *band*. The middle of the band will be located in ϵ_{cl}, the energy cost of the vacancy in the classical limit, and the width of the band will be proportional to the tunneling amplitude t'. If the bottom of the band is at $\vec{k} = 0$, in the vicinity of this point we can expand

$$\epsilon(\vec{k}) = \epsilon_0 + \frac{k^2}{2M} , \tag{B.23}$$

where M is the corresponding effective mass. As long as ϵ_0 is positive, the perfect crystal structure is stable, and there are no defects in its ground state.

Clearly, with sufficiently strong quantum fluctuations, ϵ_0 may become negative. At this point, the ground state ceases to be stable with respect to the *spontaneous* creation of the vacancies. A phase transition to a new ground state occurs, and the nature of this transition depends on the statistics of the defects, as well as on their mutual interaction. Close to the transition point, the number of the vacancies is low, and therefore these can be treated as a dilute gas. If the vacancies are bosons, as in the case of He^4, the total energy of the crystal with N vacancies can be written as

$$E = N\epsilon_0 + \frac{2\pi a}{MV} N^2 , \tag{B.24}$$

where a is the scattering amplitude for the vacancies, and V is the volume of the crystal. We shall assume that the interaction between the vacancies is repulsive, and correspondingly $a > 0$. Under such conditions, the equilibrium density of the vacancies in the crystal at $T = 0$ is obtained by minimizing (B.24), and reads

$$\frac{N}{V} = \frac{-\epsilon_0 M}{4\pi a} . \tag{B.25}$$

It is easily seen that the phase transition is of the second order, the order parameter being $\sqrt{N/V}$. The ground state contains a finite number of *zero-point vacancies*, a fraction of which is *Bose condensed* in the lowest eigenstate at $\vec{k} = 0$.

Appendix C
The Monte Carlo sampling algorithm for the case of bond vacancies

In this appendix, we briefly comment on the algorithm we used for the Monte Carlo sampling of the wavefunction (4.35). As pointed out in section 4.3, in the important configurations, holes are mostly surrounded by arrows (on nearest neighbouring sites) which point towards them (Fig.4.18). If we want our algorithm to produce configurations which have a good probability to be accepted, these should comply with the last condition as much as possible. A straightforward way how to implement such sampling would be the following: we choose a site at random, and first test whether it is occupied by an arrow or by a hole. In case of an arrow, we just try to flip it to another orientation, if allowed by the constraint, in the same way as we did in section 4.2. In case of a hole, we further test the neighbouring sites for presence of arrows pointing towards the hole; if we don't find any, no trial move is attempted. If we find just one such arrow, we try to exchange it with the hole; if we find more arrows, we *randomly* choose one of them and try to exchange it with the hole. Such trial move would actually be an elementary transition caused by the hamiltonian term $H^{kin\,2b}$ (2.13).

The ergodicity of this procedure is easily seen, since any configuration can be reached

by a finite sequence of moves. In order to satisfy the detailed balance condition, however, one has to be careful about the acceptance probabilities. Consider two configurations, r and s, such that these can be reached from each other by exchanging a hole with an arrow, and let P_r and P_s be the corresponding statistical probabilities. The detailed balance condition can be expressed as

$$P_r W_{rs} A_{r\to s} = P_s W_{sr} A_{s\to r} \ , \tag{C.26}$$

where W_{rs} and W_{sr} are the *'a priori'* transition probabilities, and $A_{r\to s}$ and $A_{s\to r}$ are the corresponding acceptance probabilities. Let us denote by E_r and E_s the number of arrows pointing towards the hole in the respective configurations. Since both configurations are eligible for the trial move, both numbers E_r and E_s are at least equal to one, or larger. The 'a priori' transition probabilities are then given by $W_{rs} = W/E_r, W_{sr} = W/E_s$, where W is the probability that picking a site at random we find a hole; clearly, W is just equal to the filling of the system. To be specific, suppose that $P_r \geq P_s$. It is now easy to demonstrate that the condition (C.26) will be satisfied if we adopt the following choice for $A_{r\to s}$ and $A_{s\to r}$

$$A_{s\to r} = \frac{1}{2}\sqrt{\frac{E_s}{E_r}} \ , \tag{C.27}$$

$$A_{r\to s} = \frac{1}{2}\frac{P_s}{P_r}\sqrt{\frac{E_r}{E_s}} \ . \tag{C.28}$$

Since in our case both numbers E_r and E_s can at most be equal to four, the factors of $\frac{1}{2}$ in the last equations guarantee that the resulting expressions are not larger than one, and thus may be interpreted as probabilities.

Bibliography

[1] K. Alex. Müller, H. Burkard, Phys. Rev. B **19**, 3593 (1979).

[2] R. Blinc, D. Hadži, Mol. Phys. **1**, 391 (1958).

[3] P. G. de Gennes, Solid State Commun. **1**, 132 (1963).

[4] T. Schneider, H. Beck and E. Stoll, Phys. Rev. B **13**, 1123 (1976).

[5] R. Oppermann, H. Thomas, Z. Phys. B **22**, 387 (1975).

[6] P. Pfeuty, J. Phys. C: Solid St. Phys. **9**, 3993 (1976).

[7] D. Rytz, Ph.D. thesis, Ecole Polytechnique Fédérale de Lausanne, 1983.

[8] R. Migoni and H. Bilz and D. Bäuerle, Phys. Rev. Lett. **37**, 1155 (1976).

[9] H. Bilz, G. Benedek and A. Bussmann–Holder, Phys. Rev. B **35**, 4840 (1987).

[10] M. Maglione, S. Rod and U. T. Höchli, Europhys. Lett., 4 (5), 631 (1987)

[11] K. Alex. Müller, W. Berlinger, and E. Tosatti, Z. Phys. B – Condensed Matter **84**, 277 (1991).

[12] H. Gränicher, O. Jakits, Il Nuovo Cimmento Suppl., **11**, 480 (1954)

[13] S. Nomura, S. Sawada, J. Phys. Soc. Japan **10**, 108 (1955).

[14] J. G. Bednorz and K. A. Müller, Phys. Rev. Lett. **52**, 2289 (1984).

[15] O. M. Nes, K. A. Müller, T. Suzuki, K. Fossheim, preprint 1992.

[16] E. Courtens, G. Coddens, B. Hennion, B. Hehlen, J. Pelous, R. Vacher, *13th General Conference of the European Physical Society*, Regensburg, Germany, March 28 - April 2, 1993, to be published in *Physica Scripta*

[17] M. Maglione, M. Fischer, private communication.

[18] A. F. Andreev, I. M. Lifshitz, Soviet Physics JETP, **29**, 1107 (1969).

[19] R. A. Cowley, Phys. Rev. **134**, A981 (1964).

[20] P. A. Fleury, J. F. Scott, J. M. Worlock, Phys. Rev. Lett. **21**, 16 (1968).

[21] G. Shirane, Y. Yamada, Phys. Rev. **177**, 858 (1969).

[22] Hiromi Unoki and Tunetaro Sakudo, J. Phys. Soc. Jpn. **23**, 546 (1967).

[23] P. A. Fleury and J. M. Worlock, Phys. Rev. **174**, 613 (1968).

[24] Yasusada Yamada and Gen Shirane, J. Phys. Soc. Jpn. **26**, 396 (1969).

[25] W. Cochran, Adv. Phys. **9**, 387 (1960).

[26] E. Sawaguchi, A. Kikuchi, Y. Kodera, J. Phys. Soc. Japan **17**, 1666 (1962).

[27] T. Sakudo, H. Unoki, Phys. Rev. Lett. **26**, 851 (1971).

[28] W. R. Abel, Phys. Rev. B **4**, 2696 (1971).

[29] G. A. Samara, B. Morosin, Phys. Rev. B **8**, 1256 (1973).

[30] R. P. Lowndes, A. Rastogi, J. Phys. C **6**, 932 (1973).

[31] M. Maglione, private communication.

[32] A. S. Chaves, S. P. S. Porto, Solid State Commun. **13**, 865 (1973).

[33] Hiromoto Uwe and Tunetaro Sakudo, Phys. Rev. B **13**, 271 (1976).

[34] *Statistical Physics, Part 1*, L. D. Landau, E. M. Lifshitz, Course of Theoretical Physics, Vol.5 (Pergamon Press, Oxford 1980)

[35] R. O. Bell, G. Rupprecht, Phys. Rev. **129**, 90 (1963).

[36] G. Sorge, E. Hegenbarth, Phys. Stat. Sol. **33**, K79 (1969).

[37] G. Sorge, E. Hegenbarth, G. Schmidt, Phys. Stat. Sol. **37**, 599 (1970).

[38] F. W. Lytle, J. Appl. Phys. **35**, 2212 (1964).

[39] W. Rehwald, Solid State Commun. **8**, 607-611, 1483-1485 (1970).

[40] J. D. Axe, J. Harada and G. Shirane, Phys. Rev. B **1**, 1277 (1970).

[41] R. Vacher, J. Pelous, B. Hennion, G. Coddens, E. Courtens and K. Alex. Müller, Europhys. Lett. **17**, 45 (1992).

[42] K. Inoue, Jpn. J. Appl. Phys. **24**, Suppl. 24-2, 107 (1985).

[43] A. Okazaki, M. Kawaminami, Mater. Res. Bull. **8**, 545 (1973).

[44] *Structural Phase Transitions*, A. D. Bruce and R. A. Cowley (Taylor & Francis Ltd. London 1981)

[45] *Structural Phase Transitions and Soft Modes*, Proceedings of the NATO Advanced Study Institute, Geilo, Norway, 1971, ed. by E. J. Samuelsen, E. Andersen and J. Feder (Universitetsforlaget Oslo, Bergen, Tromsö 1971)

[46] J. C. Slater, J. Chem. Phys. **9**, 16 (1941).

[47] T. Schneider, E. Stoll, Phys. Rev. B **17**, 1302 (1978).

[48] H. Uwe, K. B. Lyons, H. L.Carter, P. A. Fleury, Phys. Rev. B **33**, 6436 (1986).

[49] S. Rod, F. Borsa, J.J. van der Klink, Phys. Rev. B **38**, 2267 (1988).

[50] K. A. Müller, W. Berlinger and J. C. Slonczewski, Phys. Rev. Lett. **25**, 734 (1970).

[51] V. Dvořák in: *Modern Trends in the Theory of Condensed Matter.* Proceedings of the XVI Karpacz Winter School of Theoretical Physics, 1979, Karpacz, Poland, ed. by A. Pękalski and J. Przystawa, Lecture Notes in Physics; 115 (Springer-Verlag, 1980), p. 447.

[52] T. A. Aslanian and A. P. Levanyuk, Solid State Commun. **31**, 547 (1979).

[53] *Incommensurate Phases in Dielectrics - 1. Fundamentals*, ed. by R. Blinc, A. P. Levanyuk, Modern Problems in Condensed Matter Science, Vol.14.1 (North–Holland, Amsterdam 1986)

[54] T. A. Aslanian, A. P. Levanyuk, M. Vallade and J. Lajczerowicz, J. Phys. C: Solid State Phys., **16** (1983) 6705

[55] R. J. Elliott, C. Wood, J. Phys. C: Solid St. Phys. 4, 2359 (1971).

[56] P. Pfeuty, Ann. Phys. NY **57**, 79 (1970).

[57] M. Suzuki, Progr. Theor. Phys., **37**, 770 (1967).

[58] A. Michelson, Phys. Rev. B **16**, 577 (1977).

[59] F. D. M. Haldane, J.Phys. A: Math. Gen. **15**, 507 (1982); F. D. M. Haldane, P. Bak and T. Bohr, Phys. Rev. B **28**, 2743 (1983).

[60] R. Martoňák, Magister PhilosophiæThesis, SISSA, Trieste, 1991.

[61] M. A. Moore, H. C. W. L. Williams, J. Phys. C: Solid St. Phys. **5**, 3168 (1972)

[62] M. A. Moore, H. C. W. L. Williams, J. Phys. C: Solid St. Phys. **5**, 3185 (1972)

[63] M. A. Moore, H. C. W. L. Williams, J. Phys. C: Solid St. Phys. **5**, 3222 (1972)

[64] M. Kolb, Phys. Rev. Lett. **51**, 1696 (1983).

[65] M. N. Barber, W. Selke, J. Phys. A **15**, L617 (1982).

[66] P. Fazekas, B. Mühlschlegel, M. Schröter, Z. Phys. B – Condensed Matter **57**, 193 (1984).

[67] P. W. Anderson, Phys. Rev. Lett. **64**, 1839 (1990).

[68] G. Kotliar, A. E. Ruckenstein, Phys. Rev. Lett. **57**, 1362 (1986).

[69] R. Morf, T. Schneider and E. Stoll, Phys. Rev. B **16**, 462 (1977).

[70] T. Matsubara, H. Matsuda, Progr. Theor. Phys., **16**, 569 (1956).

[71] K. Alex. Müller, Jap. J. Appl. Phys., **24-2**, 89 (1985)

[72] X. Y. Zhang, Elihn Abrahams, G. Kotliar, Phys. Rev. Lett. **66**, 1236 (1990).

[73] *Quantum Monte Carlo Methods in Equilibrium and Nonequilibrium Systems*, Proceedings of the Ninth Taniguchi International Symposium, Susono, Japan, 1986, ed. by M. Suzuki (Springer-Verlag Berlin Heidelberg 1987).

[74] J. Tobochnik, Phys. Rev. B **26**, 6201 (1982).

[75] G. Jacucci, A. Rahman, Il Nuovo Cimento, **Vol. 4 D**, 341 (1984).

[76] J. Cao, B. J. Berne, J. Chem. Phys. **91**, 6359 (1989).